With Low Emission to High Transmission

Integrating low thermal emissivity in antireflective coatings on glasses for energy saving in greenhouse horticulture

Bram van Breugel[1], Esteban Baeza[1], Marcel Raaphorst[1], Remi Aninat[2], Mohammad Shayesteh[3], Feije de Zwart[1], Hans Linden[2] and Vincent Lieffrig[3]
1. Wageningen University & Research, 2. TNO Solliance, AGC Glass Europe

Report WPR-1040

WAGENINGEN UNIVERSITY & RESEARCH

Glastuinbouw Nederland morgen groeit vandaag

Ministerie van Landbouw, Natuur en Voedselkwaliteit

KAS ALS ENERGIEBRON

Referaat
Vanuit een energiebesparend perspectief moet de kasomhulling een zo hoog mogelijke lichtdoorlatendheid hebben om maximaal gebruik te maken van gratis zonne-energie, terwijl ze goede isolerende eigenschappen moet hebben om warmteverlies vanuit kas te voorkomen. Antireflectie coatings (AR) verhogen de lichttransmissie, emissiearme coatings (low-e) verminderen het warmteverlies. De gangbare low-e coatings verlagen echter de licht transmissie en hebben een beschermende atmosfeer nodig om degradatie te voorkomen waardoor low-e coatings standaard alleen in dubbel glas worden toegepast. Het doel van dit project was om low-e en antireflectie eigenschappen te verenigen in een enkele coating waardoor het verhogen van de lichttransmissie en verminderen van het warmteverlies wordt gecombineerd. Dit levert een duidelijke energiebesparing op.

Abstract
From an energy-saving perspective, the greenhouse cover must have the highest possible light transmission to make maximum use of free solar energy, while it must have good insulating properties to prevent heat loss from the greenhouse. Anti-reflection coatings (AR) increase light transmission, low-emission coatings (low-e) reduce heat loss. However, common low-e coatings reduce light transmission and require a protective atmosphere to prevent degradation, which is why low-e coatings are normally only used in double glazing. The aim of this project was to combine low-e and anti-reflective properties in a single coating, thus combining increasing light transmission and reducing heat loss. This leads to a significant energy saving.

Reportinfo

Report WPR-1040
Projectnumber: 3742265000
DOI number: 10.18174/541487

Dit project is gefinancierd vanuit het programma Kas als Energiebron, het innovatie- en actieprogramma voor energiebesparing en verduurzaming in de glastuinbouw van Glastuinbouw Nederland en het ministerie van Landbouw, Natuur en Voedselkwaliteit. Het onderzoek is uitgevoerd door WUR Glastuinbouw en TNO Solliance met bijdrage van Asahi Glass Company.

Disclaimer

Address

Wageningen University & Research, BU Greenhouse Horticulture
Violierenweg 1, 2665 MV Bleiswijk
P.O. Box 20, 2665 ZG Bleiswijk
The Netherlands
+31 (0) 317 - 48 56 06
glastuinbouw@wur.nl
www.wur.eu/greenhousehorticulture

Table of contents

Samenvatting

Vanuit een energiebesparend perspectief moet de kasomhulling een zo hoog mogelijke lichtdoorlatendheid hebben om maximaal gebruik te maken van gratis zonne-energie, terwijl ze goede isolerende eigenschappen moet hebben om warmteverlies vanuit kas te voorkomen. Antireflectie coatings (AR) verhogen de lichttransmissie, emissiearme coatings (low-e) verminderen het warmteverlies. De gangbare low-e coatings verlagen echter de licht transmissie en hebben een beschermende atmosfeer nodig om degradatie te voorkomen waardoor low-e coatings standaard alleen in dubbel glas worden toegepast. Het doel van dit project was om low-e en antireflectie eigenschappen te verenigen in een enkele coating waardoor het verhogen van de lichttransmissie en verminderen van het warmteverlies wordt gecombineerd. Dit levert een duidelijke energiebesparing op.

De **energiebesparing** van een nieuw lage emissie glas met AR coating is berekend met de computermodellen KasPro en Intkam Hierbij is gekozen voor een onbelichte teelt van tomaten in een standaard Venlo type kas in het Nederlandse klimaat. Als referentie situatie is naar de huidige beste stand van de techniek gekeken, een dubbelzijdig AR gecoat enkel glas met een hemisferische PAR transmissie van 90% en een emissiefactor van 86% wordt hierbij als high performance kasdekmateriaal verondersteld. Dit werd vergeleken met glazen met een medium en lage emissiefactor.

- Uit de modelberekeningen is duidelijk geworden dat het energieverbruik met 22% gereduceerd kan worden, ook in combinatie met andere energiebesparende maatregelen zoals 1 of 2 energiebesparende schermen is het verlagen van de emissiefactor van het kasdek effectief waarbij additioneel respectievelijk 19% en 17% energie bespaart kan worden.
- Ook laten de modelberekeningen zien dat zelfs bij een gelijke PAR transmissie rekening gehouden moet worden met een paar 1~3% opbrengst verlies als gevolg van het verlagen van de thermische emissiefactor, dit is een gevolg van een iets lagere CO_2 concentratie in de zomermaanden doordat er iets eerder geventileerd moet worden.
- Indien het nieuwe lage emissie glas met AR coating zou worden vergeleken met traditioneel tuinbouwglas, wat tot nu toe nog het merendeel op Nederlandse tuinbouwkassen is, zou de energiebesparing naar verhouding overigens hoger zijn en het een lichtwinst en daarmee verhoogde opbrengst opleveren. Dit geldt ook voor de hieronder beschreven prototypes.

In dit project is een **prototype glas op experimentele schaal** (met physical vapour deposition) gerealiseerd waarmee een hemisferische PAR transmissie van 88.6% en een emissiefactor van 31% is gerealiseerd. Voor deze teelt kan met een kasdek met deze eigenschappen het energieverbruik worden gereduceerd met 17%, echter zal de productie ook 1.8% lager uitvallen in vergelijking met high performance glas, 1.1% hiervan kan worden verklaard door T_{Hem} van 88.6% ten opzichte van 90% voor de referentie en 0.7% van deze reductie laat zich verklaren door een lagere CO_2 concentratie in de zomer.
Parralel aan de ontwikkeling op experimentele schaal heeft Asahi Glass Company een **prototype glass op industriële schaal** gerealiseerd (met spray pyrolyse) waarmee een hemisferische PAR transmissie van 86% en een emissiegraad van 16% wordt bereikt. Voor de modelteelt betekent dit een gereduceerd energie verbruik van 22% en een productie vermindering van 4.4% waarvan 3.2% wordt verklaard door het verschil in hemisferische PAR transmissie en 1.2% door een lagere CO_2 concentratie in de zomer maanden.

De ontwikkelde prototypes laten zien dat low-e eigenschappen verenigt kunnen worden met een AR coating en dit maar beperkt invloed hoeft te hebben op de PAR transmissie. Gekeken naar de **economische balans** van de teelt is er met de eigenschappen van de huidige prototypes een netto meerwaarde en dus investeringsruimte voor het toepassen van low-e AR gecombineerde coatings, zelfs voor de huidige prototypes vergeleken met het beste nu beschikbare high performance referentie glas. Low-e AR gecombineerde coatings bieden hiermee **een interessant perspectief voor telers** die op zoek zijn naar een business case waarin energieverbruik op een economische manier kan worden gereduceerd.

Om de gerealiseerde eigenschappen beter in context te plaatsen en een idee te krijgen of er **toekomstige potentie is voor low-e AR gecombineerde coatings** met betere eigenschappen dan de huidige prototypes zijn via verdere modelberekeningen en experimenten een aantal referentiepunten bepaald.

- Om lage emissie te combineren met anti reflectieve eigenschappen is een coating opbouw met minimaal 2 dunne lagen nodig. Om inzicht in de potentie te krijgen zijn hypothetische AR coatings met 1, 2 en 3 lagen doorgerekend waarbij 0% absorptie is aangenomen. Coatings met 1 dunne laag kunnen theoretisch een hemisferische transmissie van 94% bereiken met een coating met een brekingsindex van 1.18, hiervoor is een porositeit van 63% nodig voor een silica AR coating. In de praktijk wordt maximaal 91% behaald met enkel laags coatings (n=1.34 en porositeit 29%). Dit verschil komt waarschijnlijk doordat de hoge porositeit die voor een lagere brekingsindex nodig is leidt tot een te fragiele coating.
- Met coatings van 2 en 3 lagen kan respectievelijk iets meer en iets minder dan 92% hemisferische transmissie worden bereikt. Hierbij is een brekingsindex van 1.34 als praktische ondergrens aangehouden voor de buitenste laag. Ook is de hemisferische PAR transmissie van coatings met 2 en 3 lagen veel minder gevoelig voor de brekingsindex van de buitenste laag, als hiervoor niet-poreus kwarts (n=1.48) wordt gebruikt kan voor een 3 lagen systeem iets meer dan 91% en voor een 2 lagen systeem 90.5% hemisferische PAR transmissie worden bereikt. Door de afwezige porositeit zal dit waarschijnlijk in een zeer duurzame coating resulteren. De in theorie superieure performance qua hemisferische PAR transmissie van enkel laags AR coatings vormt dus waarschijnlijk geen belemmering voor het gebruik van 2 of 3 laags AR coatings.
- Voor de laag die een lage emissiegraad moet realiseren zijn transparante geleidende oxides (TCOs) onderzocht en is daarbij gestreefd naar:
  1. Een zo laag mogelijke absorptie in het PAR gebied.
  2. Een significante reductie van de emissiegraad
  3. Het kunnen doorstaan van het verdere productieproces voor veiligheidsglas

  De eigenschappen van TCOs hangen sterk af van de specifieke materiaalkeuze en proces condities. Als referentiepunt is via een hoog kwalitatief (maar traag en kleine schaal) depositie proces een praktische ondergrens vastgesteld voor de potentieel haalbare laagste PAR absorptie. Dit was 1.6% voor Indium Tin Oxide (ITO) en 1% voor Indium Zink Oxide (IZO) (genormaliseerd naar een 130nm laagdikte).
- Initieel is exploratief gezocht naar een TCO en depositie proces dat resulteert in een lage PAR absorptie. Echter is het voornaamste wat we hiervan hebben geleerd dat de verschillen in eigenschappen die hieruit voort komen grotendeels verdwijnen bij een thermische nabehandeling welke gebruikelijk is bij het temperen van glas. Verwonderlijk genoeg komt de PAR absorptie voor ITO hierdoor zelfs lager te liggen dan het referentiepunt met 0.6% voor 130nm ITO.
- Verder is duidelijk geworden dat het temperen van IZO ervoor kan zorgen dat de low-e eigenschappen verdwijnen. Voor ITO is een milde reductie in de low-e eigenschappen waargenomen na het temperen. Het voor PAR transmissie geoptimaliseerde prototype heeft een emissiegraad van 31% ten opzichte van 86% voor normaal glas en 16% voor het industriële prototype. Waar de laagdikte van de TCO voor een PAR transmissie geoptimaliseerde AR coating rond de 130nm ligt is er voor een lagere emissiegraad een dikkere laag nodig voor de TCOs die in dit project zijn onderzocht. Hierin zit ruimte voor verbetering omdat TCOs met een hogere elektron mobiliteit al bij dunnere lagen een optimale lage emissiegraad laten zien.

Wij mogen in de toekomst verwachten dat de ontwikkeling van glazen met low-e en AR coatings perspectief bieden voor de teler om nog meer energie te kunnen besparen. Verdere productverbetering door commerciële partijen is in de komende periode zeker mogelijk.

Summary

From an energy-saving perspective, the greenhouse cover must have the highest possible light transmission to make maximum use of free solar energy, while it must have good insulating properties to prevent heat loss from the greenhouse. Anti-reflection coatings (AR) increase light transmission, low-emission coatings (low-e) reduce heat loss. However, common low-e coatings reduce light transmission and require a protective atmosphere to prevent degradation, which is why low-e coatings are normally only used in double glazing. The aim of this project was to combine low-e and anti-reflective properties in a single coating, thus combining increasing light transmission and reducing heat loss. This leads to a significant energy saving.

The **energy saving** of the new low-e glass with AR coating is calculated with the computer models KasPro and Intkam, the effects of variation in thermal emission have been explored. A cultivation of tomatoes without artificial lighting was chosen in a standard Venlo type greenhouse in the Dutch climate. As a reference situation, the current state of the art has been considered, a double-sided AR coated single glass with a hemispheric PAR transmittance of 90% and an emissivity of 86% is considered representative for a high-performance greenhouse covering material. This has been compared with glasses with low-e and medium-e coatings.

- It has become clear from the model calculations that energy consumption can be reduced by 22%. Also, in combination with other energy-saving measures such as 1 or 2 energy-saving screens, lowering the thermal emittance of the greenhouse roof is effective, respectively 19% and 17% of additional energy saving can be realised through lowering the emissivity of the cover.
- The model calculations also show that even with an equal PAR transmission, a few 1 ~ 3% yield loss can be expected as a result of lowering the thermal emittance of the cover, this is a result of a slightly lower CO_2 concentration in the summer months because of an increased need to ventilate to control the temperature in the greenhouse.
- If the new low-e glass with AR coating were to be compared with traditional horticultural glass, which until now is mainly used in Dutch horticultural greenhouses, the energy saving would be relatively higher and it would generate light gain and thus a higher yield. This also applies to the prototypes described below.

In this project, **a prototype glass on an experimental scale** (with physical vapor deposition) has been made which realized a hemispherical PAR transmission of 88.6% and an emissivity of 31%. For this crop cycle, with a greenhouse cover with these properties, energy consumption can be reduced by 17%, but production will also be 1.8% lower, 1.1% of this can be explained by T_{Hem} of 88.6 % compared to 90% for the reference and 0.7% of this reduction is caused by a lower CO_2 concentration.
Parallel to the development on an experimental scale, Asahi Glass Company has realized **a prototype glass on an industrial scale** (with spray pyrolysis) with a hemispherical PAR transmission of 86% and an emissivity of 19%. For our reference cultivation this means a reduced energy consumption of 22% and a production reduction of 4.4%, 3.2% of this can be explained by the lower hemispherical PAR Transmission compared to 90% for the reference and 1.2% of this reduction is caused by a lower CO_2 concentration.

The developed prototypes show that low-e properties can be combined with an AR coating and that this can be done with a very limited influence on the PAR transmission. Looking at the **economic balance** of the cultivation, with the properties of the current prototypes, there is a net added value and therefore room for investment for applying low-e AR combined coatings, even for the current prototypes. Low-e AR combined coatings thus **offer an interesting perspective for growers** who are looking for a business case in which energy consumption can be reduced economically.

In order to provide context for the realized properties and to get an idea of the **future perspective** and potential room for improvement for low-e AR combined coatings, a number of reference points were determined through further model calculations and experiments.

- To combine low emission with anti-reflective properties, a coating structure with at least 2 thin layers is required. To gain insight into the potential of 2- and 3-layer AR stacks, hypothetical AR coatings with 1, 2 and 3 layers were calculated, assuming 0% absorption. Coatings with 1 thin layer can theoretically achieve a hemispherical PAR transmission of 94% with a coating with a refractive index of 1.18, this requires a porosity of 63% for a silica-based AR coating. In practice, a maximum of 91% is achieved with single-layer coatings (n = 1.34 and porosity 29%). This difference is probably because the high porosity required for a lower refractive index leads to a coating that is too fragile.
- With 2- and 3-layer coatings, slightly more and slightly less than 92% hemispheric transmission can be achieved, respectively. A refractive index of 1.34 has been used as a practical lower limit for the outermost layer. Also, the hemispherical PAR transmission of 2- and 3-layer coatings is much less sensitive to the refractive index of the outer layer, if non-porous quartz (n = 1.48) is used for this, it can be slightly more than 91% for a 3-layer system and for a 2 layer system 90.5% hemispheric PAR transmission can be achieved. Due to the absence of porosity, this could potentially result in a very durable coating. The theoretically superior performance in terms of hemispherical PAR transmission of single layer AR coatings is therefore unlikely to be an obstacle to the use of 2- or 3-layer AR coatings.
- Transparent conductive oxides (TCOs) have been investigated for the layer that should contribute low-e properties to the AR stack, we aimed for:
  1. The lowest possible absorption in the PAR region.
  2. A significant reduction of the emissivity
  3. Being able to withstand the further production process for safety glass

  The properties of TCOs are known to strongly depend on the specific choice of materials and process conditions. As a reference point, a practical lower limit for the potentially attainable lowest PAR absorption has been established via a high-quality (but slow and small-scale) deposition process. This was 1.6% for Indium Tin Oxide (ITO) and 1% for Indium Zinc Oxide (IZO) (normalized to a 130nm layer thickness).
- Initially, a TCO and deposition process was investigated that resulted in a low PAR absorption. However, the main thing we have learned from this is that the differences in properties that arise from variation in deposition conditions largely disappear with a thermal after-treatment that is common in tempering glass. Surprisingly, the PAR absorption for ITO becomes even lower than the reference point with 0.6% for 130nm ITO regardless of the deposition recipe.
- Furthermore, it has become clear that tempering IZO can cause the low-e properties to disappear. For ITO a mild reduction in the low-e properties has been observed after tempering. The prototype optimized for PAR transmission has an emission level of 31% compared to 86% for normal glass and 16% for the industrial prototype. Where the layer thickness of the TCO for a PAR transmission optimized AR coating is around 130nm, a thicker layer is needed for the TCOs investigated in this project for a lower emissivity. There is room for improvement here because TCOs with a higher electron mobility show an optimal low emissivity at thinner layers.

In the future, we can expect that the development of glasses with low-e and AR coatings will offer the grower a perspective to save even more energy. Further product development by commercial parties is required and possible in the coming period.

1 Introduction

The ideal greenhouse cover has as much light Transmission as possible, while having good insulating properties to prevent heat loss. Although, the transition from double glazing to triple glazing is currently happening in the building sector, single pane glass is still used almost exclusively in glasshouse horticulture, because the requirements for light transmission far outweigh those of insulation. However, recent concerns of gas supply are changing the requirements of the future. Increased energy efficiency through insulation might become essential.

The VenlowEnergyKas demo project has shown that 50% energy savings can be achieved with a double-glazed greenhouse cover. This was achieved by applying a *layer with low infrared emission* (*low-e*) on one surface inside, which reduces the light transmission but is essential for good insulation. By applying anti-reflection (AR) coatings on the other 3 surfaces and using high light transmission glass composition, almost the same light transmission was achieved as "standard horticultural glass". This was made possible because AR coatings became available on a large scale and at competitive prices around that time.

Due to this development, the "standard" horticultural glass changed, the reference situation nowadays is becoming a single glass greenhouse cover with double AR coating. As a result, the sector opts for the extra light instead of the possible energy savings.

1.1 Goal

By **combining AR with low-e properties in the same coating** light transmission can be increased, insulating glazing becomes much more transparent and highly insulating **double glazing** could become a true asset in a growers' business case.
As the sector is getting used to the benefits of coated glass, a **single glazing** provided with an antireflective low-e coating could serve as an attractive alternative to the ultimate insulation of double glazing as this would be a relatively small step in terms of additional costs but could still provide significant energy savings, without extra weight.
In order for the sector to actually switch to greenhouse covers with high reduction of energy losses, the energy-saving low-e property must be combined with the benefits of an AR coating to ensure high crop production. Next to that such new materials must be economically feasible.

1.2 Technical objectives

The aim of the project is to develop coatings for single pane glass that combine low-e with AR properties whereby the energy saving properties are not at the expense of light transmission or at least will be so minimal that the cost savings of the better insulation outweigh any decrease in production.
The potential benefit for greenhouse applications of combining low-e with AR coating in single glazing and double glazing units will be evaluated via computer modelling and measurements on simple stacked combinations of samples. Samples will be measured following NEN2675 (Greenhouses – determination of optical properties of greenhouse covering and screen materials), they will be modeled via NEN 673 (Glass for buildings – determination of the u-value) and via KASPRO (Dynamic greenhouse climate and energy model).

1.3 Energy objectives

Previous research in the VenLowEnergy greenhouse has shown that with a double glazed greenhouse cover with additional screens, more than 50% energy can be saved in vegetable cultivation. The energy benefit of low-e coatings is caused by reflecting thermal infrared radiation (i.e. 'heat radiation') and therefore keep heat (thermal energy) inside the greenhouse. At the same time these coatings might show some small losses in the entrance of near infrared and visible light (solar energy). By tuning the low-e coatings for specific greenhouse requirements, it is possible to obtain a better light and solar energy input to the VenLowEnergy greenhouse. By incorporating the low-e properties in anti-reflective coatings, the extra light transmission will contribute positively to the energy balance of the greenhouse and light available for crop growth and development.
Moreover, by demonstrating low-e AR integration of functionalities on a single pane, energy saving could be realized at relatively low additional greenhouse investments and introduce an intermediate step for the sector to adopt highly insulating covers. It is expected that these options could swing the balance between production and energy saving towards energy saving as an asset to the grower.

1.4 Other objectives

By demonstrating low-e AR coating integration of functionalities on a single pane, energy saving could be realized at relatively low additional greenhouse investments and introduce an intermediate step for the sector to adopt highly insulating double covers in the future. It is expected that these options could swing the balance between production and energy saving towards energy saving as an asset to the grower.
Together with experts from the PV industry (TNO Solliance) and the glass industry (Asahi Glass Company, AGC), the most significant influences in terms of choice of materials and processing on costs and performance is identified. This project does not yet include a full-scale testing, which might be a future step in a follow-up project in order to demonstrate the technology in a horticultural test site.

2 Anti-reflective and low emissivity technologies

In this project we explore different combination of AR coatings (increase of light) and low-e coatings (energy saving) in order to come to better solutions in terms of light transmission and energy saving than now available in greenhouse industry.

Standard low-e coatings, which aim to reflect thermal infrared radiation, have suboptimal optical quality as they often contain a metallic or metal oxide layer, which also tend to have a higher reflection in the visible (and PAR) part of the spectrum. Interface reflection occurs at the glass/air interface, normally about 4% per interface. AR coatings make this interface optically less abrupt and lower the reflection. Unfortunately, a low-e interface has a higher reflection than normal glass/air interface. Luckily, the principle of AR coating can also be applied on top of a of a low-e coating to reduce the relatively high reflection in the visible. Note that the mechanism of infrared reflection is different and can be tuned compared to the visible reflection. Therefore, we can reduce the visible reflection of a low-e coating with antireflection, without compromising its energy saving quality. Obviously, the requirements for the AR coating on top of a low-e coating is different than for normal glass. Also, the low-e coating might need some co-development to give the best combination of optical and energy saving qualities. Therefore, the coating stack needs to be designed for this new situation. Moreover, for greenhouses, a specific demand of angle of incidence has to be taken into account.

2.1 Greenhouse requirements

Plant photosynthesis, the basis of crop growth and development, requires the right amount of light, CO_2, temperature, water, nutrients to be optimally available at all times in order to be efficiently used by the crop. If any one of these resources or conditions is not optimal this becomes the limiting factor and slows down the entire process. In modern high tech greenhouses, the temperature, water, nutrients and to some degree CO_2 can be maintained at optimal levels via active control. The available light is either dependent on the natural sunlight and can be regulated by screens or it can be controlled using artificial lighting, the latter option is of course relatively expensive in terms of capital investment and energy costs compared to the freely available sunlight which makes it imperative to make optimal usage of this free resource.

Natural sunlight reaching earth's surface consists of electromagnetic radiation with wavelengths in the range from 300 nm to roughly 2500 nm. Only the part between 400 and 700 nm contributes to carbohydrate production via photosynthesis, in this range all photons contribute more or less equally (Hemming *et al.* 2004). The other part of the spectrum mainly contributes to energy input to the greenhouse. Most sunlight entering the greenhouse is transferred into thermal infrared radiation beyond 2500 nm is emitted again from the greenhouse. The goal of this project is to get as much as possible PAR light into the greenhouse and prevent the emission of thermal infrared radiation outside the greenhouse.

2.2 Anti-reflective coatings (AR)

As the Transmission of PAR under hemispherical incidence is beneficial for greenhouse operation the industry has up to the time of writing used insulating double glazing units only in limited applications (mainly pot plant operations) for solid economic reasons: increased investment. Instead, the industry is moving to single pane glazing with antireflective (AR) coatings to further the Transmission PAR, energy saving is a.o. realized by using moveable thermal screens.

An antireflective effect on a glass can be realized via different designs. All aim to reduce the reflection caused by the interface between air and glass where the refractive index changes from 1 for air to ~1.52 for conventional soda lime float glass. This interface is engineered to become two or more distinct interfaces, the reflections from these distinct interfaces can cancel out via destructive interference leading to an antireflective effect.

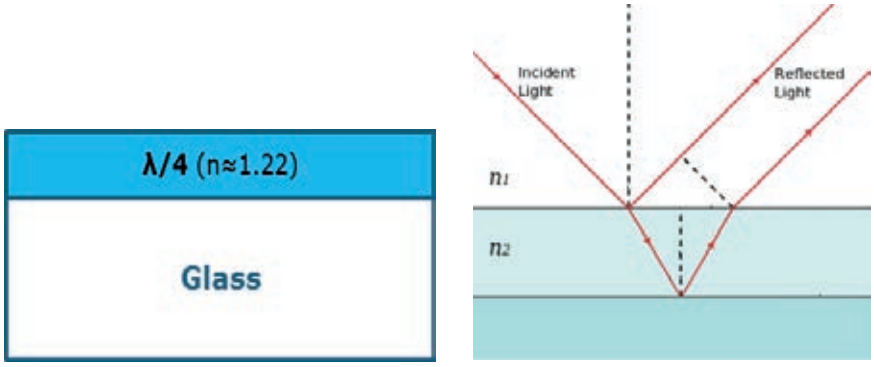

Figure 1 *Antireflective effects can be realized by adding thin layers effectively changing an interface into in this case 2 interfaces generating 2 distinct reflecting waves that can interfere destructively (source: from https:// en.wikipedia.org/wiki/Thin-film_interference).*

The simplest design consists of a layer with a refractive index in between air and glass to generate 2 reflections with roughly the same amplitude which interfere destructively for a layer thickness equal to a quarter wavelength of the light. The challenge for this design is the fact that there are no materials available with an optimum bulk refractive index required for an AR coating on glass which would be 1.18 to 1.22 depending on the angle of incidence for which the coating is designed. By utilizing multiple layers materials with other refractive indexes can be chosen.

2.2.1 Anti-reflection and the Fresnel equations

The interface reflection for all abrupt changes in refractive index can be calculated by the Fresnel equations which consists of 2 formulas for the s- and p-polarized interface reflection ($R_{s,intf}$ and $R_{p,intf}$ respectively):

$$R_{s,intf} = \left|\frac{n_1 \cdot \cos\theta_i - n_2 \cdot \cos\theta_t}{n_1 \cdot \cos\theta_i + n_2 \cdot \cos\theta_t}\right|^2$$

$$R_{p,intf} = \left|\frac{n_1 \cdot \cos\theta_t - n_2 \cdot \cos\theta_i}{n_1 \cdot \cos\theta_t + n_2 \cdot \cos\theta_i}\right|^2$$

θ_i is the angle of incidence, θ_t the angle of transmission, n_1 is the refractive index of the medium where the light is incident and n_2 is the refractive index of the medium in which the light is transmitted. For a single glass sheet there are 2 interfaces from air to glass and from glass to air (upper side and lower side of the glass).

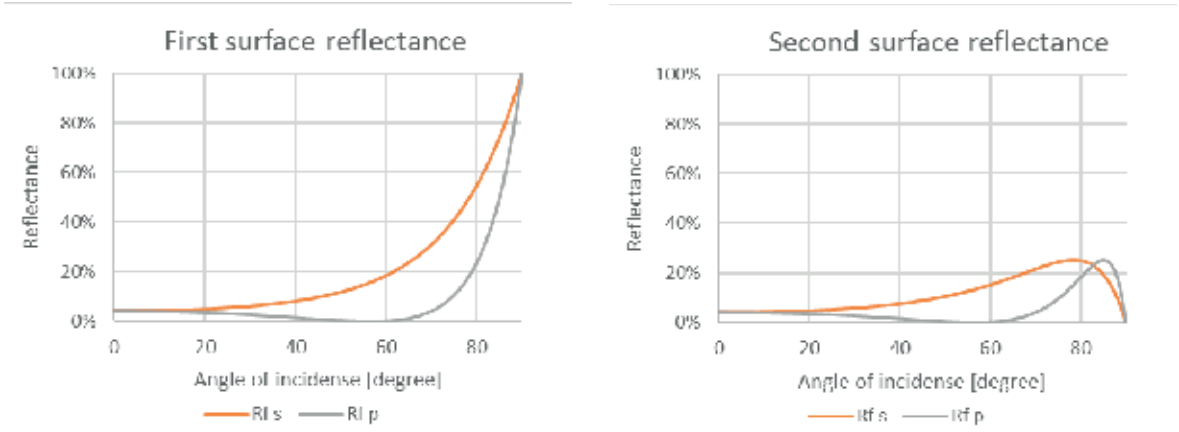

Figure 2 *Fresnel interface reflection on a glass plate, left the reflection of the initial interface (upper side of the glass), right the reflection from the second surface (lower side of the glass) which is less because the incident light was already reduced by the first interface reflection.*

Since a small fraction of light is being reflected on each interface a part of the incident light bounces back and forth multiple times before it becomes either Transmission or reflection this series of reflections results in the following expressions:

$$R_{s,p} = R_{s,p,intf} \cdot \left(1 + \frac{\left(1-R_{s,p,intf}\right)^2 \cdot \tau^2}{1-R_{s,p,intf}{}^2 \cdot \tau^2}\right)$$

$$T_{s,p} = \frac{\left(1-R_{s,p,intf}\right)^2 \cdot \tau}{1-R_{s,p,intf}{}^2 \cdot \tau^2}$$

Where $R_{s,p}$ is the resulting or p polarized reflection, $R_{s,p,intf}$ is the s or p polarized interface reflection from the fresnel equations and τ is the internal Transmission accounting for the absorption by the glass plate.

2.2.2 Thin layers and destructive interference

When two or more reflections are generated very close to each other interference can occur. For this to happen the optical path difference needs to be smaller than the coherence length of the incident light. The coherence length is dependent on the bandwidth of the light source or detector, for the PAR region this is roughly 930 nm. For reflections below this path length the amplitudes of the reflections are calculated using the version of the Fresnel equations below.

$$r_{s,intf} = \frac{n_1 \cdot \cos\theta_i - n_2 \cdot \cos\theta_t}{n_1 \cdot \cos\theta_i + n_2 \cdot \cos\theta_t}$$

$$r_{p,intf} = \frac{n_1 \cdot \cos\theta_t - n_2 \cdot \cos\theta_i}{n_1 \cdot \cos\theta_t + n_2 \cdot \cos\theta_i}$$

Where r is the reflection amplitude (in our earlier formula above the reflected energy R was calculated instead).

The optical path difference between the two reflections is calculated geometrically and is only dependent on the angle of Transmission θ_2, the thickness d2 and refractive index of the thin layer n2.

$$OPD = 2 \cdot n2 \cdot d2 \cdot \cos(\theta_2)$$

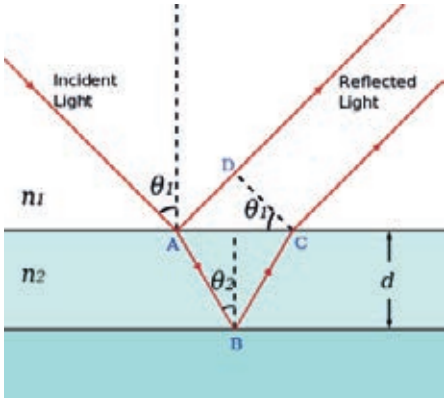

Figure 3 *Optical path difference between two reflections is determined geometrically by the difference between A -> D times n1 and A -> B -> C times n2 (source: from https://en.wikipedia.org/wiki/Thin-film_interference).*

The phase difference φ is the optical path difference divided by the wavelength λ time 2 pi for the phase difference in radians.

$$\varphi = \frac{OPD}{\lambda} \cdot 2\pi$$

When the phase difference is 180 degrees or pi radians two waves interfere completely destructively, since wavelengths between 400 and 700nm are all contributing to photosynthesis and this light is coming in from the complete hemisphere the optical path difference and subsequent phase difference varies greatly over this range.

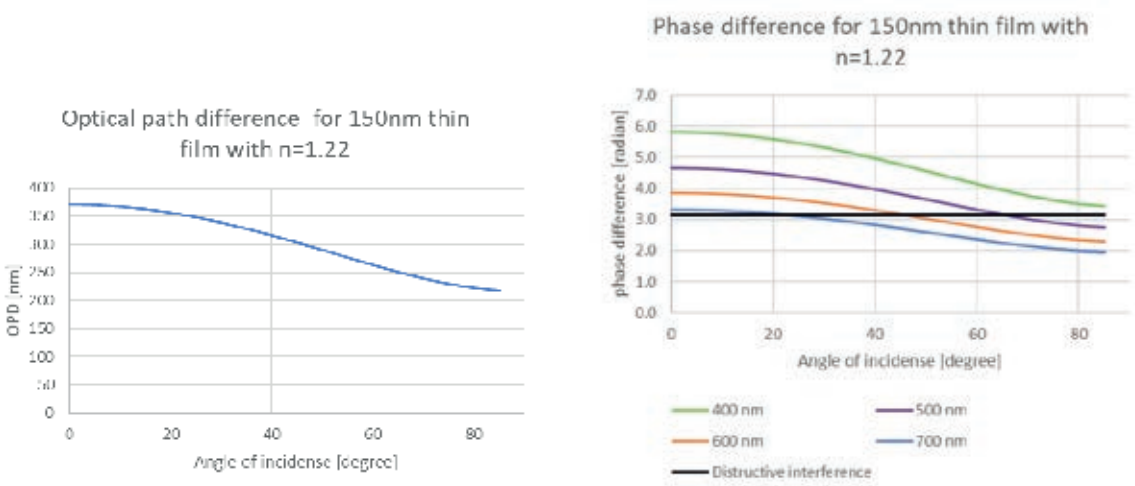

Figure 4 *Left the optical path difference for a 150 nm thin layer varying with the angle of incidence, on the right the resulting phase difference for the same thin layer for multiple wavelengths varying with angle of incidence.*

As can be seen in Figure 4 where the phase difference for normal incidence is causing almost completely destructive interference for 700nm incident light while being nearly constructive for 400nm light.

Destructive interference is most effective when the 2 interfering waves of the same polarisation have the same amplitude. As can ben seen in Figure 6 when we consider an AR coating for glas, n=1.52, at normal incidense the amplitudes match exactly at $n = \sqrt{1.52} = 1.22$ which is the refractive index most often encountered when

simple AR coatings are discussed. When considering hemispherical incident light other angles of incidense come into play and the amplitudes of the interfering waves cannot be matched for al angles of incidense at the same time. This broad range of angles of incidense that are important for Transmission under hemispherical incidense makes a perfect AR coating impossible.

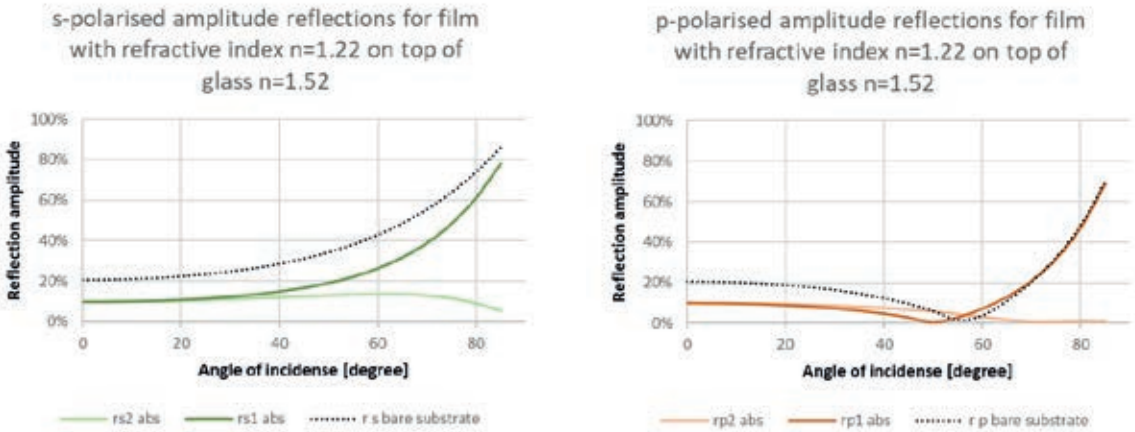

Figure 5 *Left 1st and 2nd amplitude reflection from thin layer with n=1.22 on glass with n=1.52, left the s- and right the p-polarised reflection.*

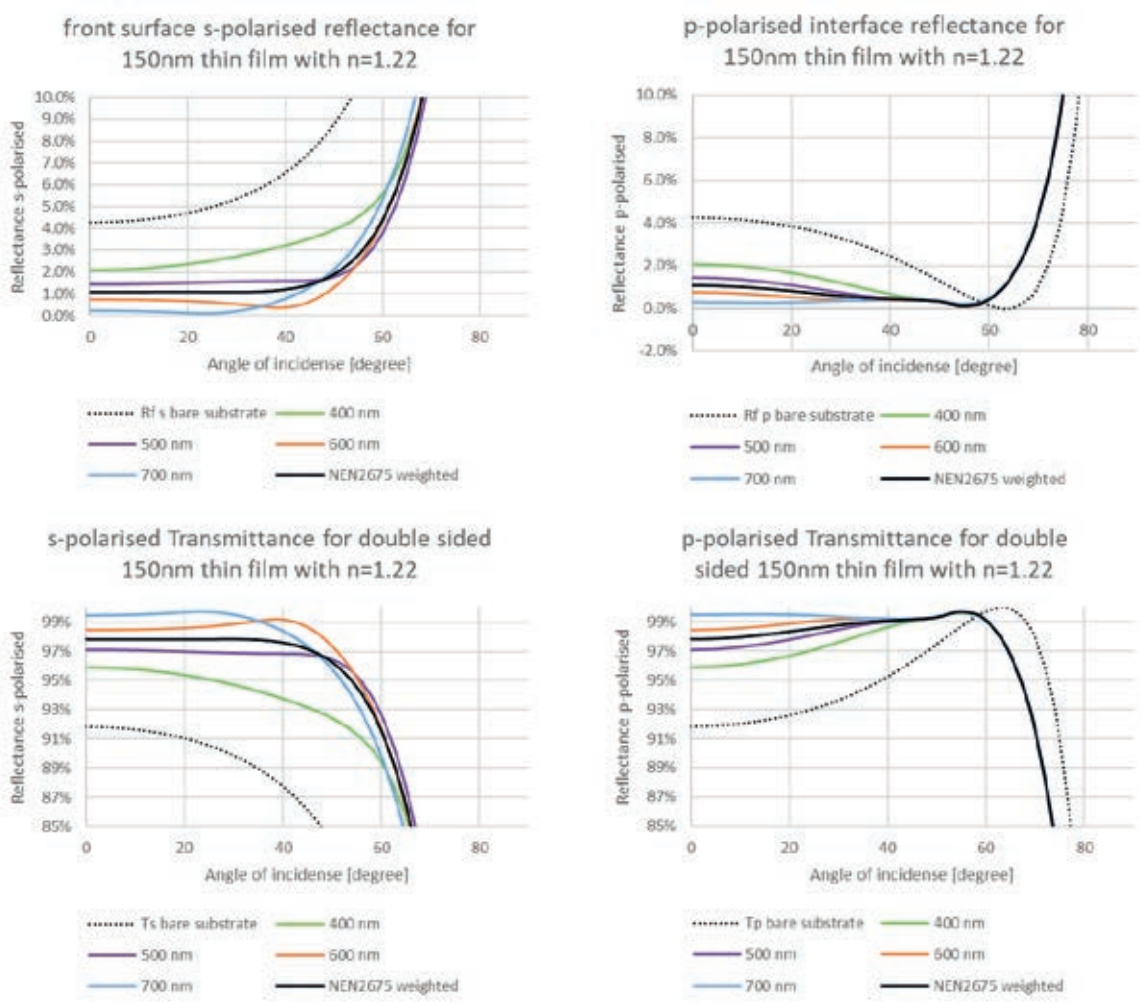

Figure 6 *At the top the interface reflection and bottom resulting Transmission for s and p polarised light depending on the angle of incidence for multiple wavelengths.*

Besides a full range of angles of incidence greenhouse application also requires effectiveness over a broad spectral range that encompasses the photosynthetically active radiation or PAR range from 400 to 700 nm. In Figure 7 is shown how the resulting reflection and Transmission for multiple wavelengths and angles of incidence is affected by one and the same coating.

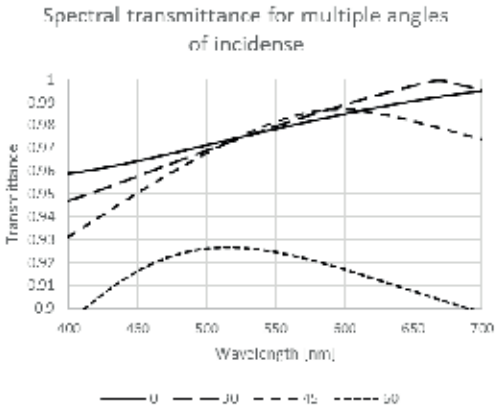

Figure 7 *Spectral distribution of Transmission at multiple angles of incidence for a 150nm coating with n=1.22 on glass.*

2.2.3 Parameter study on single layer AR stack design

Using the method described in the previous paragraph we can now take a look at how parameters like refractive index and layer thickness affect the hemispherical PAR Transmission. A 4 mm thick low iron glass was chosen as substrate and parameters of the bottom and top thin layers are given the same values, so the normal and hemispherical PAR Transmission shown in Figure 9 is the result of both AR coatings having this layer thickness and refractive index.

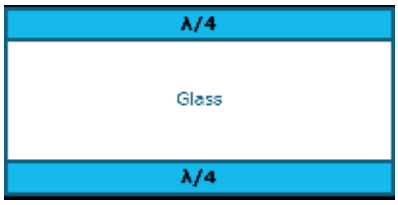

Figure 8 *Glass design with coatings on both sides used for parameter study.*

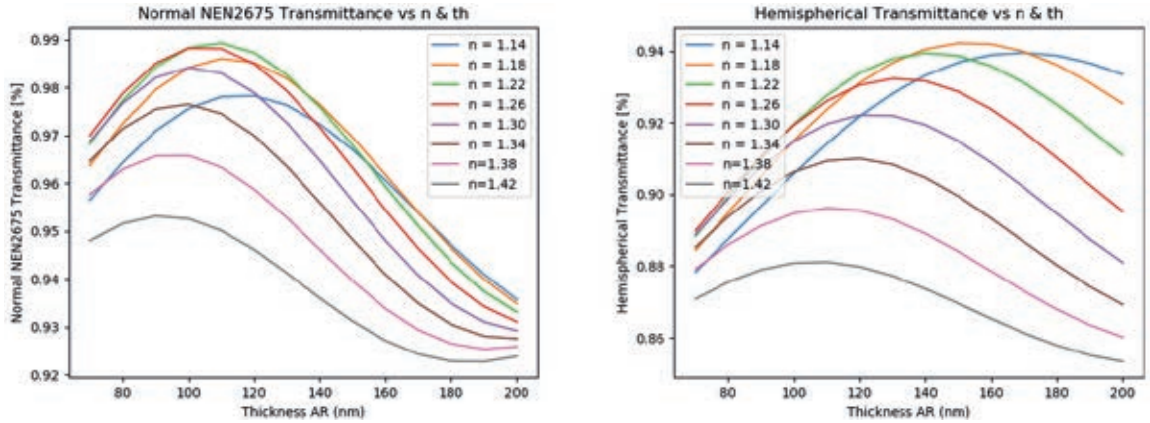

Figure 9 *NEN2675 PAR Transmission, left under normal incidence and right under hemispherical incidence.*

As expected for normal incidence the optimum refractive index is at $n = \sqrt{1.52} = 1.22$ and an optimal thickness of 110 nm which is 110·1.22=134 nm optical path length which is roughly ¼ of the central wavelength in the PAR range. For hemispherical incidence on the other hand a slightly lower refractive index of 1.18 and a thicker layer of 150 nm is the optimal AR coating for this design.

2.2.4 State of the art antireflective coatings applied in the greenhouse market

To reach a good anti-reflection effect, thus a suitably low refractive index layers on glass the industry has focused on creating nano porosity in thin layers to make antireflective coatings. These so called mesoporous silica layers are created either by etching, deposition of nanoparticles or templating silica layers with polymer nanoparticles which are evaporated out of the layer during heating in the tempering process to strengthen the glass. In each approach the refractive index of silicon oxide is lowered by creating an effective refractive index that is a mix of SiO_2 and air.

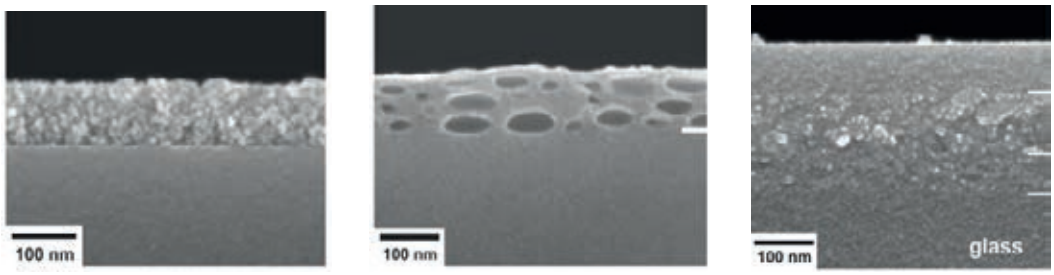

Figure 10 *Commercial antireflective coatings created by: a) deposited silica nanoparticles, b) latex templated silica, c) a dense multilayer design (source: Löbman, 2017).*

Via the effective medium approach, the refractive index can be tuned a wide range of desirable values but there are certain consequences related to lowering the refractive index via this approach. For one the scratch resistance diminishes with increasing porosity (Löbman, 2017; Thomas, 1992) and for latex templated mesoporous silica the refractive index shows poor stability due to hysteresis in the adsorption/desorption behavior of atmospheric moisture via capillary condensation. As shown in Guillemot, 2010a, b), in order to reach a refractive index below 1.29 via the latex templated mesoporous silica required a degree of porosity that causes the pores to become accessible to atmospheric moisture, as a consequence the authors concluded their approach to be suitable for antireflective applications only for the range 1.29 to 1.48 where their mesoporous silica thin layers were produced with closed porosity even though the refractive index could be tuned down to 1.15 in the regime where their layers showed open porosity.

Even though using these techniques a hemispherical PAR Transmission of 94% could easily be fabricated it is likely, due to the tradeoffs stated in the previous paragraph, that the state-of-the-art double sided antireflective coated single glazing that we see being applied for high tech greenhouse construction usually has a hemispherical PAR Transmission up to 91%.

For this reason, it is reasonable to choose 4mm low iron single glazing with 120nm thin layer with a refractive index of 1.34 as antireflective coating on both sides as the reference for the current state of the art for greenhouses glazing. This configuration has a NEN2675 weighted hemispherical PAR Transmission of 91.4% relative to 84.3% for the uncoated base glass.

2.2.5 Parameter study on double and triple layer hypothetical AR stacks

Next to single layer AR stacks (2.2.3) also double and triple layer AR stacks can be design. The principle is shown in Figure 11.

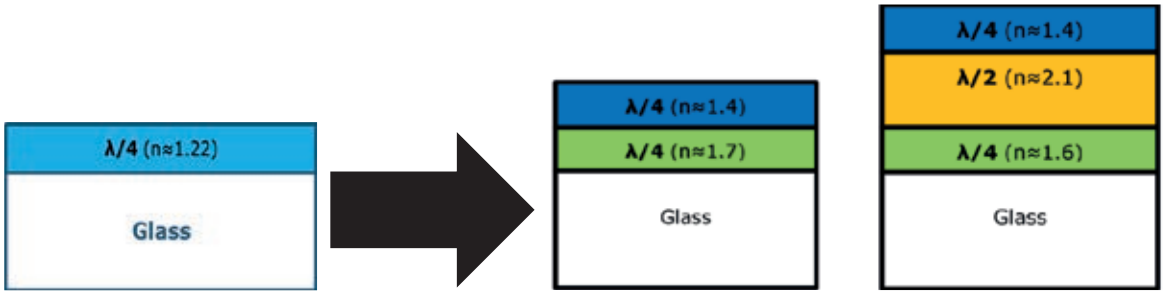

Figure 11 *Antireflective effects can be realized via multiple layer designs instead of one layer design.*

In order to get an idea of the potential optical performance that can be obtained while integrating high refractive index TCO layers in an AR stack a parameter study has been conducted for double quarter wave and triple layer AR stacks with quarter, halve, quarter wave configurations. To get insight in the hypothetical maximum performance the layers in the AR stack had their extinction coefficient set to zero. This would be reasonable for mesoporous silica or for instance for an alumina intermediate quarter wave layer but definitely not for a TCO layer. In this way the properties of a TCO can be compared relative to an ideal TCO for this application.

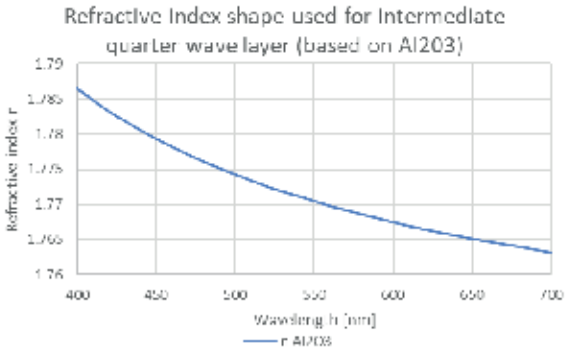

Figure 12 *Refractive index used for the intermediate quarter wave layer in this study.*

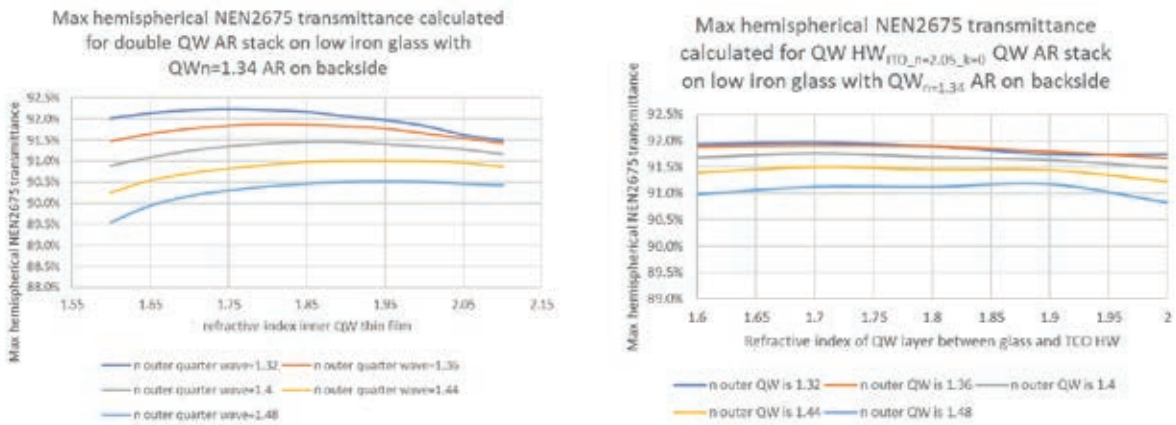

Figure 13 *Maximum hemispherical Transmission calculated as a result of different refractive index in different configurations to create an anti-reflection effect.*

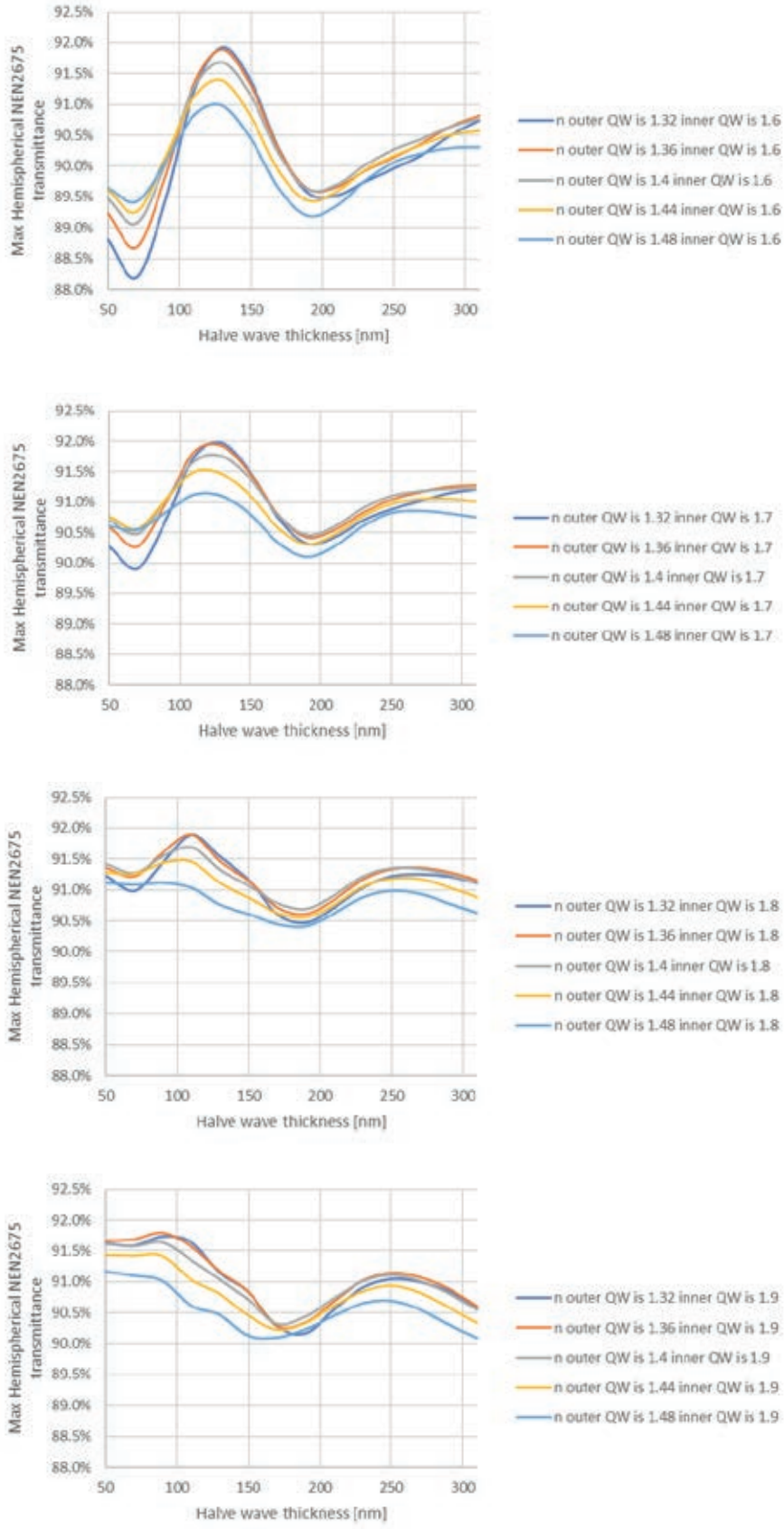

Figure 14 *Maximum hemispherical Transmission calculated depending on the halve wave thickness and different refractive index in different configurations to create an anti-reflection effect.*

The parameter study has been carried out for double and triple layers in order to obtain an anti-reflection effect as a result of varying refraction index. The goal of the variation in refractive index would be to obtain the highest possible anti-reflection effect, thus the highest possible hemispherical light Transmission. For the study the following parameter ranges are used. Layers show no absorption in this parameter study.

- Double layer AR parameter range.
  - n_{outer}=1.34 to $n_{denseSiO2}$.
  - n_{inner}=1.6 to 2.1.
- Triple layer AR parameter range.
  - n_{outer}=1.34 to $n_{denseSiO2}$.
  - n_{middle}=2 to 2.2.
  - n_{inner}=1.6 to 1.8.

Figure 13 and Figure 14 show the results of this parameter study on hemispherical light Transmission.

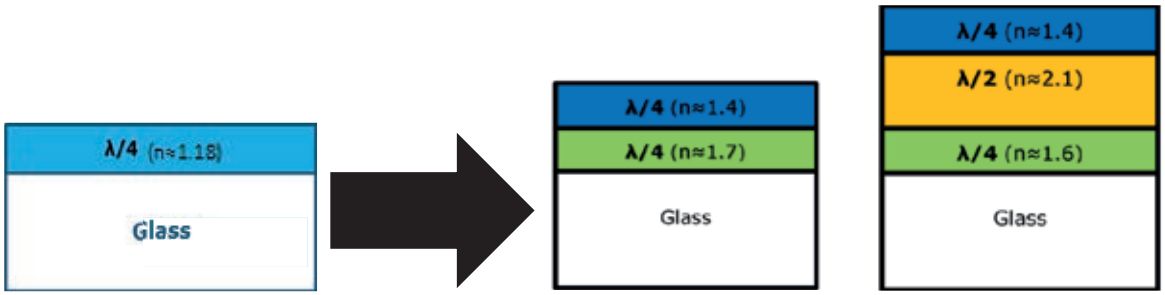

Figure 15 *Conclusion of the optimum refractive index in different configurations to create an optimum anti-reflection effect, thus maximum hemispherical Transmission.*

From the results shown above, we can conclude that in theory the most simple AR coatings with a single quarter wave layer with low refractive index show a higher performance than the double quarter wave AR stacks and these show a higher performance than the triple layer AR stacks, this is to be expected because of the wide range in the angles of incidence and wavelength that contribute to the hemispherical PAR Transmission.

In practice the comparison is more subtle since the low refractive index materials needed for the highest performance single layer AR stacks are limiting the durability.

- The industry currently seems to have settled on approximately a 120nm thin layer with n≈1.34 which reaches T_{hem}≈91% instead of the 150nm thin layer with n≈1.18 that can reach T_{hem}≈94%.
- Double and Triple layer AR stack with an outer thin layer with the same n≈1.34 refractive index have a slight advantage in that they can potentially reach T_{hem}≈92%
- For a more dense and potentially more durable outer thin layer of n≈1.4 double layer AR stacks clearly outperform single layer AR stack, respectively T_{hem}≈91.5% versus T_{hem}≈ % and a triple layer AR stack outperforms the double layer version slightly.
- For an even denser outer thin layer of 1.44 or 1.48 the advantage of the triple layer AR stack versus the double layer AR stack increases a bit more to 0.5%,

2.3 Thermal emissivity coatings (low-e)

Greenhouses exchange thermal energy with the outside world directly via ventilation (actively controlled and unintentional via leakage) or indirectly through its cover via conduction to the outside air (amplified by the convective activity of the air) or via radiative exchange.

When thermal radiation interacts with a material it can be transmitted, reflected and absorbed, the total of these must be unity due to conservation of energy. The absorption of a material must equal the emissivity to prevent two bodies at equal temperature to spontaneously decrease their entropy and violate the second law of thermodynamics, this is expressed by Kirchhoff's law:

$$\varepsilon + \tau + \rho = 1$$
$$\varepsilon_\lambda = \alpha_\lambda$$

Where ε is the emissivity, ε_λ the emissivity at a specific wavelength, α_λ the absorption at a specific wavelength, τ the Transmission and ρ the reflection.

A greenhouse sends out energy depending on the cover temperature and emissivity towards everything in its field of view and receives radiative energy depending on the temperature of the objects in its field of view. Most of the field of view consists of the sky which on clear nights can reach very low apparent temperatures because the atmosphere's radiative Transmission allows for direct radiative heat exchange with outer space. Radiative energy is exchanged via Stefan Boltzmann's law:

$$P = \varepsilon \cdot \sigma \cdot A \cdot T^4$$

Where P is the radiated power, A is the bodies surface area, T the bodies temperature in Kelvin, σ is the constant of Stefan-Boltzmann and ε the emissivity of the body.

Power is radiated in the form of electromagnetic waves and the spectral distribution depends on the temperature of the radiating object; this is described by Planck's law:

$$I(\lambda, T) = \frac{2hc^{2^{\cdot}}}{\lambda^5} \cdot \frac{1}{e^{\frac{hc}{k_B T \lambda}} - 1}$$

Where I is intensity in $W \cdot nm^{-1} \cdot k^{-1}$, h is Planck's constant, k_B is Boltzmann's constant, c is the speed of light in vacuum, T the bodies temperature in Kelvin and λ the wavelength.

Very hot objects like the sun at roughly 5780 Kelvin radiate in the visible part of the electromagnetic spectrum with its peak intensity at 500 nanometers. The lower the temperature of an object the further the peak intensity shifts into the infrared, at 25 degrees Celsius (293K) the peak radiative intensity is around 9 micrometers.

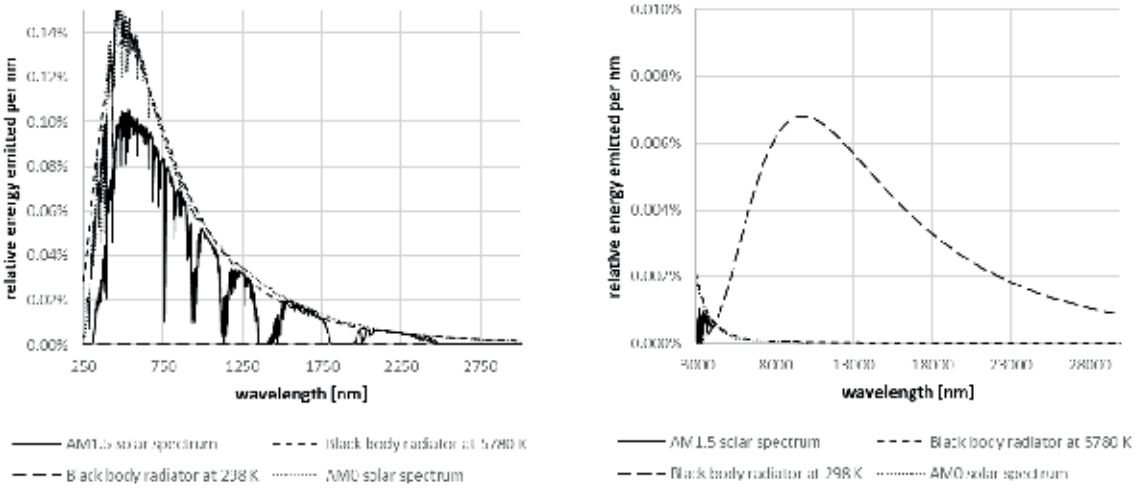

Figure 16 *Spectral intensity distribution for sunlight radiation (left) and thermal infrared radiation (right) for an object at room temperature of 298 Kelvin, note the changeover in scaling of the axes.*

As can be seen in Figure 16, an object like a greenhouse receives radiative energy from the sun in a completely different spectral range compared to the spectral range where it loses energy by emitting radiative energy.

2.3.1 Low emissivity and the Drude model

A low emissivity coating aims to switch from transmitting in the spectral range of sunlight to reflecting in the spectral range where objects at ambient temperature (~298K) are emitting. For the (AM1.5) solar spectrum only 5% of the energy is radiated in the range of 2000nm and upwards, while a black body at 25 degrees Celsius (298K) only 5% of the radiated energy is in the spectral range below 6300nm as shown in Figure 17. So, for a maximum heat gain from sunlight a low-e coating should switch from Transmission to reflection between 2000 and 6300 nm.

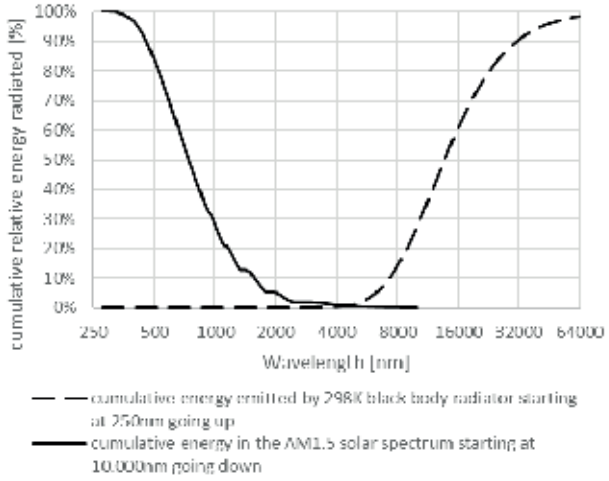

Figure 17 *Cumulative energy emitted over the electromagnetic spectrum, for the solar spectrum starting at 10000nm accumulating going to shorter wavelengths and for an ambient temperature object starting at 250nm accumulating going to longer wavelengths.*

The optical properties of materials are mainly determined by how its electron respond to the incident electromagnetic waves (due to the mass of the nucleus relative to the electrons means that ionic response to electromagnetic forces are only significant at extremely low frequencies). These dielectric properties are expressed in the complex function:

$$\varepsilon(E) = \varepsilon_1(E) + i \cdot \varepsilon_2(E)$$

Where ε is the dielectric proportionality constant between the applied electric field and the electric displacement field and depends on the frequency E of the electromagnetic field, in this case in electron volts.

$$N(E) = \sqrt{\varepsilon(E)}$$

The complex refractive index N is the square root of the dielectric function and consists of

$$N(E) = n(E) - i \cdot k(E)$$

Where n is the refractive index and k the extinction coefficient.

At thermal infrared frequencies these dielectric properties are determined by the electron's freedom to move over relatively long ranges within the materials. For instance bound electron that have formed covalent bonds have resonance frequencies in this range and show sharp spikes in the absorption spectrum. Free electrons in conductors do not have a resonance frequency in this range but are able to respond over a broad infrared range. The dielectric function for conductors can be described using Drude's model:

$$\left(-\frac{A_D}{E^2 + {\Gamma_D}^2}\right) + i \cdot \left(\frac{A_D \cdot \Gamma_D}{E^3 + {\Gamma_D}^2 \cdot E}\right)$$

Where E is the photon energy in eV and A_D and Γ_D are the amplitude and broadening parameters which are expressed by

$$A_D = \frac{e^2 N_{Opt}}{m^* \cdot \varepsilon_0}$$

$$\Gamma_D = \frac{e}{m^* \cdot \mu_{Opt}}$$

Where e is the electron charge, N_{Opt} the optical electron density, m_{Opt} the optical electron mobility and m^* the effective electron mass.

In essence the electron density determines the resonance frequency, above this frequency (at shorter wavelengths) the electrons cannot react fast enough and contribute very little to the dielectric function, at frequencies lower than this resonance frequency (longer wavelengths) the electrons respond fast enough to generate a strong electric displacement field giving rise to a high reflectivity.

In the figure below the effect of the electron density on reflectivity is shown from Simonis *et al.* (1979).

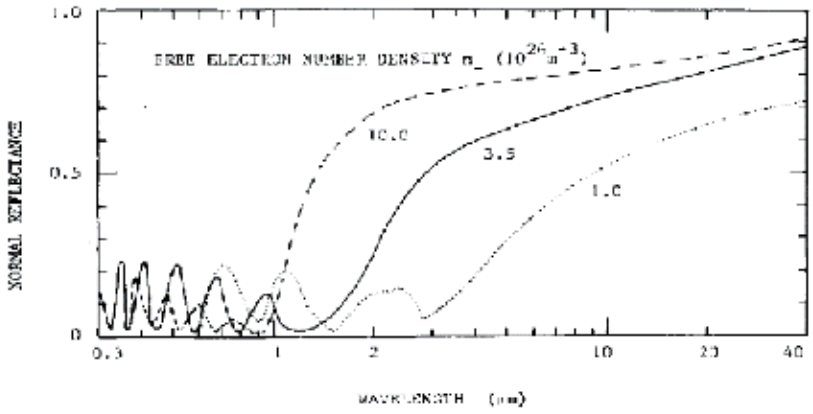

Fig. 4. Calculated normal reflectance for different n_--values. Layer thickness $d = 0.5\ \mu m$, $\mu_- = 1.5 \times 10^{-3}$ m^2/Vs and $m^* = 0.25 m_0$.

Figure 18 *The effect of free electron density on the reflection spectrum of a conductor showing that a higher electron density leads to reflectivity at shorter wavelengths, specifically: "calculated normal reflection for different electron densities. Layer thickness d=500nm, electron mobility m=15 cm^2/Vs and effective electron mass m*=0.25m^0." (Simonis et al. 1979).*

The electron mobility determines the damping of the frequency response and the lower the mobility the broader the changeover towards reflectivity becomes as shown below from the same reference as above.

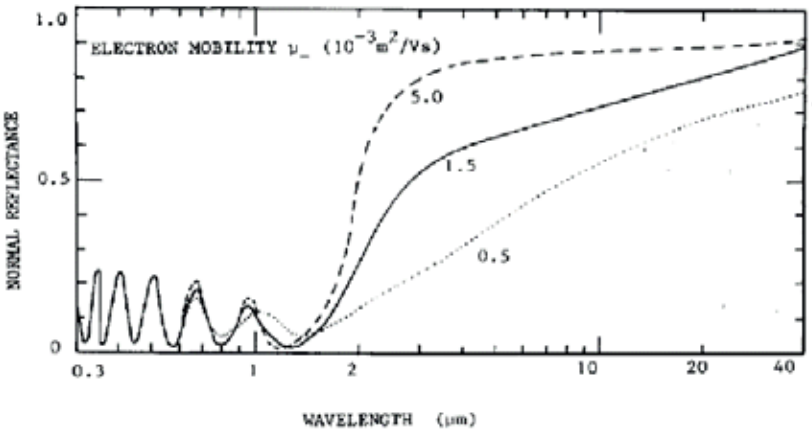

Fig. 5. Calculated normal reflectance for different μ_--values. Layer thickness $d = 0.5\ \mu m$, $n_- = 3.5 \times 10^{26}$ m^{-3} and $m^* = 0.25 m_0$.

Figure 19 *The electron mobility determines the damping of the frequency response, lower electron mobilities effectively broadening the changeover to reflectivity. Specifically: "calculated normal reflection for different electron mobilities. Layer thickness d=500nm, electron density NOpt=3.5·1020 cm^{-3} and effective electron mass m*=0.25m^0" (Simonis et al. 1979).*

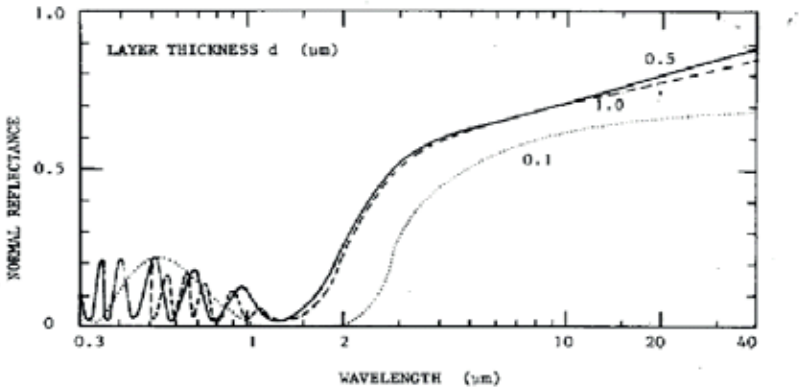

Fig. 6. Calculated normal reflectance for varying layer thicknesses. Effective mass $m^* = 0.25 m_0$, $n_- = 3.5 \times 10^{26}$ m^{-3} and $\mu_- = 1.5 \times 10^{-3}$ m^2/Vs.

Figure 20 *The effect of layer thickness on reflection showing that for this specific combination of electron mobility, density and effective mass the layer thickness has significant influence on the reflection up to a certain point above which it no longer has a significant impact. Specifically: "calculated normal reflection for varying layer thicknesses. Effective electron mass m*=0.25m^0, electron density NOpt=3.5·1020 cm^{-3} and electron mobility m=15 cm^2/Vs (Simonis et al. 1979).*

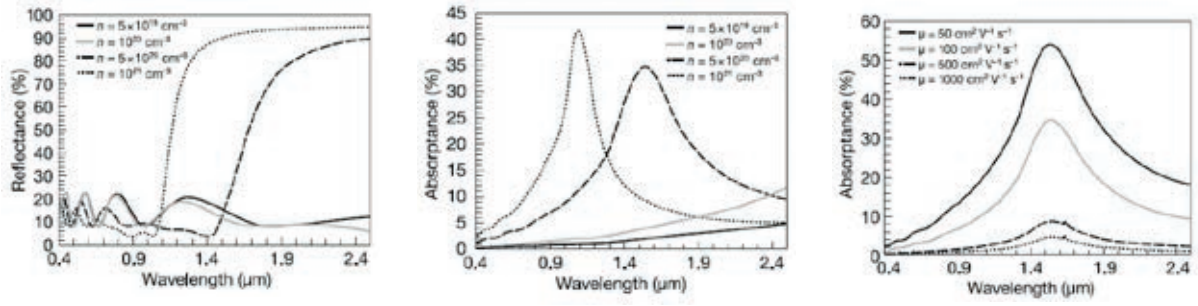

Figure 21 *On the left: reflection of 500nm thin layers with the same electron mobility of 100 cm^2 V-1 s-1 and varying electron densities. In the middle: the absorption of the same layers as in the left plot. On the right: is the absorption plotted for the layer with 5·1020 per cm^3 electron density for varying mobilities. (Timothy et al. 2000).*

For greenhouses, the film thickness of the TCO is limited because there is a clear optimum for the hemispherical transmission for a film thickness of 130nm. As a result, for the lowest possible emission or the density of free electrons will have to increase and / or the mobility. If the electron density is too high, the tail of the absorption peak that is around the plasma resonance frequency will be too much in the PAR region. A higher mobility can be freely pursued as this will only lead to a lower emission and to reduced absorption around the plasma resonance frequency. The good news is that higher mobility is also the most useful property for areas such as solar cells, because thinner layers lead to a lower use of Indium in ITO layers and less NIR absorption in the PV cell and to a higher NIR reflection net because it NIR on the rear non-transparent conductor reflects.

3 Energy saving by AR and low-e glasses

In this work package the energy saving potential of glasses with AR and low-e coatings is investigated with the help of models. The effect of AR and low-e glasses on greenhouse microclimate, the use of resources (energy) and the yield was simulated. For that different types of glasses have been used:
1.an existing glass prototype (89+ glass) which combines a FTO type low-e coating with an AR coating facing outwards and an AR coating facing the inside
2. a hypothetical glass (91+ glass) with a medium low emissivity and an AR coating on both sides
3. an existing glass (91+ glass) with standard AR coatings on both sides (reference)
All calculations are made with and without energy saving screens. This has been done for a typical Dutch greenhouse type and Dutch climate conditions. These numbers can be later used to perform an economic analysis and understand under which scenarios a newly developed glass combining low-e AR would become the most profitable option for the grower.

3.1 Kaspro: general model description

The study was carried out using a dynamic integral climate and crop growth model. KASPRO (de Zwart, 1996) has been used as the basic greenhouse climate model. KASPRO can dynamically simulate a full-scale virtual greenhouse based on the construction elements, greenhouse equipment, different covering materials and their main optical properties (transmission τ, reflection ρ and absorption a) and the set points to be maintained in the inside climate in relation to the outside climate of a given location. Outputs provided are several climate parameters, such as greenhouse air temperature, relative humidity, carbon dioxide (CO_2) concentration and resource consumption (e.g. water and energy). The model is based on the computation of relevant heat and mass balances (Bot, 1983). The heat balances describe both the convective and radiative processes. The mass balances are constituted from exchange processes of gases (air, water vapor, etc.) through leakage and ventilation (de Jong, 1990). They include canopy transpiration (Stanghellini, 1987) and condensation on cold surfaces. The mass balances around the CO_2 concentration are based on losses of CO_2 by ventilation and photosynthesis, and gains by artificial dosing and crop respiration. Greenhouse climate is controlled by simulation of commercially available climate controllers. The total set of differential equations is solved numerically. More details on the model can be found in de Zwart (1996) with several additional modules described in Luo, *et al.* (2005), Katsoulas *et al.* (2015) and Graamans *et al.* (2018).

3.1.1 Light transmission model

KASPRO allocates 50% of the solar radiation to photosynthetic active light (PAR). The UV fraction is neglected, so the other 50% is attributed to NIR (Monteith, 1973). In addition to the spectral division, solar radiation is also divided into direct and diffuse components. Direct radiation reaches the earth surface with a certain angle of incidence, given by the solar position which varies during the day and seasons. The algorithm (Bot, 1983) expresses the angle of incidence of solar radiation as a function of time, latitude and longitude. Diffuse radiation is omnidirectional although it has a distribution function for the intensity of radiation over the hemisphere and KASPRO uses the standard overcast sky approach (Bot, 1983). The incoming direct and diffuse radiation (I_{dir} and I_{diff}, respectively) can be absorbed (a), reflected (ρ) or transmitted (τ) by the greenhouse roof in different ways. For the simulation of a specific greenhouse cover, KASPRO requires the following input: τ_{PAR} (hemispherical PAR light transmission of the cover), τ_{sun} (solar radiation transmitted by the cover), τ_{TIR} (Thermal Infrared transmission of the cover), ε_{TIR} (emissivity of the cover) and C_p (specific heat coefficient of the cover material, J g^{-1} K^{-1}). KASPRO then calculates the transmission of a multi-span infinite greenhouse cover for direct radiation as a function of greenhouse geometry (roof slope, gutter distance, greenhouse orientation etc.) and solar position. A detailed description can be found in Vanthoor (2011).

3.1.2 Basic crop yield model

The estimation of the potential tomato dry matter production was carried out by coupling the microclimate (temperature, light, and CO_2 concentration) simulated by KASPRO with the tomato yield model of Vanthoor (2011) which is based on the photosynthesis model of (Goudriaan & Van Laar, 1994).

3.2 Performance analysis: detailed model input description

3.2.1 Climate data set

For the simulations we have used a yearly climate data set of De Bilt (The Netherlands) which corresponds to a reference (or typical) meteorological year (which we call SEL2000) with a methodology with was first developed by Breuer and van de Braak (1989).

3.2.2 Simulated glasses

An existing glass cover combining a low-e coating and a double AR coating and a hypothetical glass cover combining a medium emissivity with a double AR coating have been simulated and compared to a reference (existing) glass cover with a double AR coating. The most important optical properties of the simulated covers are summarized in Table 1. Finally, it is important to highlight that the low-e coating has been simulated on the external layer of the glass cover, because if the coating would be in the internal layer, the condensation would create a high emissivity layer eliminating the low-e effect.

Table 1
Summary of most relevant optical properties of the simulated glass covers.

	Hemispherical Transmission	Them* KasPro	NIR reflection (hemispherical)	Emissivity
Reference 2AR glass	90%	85.5%	Default (12%)	Default (86%)
Existing low-e 2AR glass	86%	81.7%	23%	16%
Hypothetical medium-e 2AR glass	90%	85.5%	Default (12%)	50%

*includes the effect of covering and the greenhouse roof.

3.2.3 Main input parameters

We have simulated a typical Dutch Venlo glasshouse, whose basic dimensions as included in the simulations can be observed in Table 2. A typical growing cycle for tomato in The Netherlands with
Transplant on 15th December and end of cycle 20th November of the following year was simulated. The heating power was large enough to cover all heating peaks (200 W/m^2) as well as the hot water buffer size (200 m^3) in any of the simulated scenarios, so that all simulations would be comparable (Table 3). For the simulations, we have considered three possibilities in relation to the use of screens for energy saving:

1. No energy saving screens.
2. One transparent shading screen used also during daytime hours with low radiation.
3. Two screens: a transparent and an aluminized one.

For the simulations with a semi-transparent energy saving screen, we have considered a Luxous 1347 fr (Ludvig Svensson, 2020a) screen (Table 4) and for the simulations with an aluminized screen we have considered a Tempa 8672 (Ludvig Svensson, 2020bhttps://www.ludvigsvensson.com/en/climate-screens/climate-screens-products/all-climate-screen-products/tempa-8672-d) screen.

Table 2

Summary of main geometrical parameters of the simulated glasshouse.

Area:	40,000	m²
Height gutter:	7	m
Roof slope:	22	deg
Span width:	4	m
Section length:	5	m
Leakage:	$7.50E^{-05}$	$m^3\,m^{-2}\,s^{-1}$ /m s^{-1}
Window length:	1.67	m
Window height:	1.5	m
fr_Window*:	5%	

*Ratio of open ventilation area to greenhouse area.

Table 3 shows the essential details of the simulated heated system.

Table 3

Heating system.

Heating system	
Primary heating network:	Low
Low pipes diameter:	51 cm
Number low heating pipes per span:	5
Top pipes diameter:	32 cm
Number of top heating pipes per span:	2.5
Boiler power:	200 W/m²
Hot water buffer volume:	200 m³/ha

Table 4 shows the essential details on the semi-transparent screen configuration and set points used for the simulations.

Table 4

Transparent screen setpoints.

Transparent screen		
Screen system:		
Screen type[1]:		
Max Tout screen[2]	Date	Setpoint for screen usage
	13-11	
	16-2	
	01-6	
	1-10	
Screen cloas below[3]	1st condition: external solar irradiance below:	2nd condition: outside temperature drops below:
	300 W/m^2	-10°C
	200 W/m^2	-5°C
	150 W/m^2	8°C
	75 W/m^2	10°C
	2 W/m^2	20°C

1 The name of the screen is written here. Kaspro then reads screen properties from a .txt file in which all screen properties have been written.

2 When external temperature is above this value, the screen is not used.

3 Screen is used whenever temperature is below the first value, only if external solar radiation is below the second value.

Table 5

Aluminized screen setpoints.

Alumunized screen		
Screen system:		Energy screen
Screen type[1]:	Date	Setpoint
Max Tout screen[2]:	13-11	14°C
"	16-2	12°C
"	01-6	10°C
"	1-10	12°C
Screen close below[3]:		5 W/m^2

1 The name of the screen is written here. Kaspro then reads screen properties from a .txt file in which all screen properties have been written.

2 When external temperature is above this value, the screen is not used

3 Screen is used whenever radiation is below this value

Table 6

Temperature setpoints for heating and ventilation, humidity and CO_2 setpoints.

Set points	Date Setpoint	
Heating temperature (°C):	15-12	19
Heating temperature (°C):	26-12	21 17 17.5
Heating temperature (°C):	16-1	23 23 16 19
Heating temperature (°C):	16-2	21 21 14 17
Heating temperature (°C):	20-4	20.5 20.5 14 16.5
Heating temperature (°C):	26-6	19.8 19.8 14 17.5
Heating temperature (°C):	10-9	20 14 17 17
Heating temperature (°C):	13-11	20
Dead zone(°C)[1]:	15-12	4
Dead zone(°C)[1]:	1-3	3
Dead zone(°C)[1]:	1-4	2
Relative humidity (%):		90
CO_2 (ppm):		700
CO_2 dosing rate (kg/ha h):		120

1 Ventilation temperature set point is heating set point plus this value

3.3 Results

3.3.1 Energy saving

In the figures below the energy used for heating are plotted over the course of the growing season for the described scenarios.

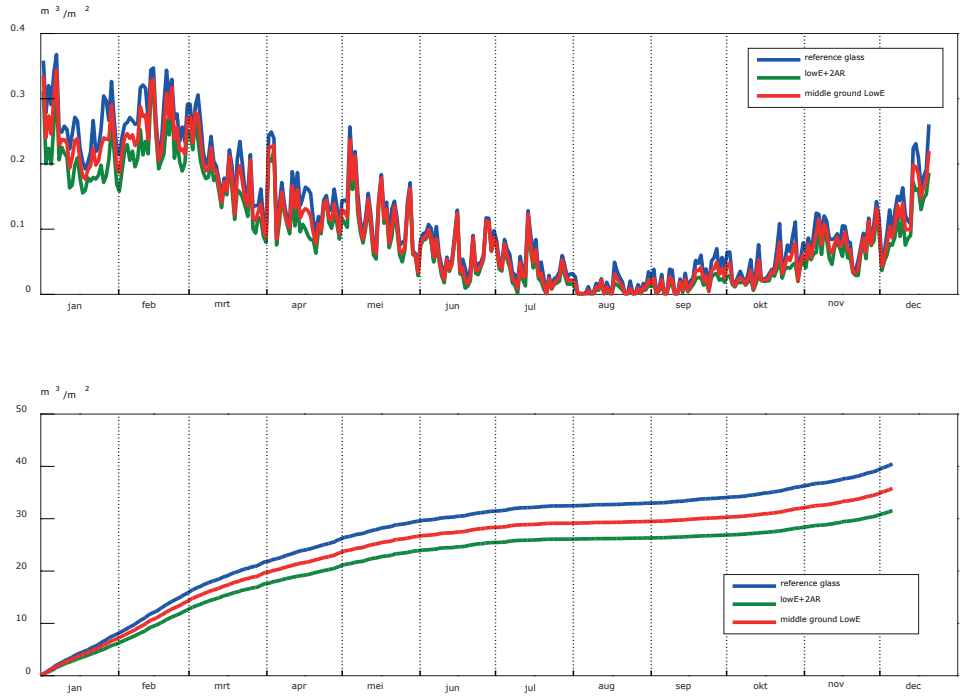

Figure 22 *Daily and cumulative natural gas use ([m^3gass /m^2greenhouse per day] and [m^3gass /m^2-greenhouse] respectively) for heating in the simulations when no energy saving screen was used.*

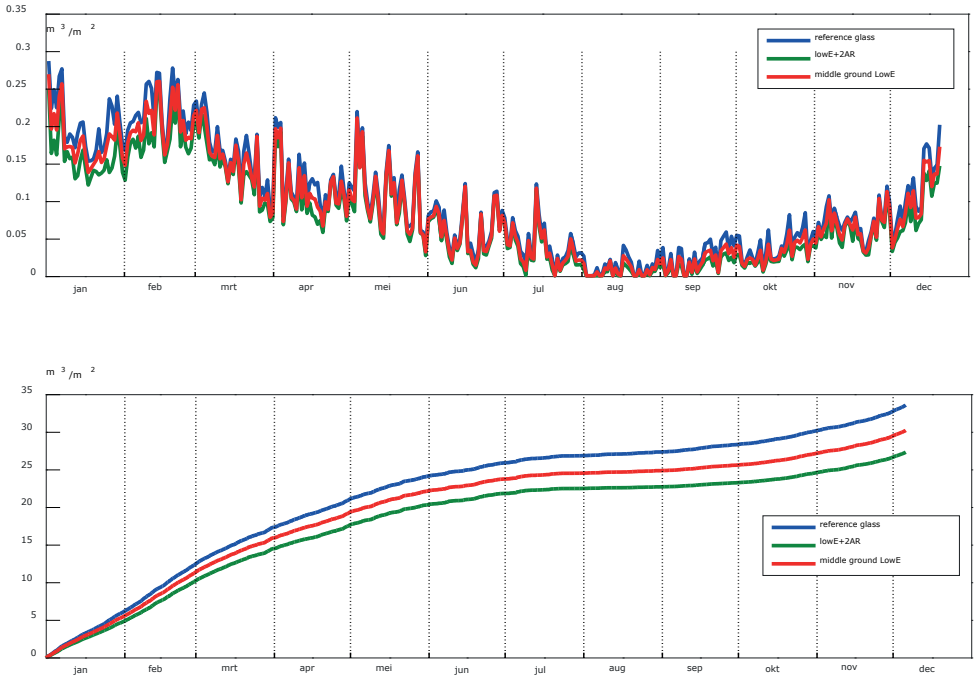

Figure 23 *Daily and cumulative natural gas use ([m³gass /m²greenhouse per day] and [m³gass /m²-greenhouse] respectively) for heating in the simulations when a semi-transparent energy saving screen was used.*

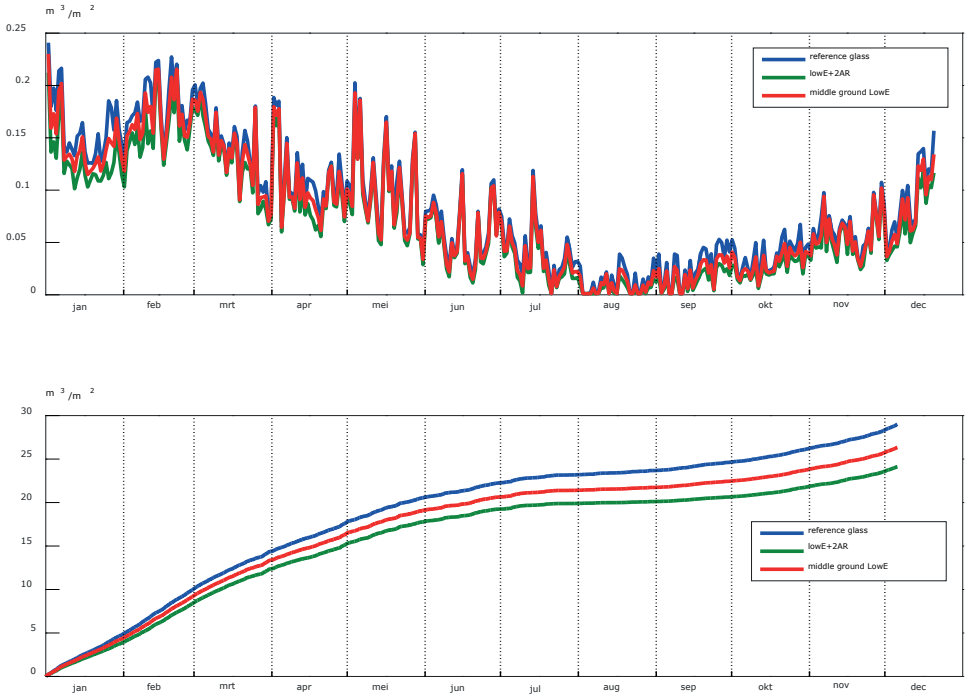

Figure 24 *Daily and cumulative natural gas use ([m³gass /m²greenhouse per day] and [m³gass /m²-greenhouse] respectively) for heating in the simulations when both an aluminized and a semi-transparent energy saving screen were used.*

Regardless of the presence or not of one or two energy saving screens, the maximum energy saving is obtained with the low-e 2AR glass, followed by the middle emissivity 2 AR theoretical glass and by the reference 2AR glass, as expected (Figure 22, Figure 23 and Figure 24). Also, differences are obviously minimized during the summer and are larger during the colder months. The absolute higher energy use is under the configuration with reference glass and no energy saving screen (around 40 m^3/m^2) and the minimum energy use is with the combination of a low-e 2AR glass and two energy saving screens (less than 25 m^3/m^2).

3.3.2 Microclimate and tomato yield

Although a small difference in daily yield is observed between the low-e 2AR glass and the other two glass types during the whole cycle, this difference is more clear during the summer months, and therefore, it appears under all the simulated scenarios, whether there are energy saving screens or not (Table 7, Table 8 and Table 9).
The cumulative yield values show that there is a small difference in yield in favor of the reference glass also in relation to the theoretical middle ground glass, which is not clearly perceptible in the daily values graph.

Table 7

Daily evolution (kg/m^2 day) and cumulative (kg/m^2) potential tomato yield under the scenarios simulated without an energy saving screen.

No screen

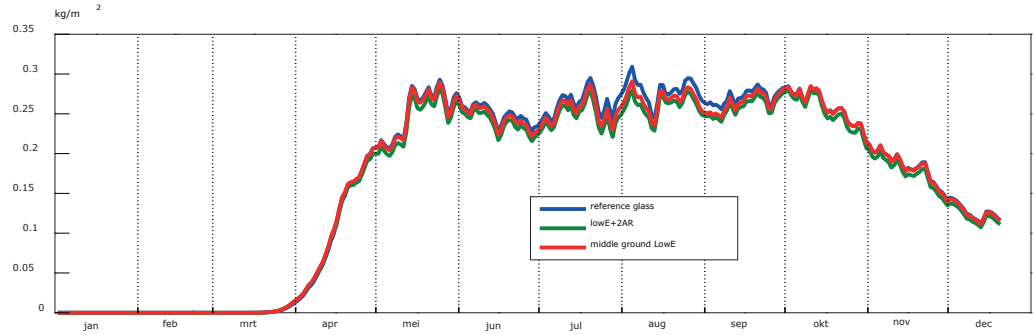

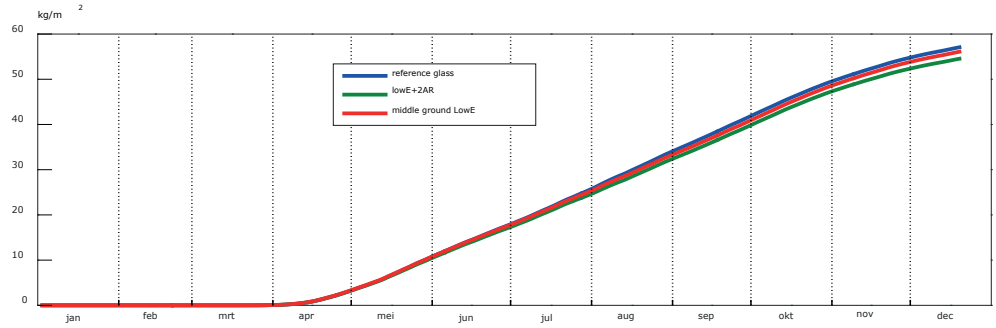

Table 8

Daily evolution (kg/m² day) and cumulative (kg/m²) potential tomato yield under the scenarios simulated with a semi-transparent energy saving screen.

Semitransparent energy saving screen

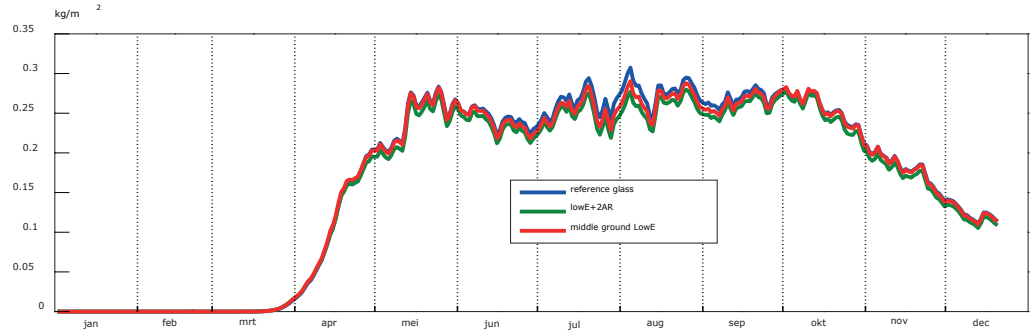

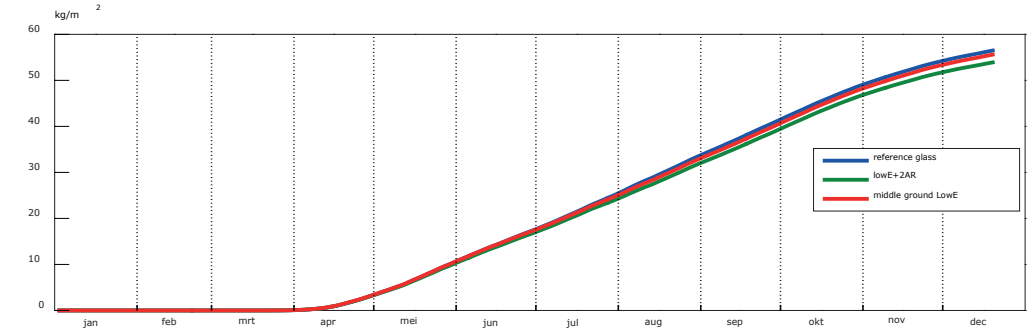

Table 9

Daily evolution (kg/m² day) and cumulative (kg/m²) potential tomato yield under the scenarios simulated with both a semi-transparent and an aluminized energy saving screen.

Semitransparent energy saving screen

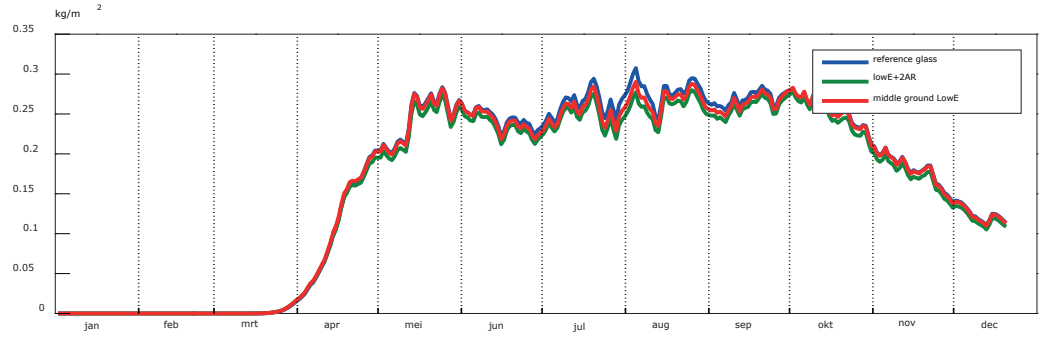

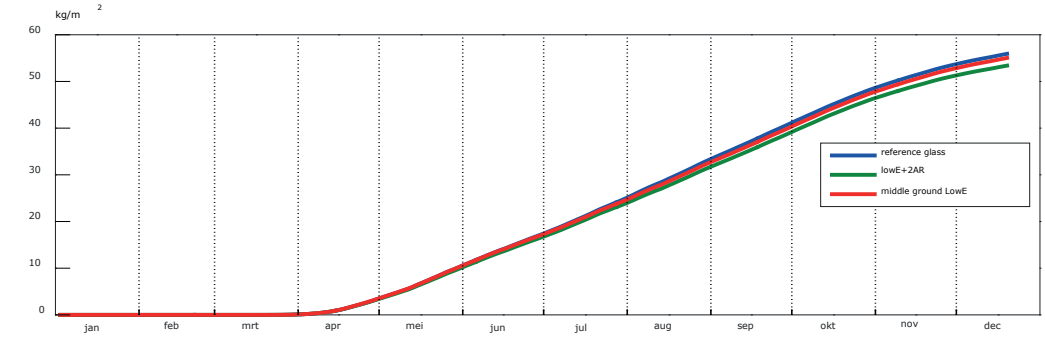

In order to understand the differences in predicted tomato yield that occur during the summer, we need to have a closer look at the microclimate. For this analysis we will focus on the scenarios without energy saving screens/The low-e and the medium-e coatings will lower the radiative heat losses during the daytime. Thus, in order to maintain the temperature set point established, the windows will have to open more under the low-e and medium-e glasses than under the reference 2AR glass during most of the daytime (until they are fully open around noon), which indeed can be observed when we plot the cyclic mean values along the 24 hours for the summer period of percentage of opening of the leeward vents (Figure 25). As a consequence, the CO_2 concentration during early hours of the day and late hours of the afternoon is lower under the low-e glasses than under the reference, due to the higher CO_2 lost to the outside air (Figure 25) which has the consequence of lowering the yield, mostly during these months, when more ventilation is required.

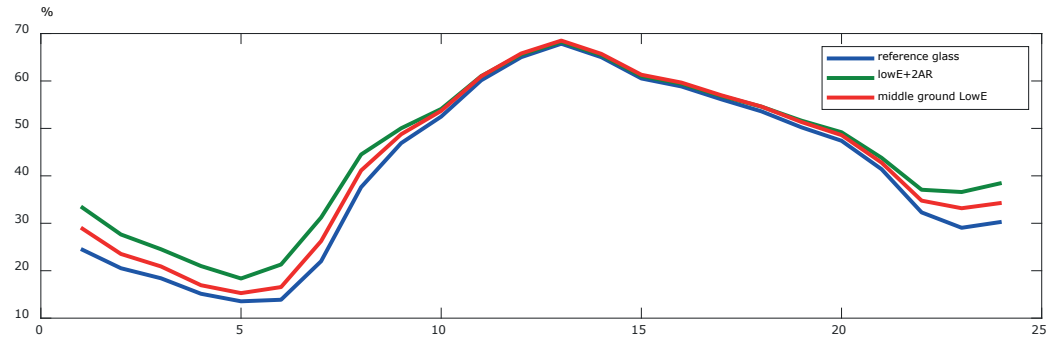

Figure 25 *24 hours cyclic mean of the opening of the leeward vents (%) during the summer period.*

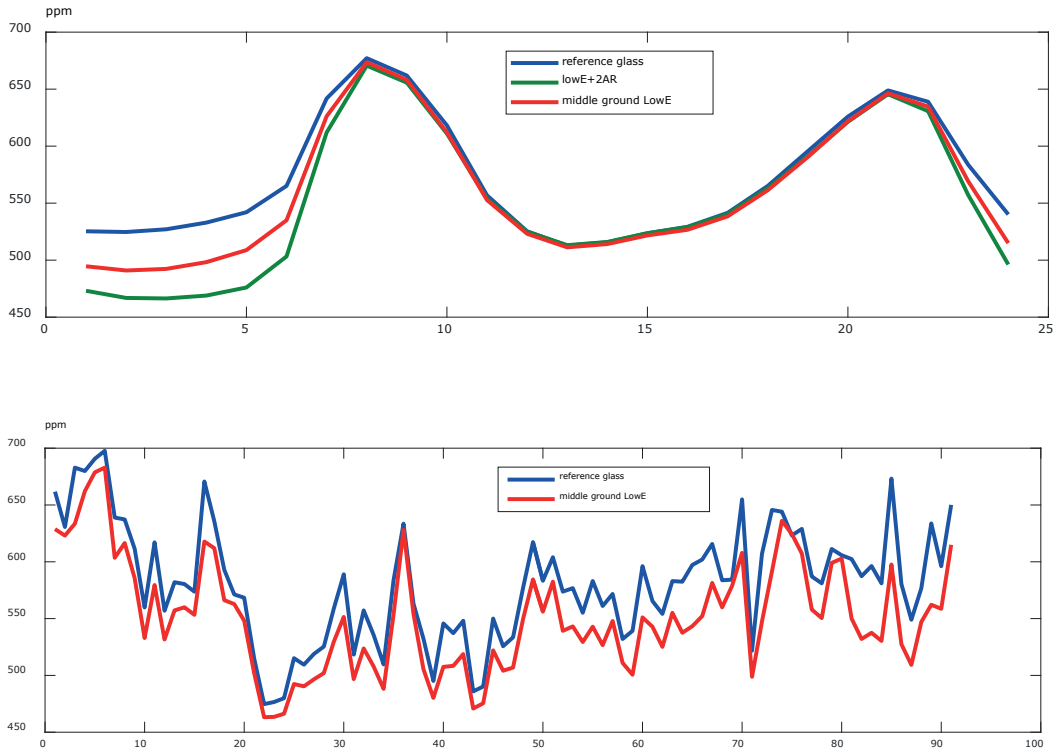

Figure 26 *24 hours cyclic mean of CO_2 concentration (ppm) during the summer period.*

Another aspect which is affected by the presence of a low-e coating is the water vapor balance. The low and medium-e coatings induce larger relative humidity values (%), especially during the winter period (Figure 27). This is because the low-e coating induces a higher cover temperature (Figure 28) and therefore, less condensation, so water vapor stays in the air, increasing R.H.

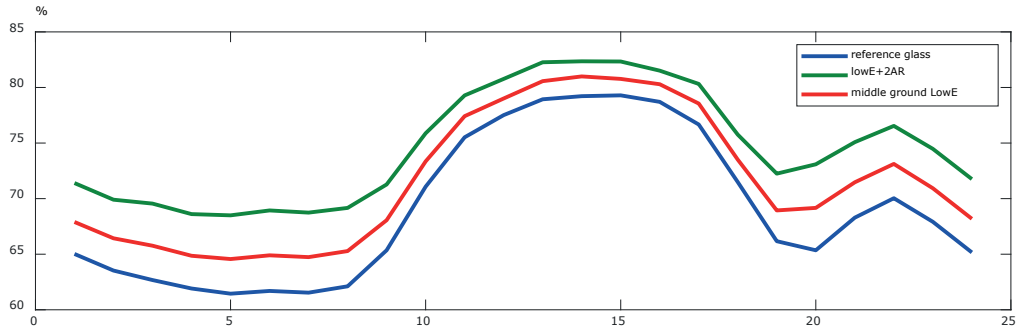

Figure 27 *24 hours cyclic mean of relative humidity (%) during the winter period.*

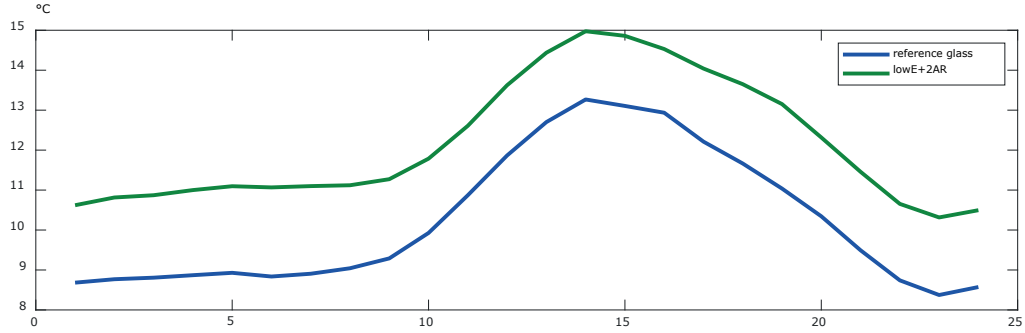

Figure 28 24 hours cyclic mean of cover temperature (°C) during the winter period.

This increase in R.H. values might have consequences in the incidence of diseases on the crop, since it may induce condensation on crop organs that get colder than dew temperature because of radiative losses. However, this is very unlikely to happen under the low-e cover, because the crop temperature will be higher on to crop parts which are more exposed to the cover. In any case, this increase in R.H. values also occurs when the greenhouse insulation increases due to the use of an energy saving screen. If only one transparent screen is used under a reference glass, the R.H. is still lower than under the low-e 2AR glass, but if two screens are used, then values become higher than under the low-e 2AR glass (Figure 29).

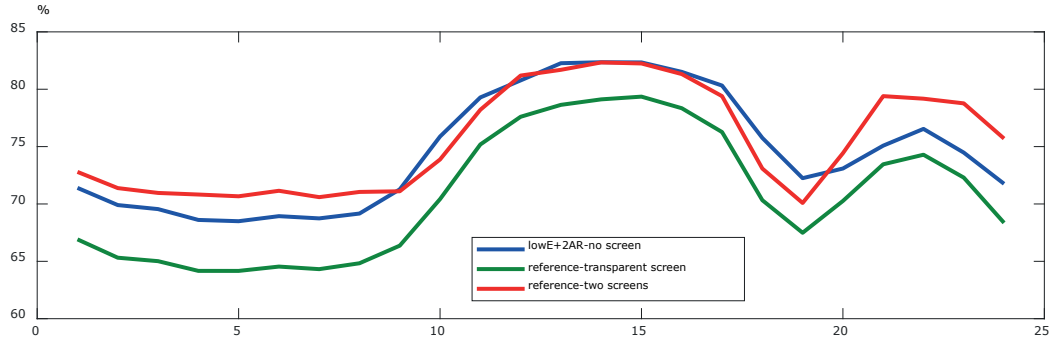

Figure 29 *24 hours cyclic mean of R.H. (%) during the winter period.*

* a) No screen scenarios.

** b) Semi-transparent screen scenarios.

*** c) Double screen scenarios.

Last but not least, also the peak load of energy consumption due to heating is affected by a covering with low-e coating (Figure 30). The lower the emissivity, the less peak hours of heating is needed.

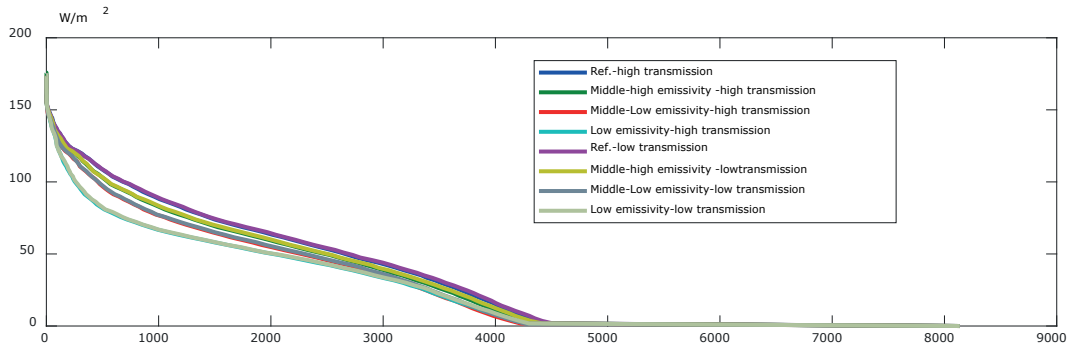

Figure 30 *Year-round duration curve for heating requirement for different configurations of the covering.*

3.3.3 Summary

In percentage, the amount of energy saved by the low-e coated glass is higher (22.2%) than that saved by a single semi-transparent energy saving screen (17%), although the yield penalization is also higher (4.4%) than with the screen (1%) (Table 10 and Table 12). With the screen, the small yield penalization is associated to the shade projected by the screen during daytime hours when it is folded. However, for a middle ground glass with medium-e, the decrease in energy use in percentage is lower (11.6%) than that achieved by the semi-transparent screen (15.6%). Therefore, in order to compete with a screen in quantitative energy saving, it seems clear emissivity must be seriously lowered by the coating. Of course, the use of two screens also saves more energy (28.4%) than using a low or a medium-e coating (22.2% and 11.6%).

Finally, combining the low-e with the use of one or two screens, an even larger quantitative energy saving is obtained, but lower in percentage than the result achieved for the absence of screen (Table 10). The combination of a low-e glass with one semi-transparent screen saves slightly more energy than a reference glass with two screens in absolute values (29 m^3/m^3 vs 27.3), but again, the yield loss caused by the two screens (2%) is lower than that caused by the low-e and the transparent screen (5.4%).

Table 10

Quantitative summary of total energy use, energy saving (m^3/m^2 and %) for the three simulated glass covers, with and without energy saving screens.

	Total energy use [m^3/m^2]		
	Energy saving [m^3/m^2]		
	Energy saving [%]		
	No screen	One semi-transparent energy-saving screen	Two energy-saving screens (one semi-transparent and one aluminized)
Reference 2AR glass • THem=90% • ε=86%	40.5	33.6	29
		-6.9	-11.5
		-17.0%	-28.4%
Medium-e 2AR hypothetical glass • THem=90% • ε=50%	35.8	30.2	26.3
	-4.7	-10.3	-14.2
	-11.6%	-25.4%	-35.1%
Low-e 2AR glass • THem=86% • ε=16%	31.5	27.3	24.1
	-9.0	-13.2	-16.4
	-22.2%	-32.6%	-40.5%

Table 11

Quantitative summary of total yield, yield loss (kg/m^2 and %) for the three simulated glass covers, with and without energy saving screens.

	Yield [kg/m^2]		
	Yield loss [kg/m^2]		
	Yield loss [%]		
	No screen	One semi-transparent energy-saving screen	Two energy-saving screens (one semi-transparent and one aluminized)
Reference 2AR glass • THem=90% • ε=86%	57.1	56.5	56.0
		-0.6	-1.1
		-1.1%	-1.9%
Medium-e 2AR hypothetical glass • THem=90% • ε=50%	56.2	55.7	55.1
	-0.9	-1.4	-2
	-1.6%	-2.5%	-3.5%
Low-e 2AR glass • THem=86% • ε=16%	54.6	54.0	53.5
	-2.5	-3.1	-3.6
	-4.4%	-5.4%	-6.3%

Table 12

Quantitative summary of energy saving (m^3/m^2) and yield loss (kg/m^2) caused by the screens, for the three different simulated glass types.

	Energy saved by Low-e (%)			Yield decrease caused by Low-e (%)		
	a)*	b)**	c)***	a)*	b)**	c)***
Reference 2AR glass • THem=90% • ε=86%	-	-	-	-	-	-
Medium-e 2AR hypothetical glass • THem=90% • ε=50%	11.6%	10.1%	9.3%	1.6%	1.6%	1.6%
Low-e 2AR glass • THem=86% • ε=16%	22.2%	18.7%	16.9%	4.4%	4.4%	4.4%

* No energy screen.

** One semi-transparent energy-saving screen.

*** Two energy-saving screens (one semi-transparent and one aluminized).

	Energy saved by screens (%)			Yield decrease caused by screens (%)		
	a)*	b)**	c)***	a)*	b)**	c)***
Reference 2AR glass • THem=90% • ε=86%	-	17%	28.4%	-	1.1%	1.9%
Medium-e hypothetical glass • THem=90% • ε=50%	-	15.6%	26.5%	-	0.9%	2.0%
Low-e 2AR glass • THem=86% • ε=16%	-	13.3%	23.5%	-	1.1%	2.0%

* No energy screen.

** One semi-transparent energy-saving screen.

*** Two energy-saving screens (one semi-transparent and one aluminized).

3.4 Sensitivity of energy use and yield to the thermal emissivity of the cover

In order to understand better the effect of the emissivity coefficient in the outer layer of the glass on energy use for heating, simulations have been done for 36 theoretical glasses in which the emissivity was decreased in steps of 0.5 from a maximum value of 0.85 to 0, for values of hemispherical light transmission of 89% and 86% (Table 13). These simulations have been done using the same settings described in the previous section, with an energy saving screen in use.

Table 13

Summary of the different theoretical glass covers simulated and the energy used for heating.

Cover	Them* KasPro	Emissivity	Energy use (m^3 natural gas/m^2)	Cover	Them* KasPro	Emissivity	Energy use (m^3 natural gas/m^2)
Theoretical glass-1	0.89	0.85	31.2	Theoretical glass-19	0.86	0.85	31.6
Theoretical glass-2	0.89	0.8	30.7	Theoretical glass-20	0.86	0.8	31.1
Theoretical glass-3	0.89	0.75	30.3	Theoretical glass-21	0.86	0.75	30.7
Theoretical glass-4	0.89	0.7	29.9	Theoretical glass-22	0.86	0.7	30.3
Theoretical glass-5	0.89	0.65	29.5	Theoretical glass-23	0.86	0.65	29.9
Theoretical glass-6	0.89	0.6	29.1	Theoretical glass-24	0.86	0.6	29.4
Theoretical glass-7	0.89	0.55	28.7	Theoretical glass-25	0.86	0.55	29.1
Theoretical glass-8	0.89	0.5	28.3	Theoretical glass-26	0.86	0.5	28.6
Theoretical glass-9	0.89	0.45	27.9	Theoretical glass-27	0.86	0.45	28.2
Theoretical glass-10	0.89	0.4	27.4	Theoretical glass-28	0.86	0.4	27.8
Theoretical glass-11	0.89	0.35	27	Theoretical glass-29	0.86	0.35	27.3
Theoretical glass-12	0.89	0.3	26.6	Theoretical glass-30	0.86	0.3	26.9
Theoretical glass-13	0.89	0.25	26.2	Theoretical glass-31	0.86	0.25	26.5
Theoretical glass-14	0.89	0.2	25.7	Theoretical glass-32	0.86	0.2	26.1
Theoretical glass-15	0.89	0.15	25.3	Theoretical glass-33	0.86	0.15	25.6
Theoretical glass-16	0.89	0.1	24.8	Theoretical glass-34	0.86	0.1	25.1
Theoretical glass-17	0.89	0.05	24.3	Theoretical glass-35	0.86	0.05	24.7
Theoretical glass-18	0.89	0	23.9	Theoretical glass-36	0.86	0	24.2

When emissivity and energy use are plotted (Figure 31) it is clearly visualized that the relation between energy use for heating and the emissivity of the outer layer of the glass cover is of linear nature, regardless if the hemispherical transmission has a value of 0.89 or 0.86. In this way, models can be used by glass manufacturers to make predictions on the potential energy saving that can potentially be achieved by decreasing the emissivity value of the glass.

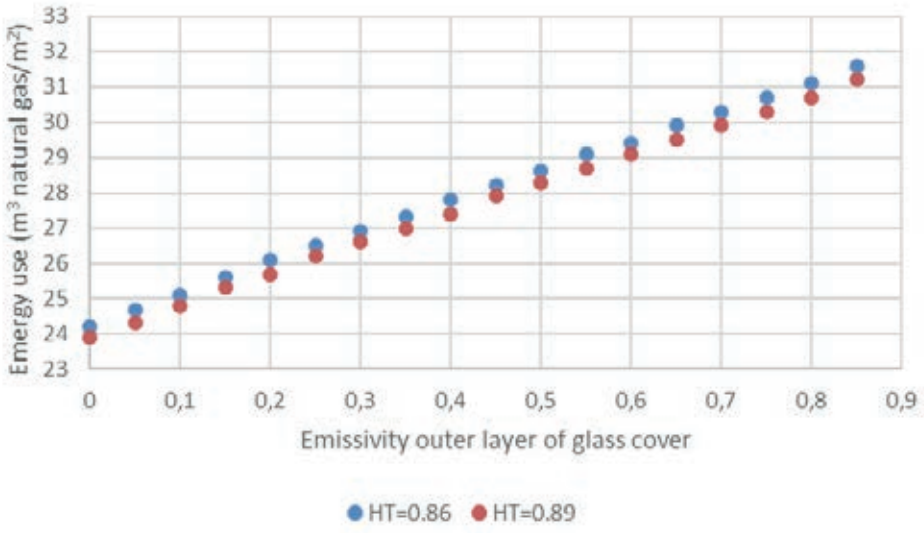

Figure 31 *Relation between the emissivity of the outer layer of the glass cover and the energy required for heating for theoretical glasses with two different hemispherical transmission values.*

These numbers also show that the maximum amount of energy that can be saved in this specific simulation by decreasing the emissivity to a minimum is approximately 7.4 (234 MJ/m^2), which represents a maximum decrease of energy use by lowering the emissivity of the glass of 23%. If such an emissivity value can be reached together the assumed hemispherical light transmission is subjected to future material development.

4 Economics of AR and low-e glasses

4.1 KWIN: general model description

The standard way of economically evaluating greenhouse systems is described in KWIN [Raaphorst *et al.* 2019[1]]. The KWIN (Quantitative Information for Greenhouse Horticulture) is a regularly published periodical with up-to-date information about production, prices of products and means of production. For cultivation plans and investment plans economic figures, 121 balances of different crops and cropping systems containing yields and cultivation-related costs are included. The information contained in this book is primarily intended as an aid in the preparation of commercial advice for greenhouse horticultural businesses by the grower himself or advice institutions. In addition, the information is also important for those who are directly or indirectly involved in greenhouse horticulture, such as suppliers, accounting firms, banks and schools. The 26th version of 2019 includes:

- Information on areas, number of companies and company size for the sector and the most important crops in the Netherlands and an estimate for the EU countries.
- Estimation of the production of several important crops in Europe.
- Investment costs of sustainable production means DPM.
- Estimates of the balance and cost per period of the most important greenhouse vegetables, cut flowers and pot and bedding plants.
- CO_2 footprint per crop and the influence of the different production means.

The KWIN is used for the economic analysis in this project. To compare treated glass with common greenhouse configurations, this chapter will focus on the impact on revenue, capital expenditure, and operational expenditure of a tomato crop without lighting. The comparison will be between 6 cases:

1. Reference 2AR glass with no screen.
2. Reference 2AR glass with one energy screen.
3. Reference 2AR glass with two energy screens.
4. Low-e 2AR glass with no screen.
5. Low-e 2AR glass with 1 screen.
6. Low-e 2AR glass with 2 screens.

4.1.1 Revenues

The revenues depend on the production and the product price. The glass type affects the production, mainly caused by the transmission of PAR, the diffuseness, and the possibility to cool the greenhouse without loss of CO_2. In this economic evaluation we do not assume any effect of the glass type on the price of the produce. But because the price of the produce in the summertime is mostly lower than in spring, 1 kg production increase in spring has a larger impact on the revenue than 1 kg production increase in the summertime.

4.1.2 Capital expenditures

The capital expenditures are calculated with the investment price and the economic life cycle of the production means. Also, the interest rate (1% per year of the new value) and a fixed maintenance rate are taken into account. For the comparison of the six cases, it's only relevant to focus on the type of glass and on the energy screens. One energy screen including installation is assumed to have an investment price 5,30 €/m^2 with 16% depreciation and 5% maintenance costs per year.
The extra price of the low-e 2AR glass compared to the standard glass with double sided antireflective coating is initially set on 8 €/m^2 for initial calculations. All glass types are assumed to have 7% depreciation costs and 0,5% maintenance costs. A price sensitivity analysis is carried out as well.

[1] Raaphorst, M.G.M., J. Benninga and B. Eveleens. 2019. Quantitative Information on Dutch Greenhouse Horticulture, Wageningen.

4.1.3 Operational expenditures

The most relevant operational expenditures for a comparison between the six cases are:
1. Gas use and gas price.
2. Labor costs (more production means more labor).
3. Sales costs (packaging, transport, auction costs, levies).
4. Nutrients.
5. Interest on crop value.

The gas use depends on the energy saving capacity of the greenhouse configuration. The other expenditures mainly depend on the production amount. The calculations in Table 14 assume a linear ratio between the production/revenue and these types of expenditure costs. The gas price is initially assumed to be 0,20 €/m^3 incl. taxes. A price sensitivity analysis is carried out as well.

4.2 Results

Table 14 shows the revenues and costs for six different cases. The low-e 2AR glass type is initially assumed to cost 8 €/m^2 more than reference 2AR coated glass, with the same light transmission as AR coated glass and an emissivity of 15%. The price of natural gas is initially set on 0,20 €/m^3 including taxes. With these assumptions, the highest profit can be reached with the case "low-e with high transmission and no screen".

Table 14
Calculation of the revenue -/- costs (=profit in €/m^2.yr) for 6 cases.

	Ref. 2AR glass no screen	Ref. 2AR glass 1 screen	Ref. 2AR glass 2 screens	low-e 2AR glass with no screen	low-e 2AR glass with 1 screen	low-e 2AR glass with 2 screens
Revenue	54.93	54.38	53.97	53.59	53.06	52.65
Investment costs	12.86	14.03	15.19	13.54	14.71	15.87
Natural gas	8.10	6.72	5.80	6.32	5.48	4.83
Total other indirect costs	6.42	6.42	6.42	6.42	6.42	6.42
labour costs crop	13.48	13.34	13.24	12.96	12.83	12.73
crop nutrition	0.98	0.97	0.97	0.95	0.94	0.93
Transport	0.41	0.41	0.41	0.40	0.39	0.39
Levies	0.33	0.32	0.32	0.32	0.31	0.31
Auction costs	0.82	0.82	0.81	0.80	0.80	0.79
interest on crop value	0.55	0.54	0.54	0.54	0.53	0.53
boxes or packaging	7.87	7.79	7.73	7.57	7.50	7.44
Total direct costs	24.45	24.20	24.02	23.53	23.30	23.12
Total costs	51.83	51.37	51.43	49.82	49.90	50.25
Profit	3.10	3.01	2.54	3.77	3.15	2.41

With a different gas price, the profit will also differ for the six cases. That is shown in Figure 32, where the profit of tomato under several cases of glass is compared to the profit of a tomato crop under standard glass with a 2AR coating without a screen. The profit differences are presented as a function of the price of natural gas. In this figure, three cases with an experimental type of glass, having a hemispherical transmission of 88.6% and an emission coefficient of 29%, are also included. With a gas price up to 0.30 €/m^3, the option of this experimental type of glass with no screen is the most profitable option. With a higher gas price, the combination of this glass type and an energy screen would increase the profitability.

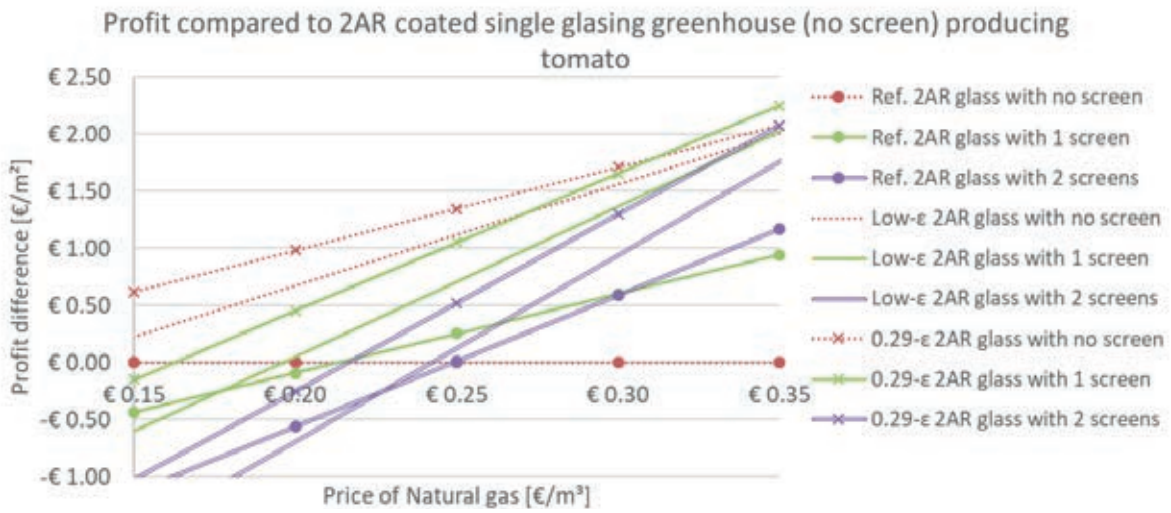

Figure 32 *Profit of eight cases compared to the case "Ref. 2AR glass without screen", assuming an investment price of 8 €/m² for low-e coating, as a function of the gas price.*

With a gas price of 0,20 €/m^3 including taxes, an energy screen is not profitable anymore for tomato (see Figure 33). For a greenhouse without an energy screen, a low-e coating with an investment price lower than 16 €/m² would still profitable. The experimental glass type with a 0.29 emission coefficient would even be profitable at prices higher than 20 €/m². For a greenhouse with an energy screen, the low-e coating is only profitable if the investment price is lower than 9 €/m². The experimental glass type would then be profitable at an investment price lower than 14 €/m².

Figure 33 *Profit of eight cases compared to the case "Ref. 2AR glass without screen", assuming a gas price of 0,20 €/m³, as a function of the investment price of a low-e coating.*

An analysis has been made particularly for the economic performance of the developed prototype glasses, the experimental demonstrator (Figure 34 and Figure 35) and also the industrial demonstrator (Figure 36 and Figure 37).

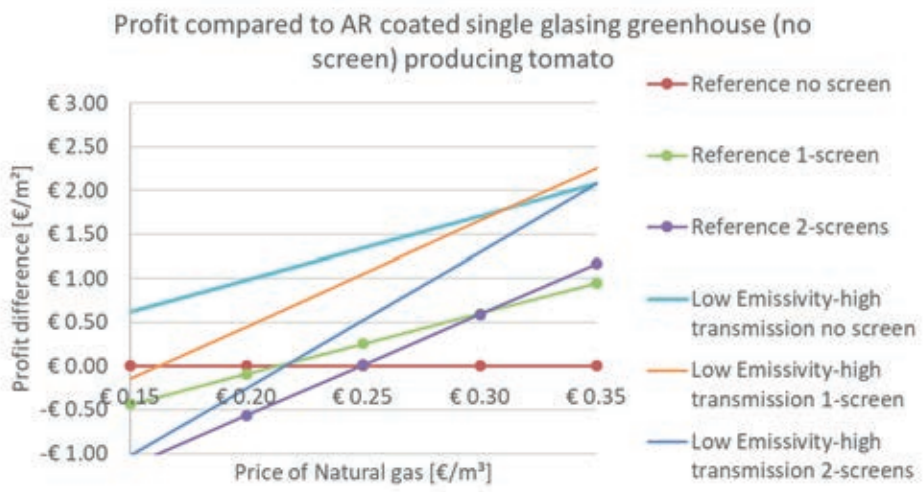

Figure 34 *Profit of the experimental demonstrator as a function of the gas price.*

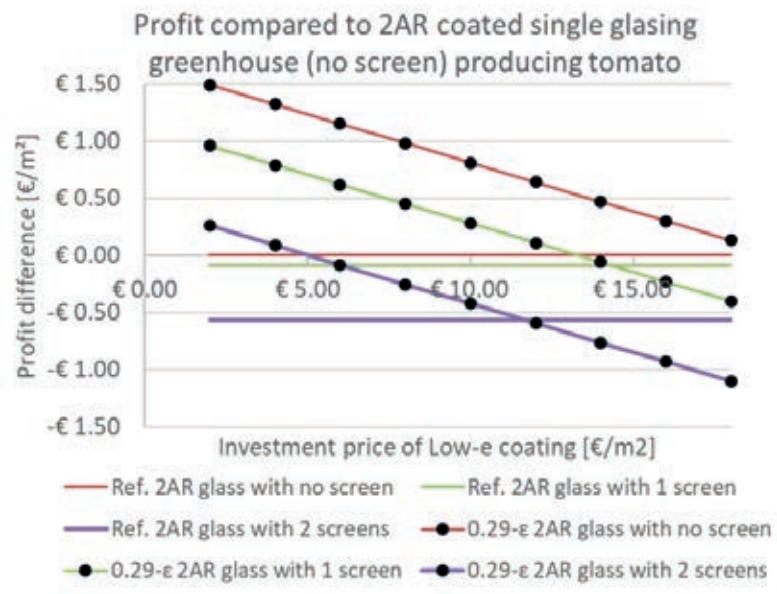

Figure 35 *Profit of the experimental demonstrator as a function of the glass investiment price.*

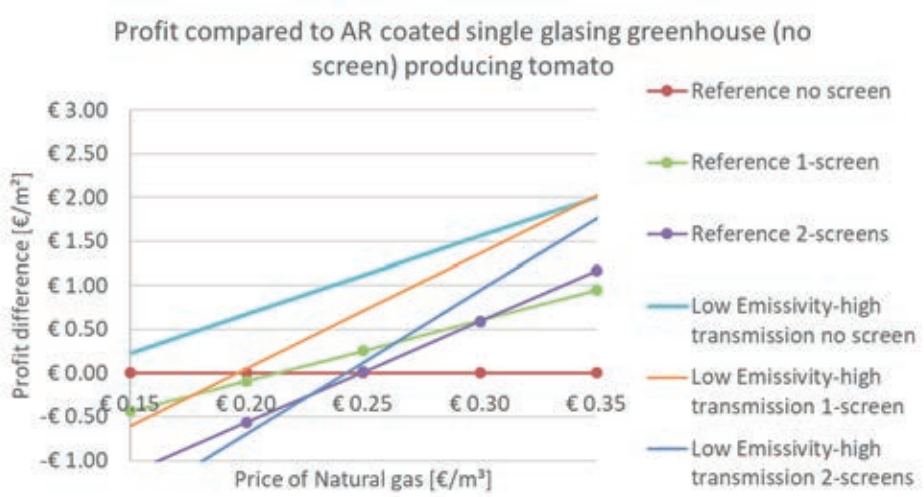

Figure 36 *Profit of the industrial demonstrator as a function of the gas price.*

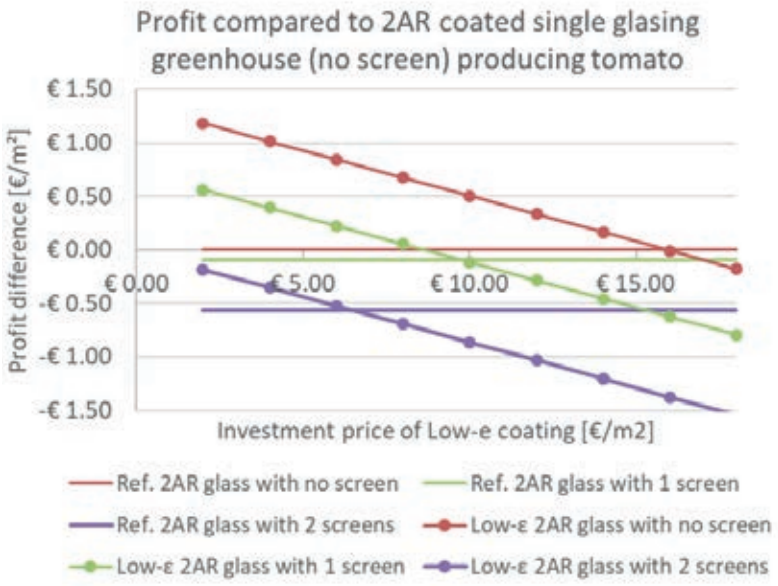

Figure 37 *Profit of the industrial demonstrator as a function of the glass investment price.*

4.3 Discussion

The calculation of the profitability depends also on the effect on the production. If the light transmission of low-e glass drops with 1%, the profit will lower with 0,24 €/m^2. Seasonal effects might apply since the effect of the low-e coating is most important in winter when crop prices are usually high (Figure 38) and energy costs are high as well.

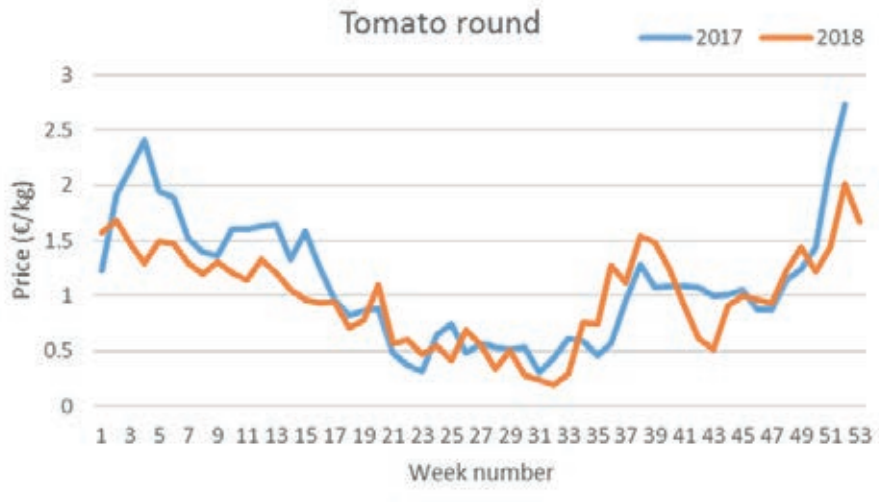

Figure 38 *Typical seasonal price fluctuations for round tomatoes in 2017 and 2018.*

The economic benefit also depends on the type of greenhouse energy system and cropping systems. Growers with a Heat and power cogeneration (CHP) usually have a lower cost price of heat compared to a traditional boiler system (Figure 39). In that case the reduction energy loss is less economic. Growers using artificial lighting also have a lower need for additional heating because the heat is a byproduct of artificial lighting which means less need for insulating greenhouse cover. Less heat is produced by LED lamps compared to HPS lamps. On the other hand, the crop production during the winter is relatively less affected by the light transmission of the cover in case of the additional use of artificial lighting.

Figure 39 *Yearly costs per square meter for tomato greenhouse equipped with a: conventional boiler, b: heat and power cogeneration.*

Last but not least, the coatings are assumed to have the same life cycle and maintenance rate as normal glass. The life cycle is usually set on 15 years, but many greenhouses live longer than 25 years. If the coatings need to be maintained within that period, the cost should also be taken into account.

5 Evaluation of transparent conducting oxides (TCOs)

5.1 Measurement methods

In the new type of low emission and high light transmission glasses different coatings are added to the glass surface combining low emissivity (low-e) functionality and anti-reflection (AR) functionality. The layer in the AR stack that is responsible for the low-e effect is a transparent conducting oxide (TCO). TCOs are a class of materials that can be made from many different compositions and its properties are known to depend strongly on the deposition conditions and after deposition processing. In this project we aimed to develop a TCO with the following characteristics:

1. The absorption in the PAR range should be as low as possible (high light transmission).
2. It should significantly reduce the thermal emissivity (low emissivity).
3. It should be able to withstand processing steps after deposition like tempering.

Low absorption in the PAR range is the strongest requirement since this allows for the highest possible hemispherical PAR Transmission which is crucial to be used as greenhouse cover. While the TCO should definitely generate a significantly lower thermal emissivity the goal is not to reduce this emissivity as much as possible but to show this property can be obtained without a detrimental impact on the PAR Transmission. The third goal stems from the tight economic balance faced by growers, being able to deposit the coating on glazing before tempering significantly eases the production process and will result in more affordable glazing for greenhouse construction.

Two types of TCO materials were tested in this project: Indium Tin Oxide (ITO) and indium zinc oxide (IZO). Both were deposited on 30cm x 30cm substrates at TNO Solliance. Measurement of light transmission and emissivity. To evaluate the light transmission and emissivity of the new glasses different measurements have been carried out.

Reflection and Transmission measurements in the range from 250 nm to 2500 nm were recorded in 5nm intervals using a Perkin Elmer Lambda 950 double beam photo spectrometer equipped with either a 150 mm integrating sphere accessory or a 270 mm integrating sphere accessory equipped with a photomultiplier and a PbS detector for the UV/VIS and NIR range respectively.

Reflection and Transmission measurements in the range from 6000 cm^{-1} to 600 cm^{-1} were recorded in 4 cm^{-1} intervals using a Perkin Elmer Frontier FTIR equipped with a 6 inch external integrating sphere equipped with a liquid nitrogen cooled wide band MCT detector produced by PIKE.

Ellipsometry measurements were carried out at 41 wavelengths in the range 363 nm to 1000 nm on an Accurion imaging ellipsometer EP4 at Surfix by Wout Knoben.

5.1.1 Determination of the refractive index

To evaluate transparent conducting oxide thin layers (TCO) for their suitability to be integrated in low-e AR stacks for horticultural applications the refractive index (n) and extinction coefficient (k) must be determined. The refractive index of materials cannot be measured directly but must be deduced from the measurements via a model.

For bulk materials like a sheet of glass the refractive index can be calculated analytically either from reflection/ Transmission measurements or from ellipsometry measurements. This can be done for each measured wavelength independently. For thin layers on a substrate the number of unknowns is increased with the layer thickness and the refractive index of the thin layer. Fortunately, entire spectra can be captured and the refractive index for the entire spectrum can be modelled using dielectric functions. By employing these dielectric functions, we make use of the fact that refractive indexes of materials at a certain wavelength are not independent of the refractive index at an adjacent wavelength. Advantages of this approach is that the results are more robust and have less influence from noise.

The software package SCOUT was used to set up a model of the substrate, thin layer stack and dielectric functions and fit this model in the observed measurements. For glass a model was set up utilizing a dielectric background, eleven Kim oscillators were used for the multiple absorption peaks throughout the spectrum and an O'Leary, Johnson, Lim (OJL) interband transition model was used for the behavior in the UV. This gives the model 49 parameters to solve based on 2250 observations (450 Transmission and 450 reflection measurements between 250 and 2500nm and 1350 reflection measurements between 1667nm and 16.7mm)

In the table below a typical fitting result for a simple glass sheet can be seen.

Table 15

Difference between measured and modelled light Transmission, reflection and absorption (sample TN19A).

	Measured	Fitted and modelled
NEN2675 weighted Transmission	91.9(214)%	91.9(213)%
NEN2675 weighted Reflection	8.0(352)%	8.0(725)%
NEN2675 weighted Absorption	0.0(434)%	0.0(062)%

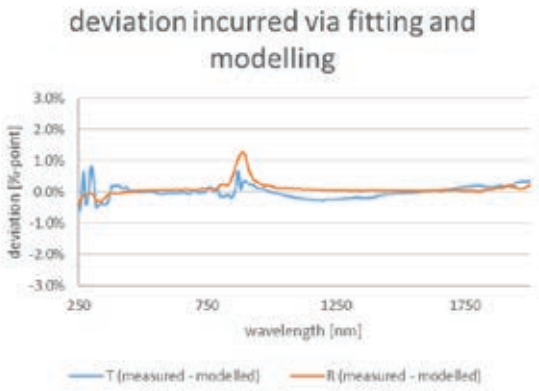

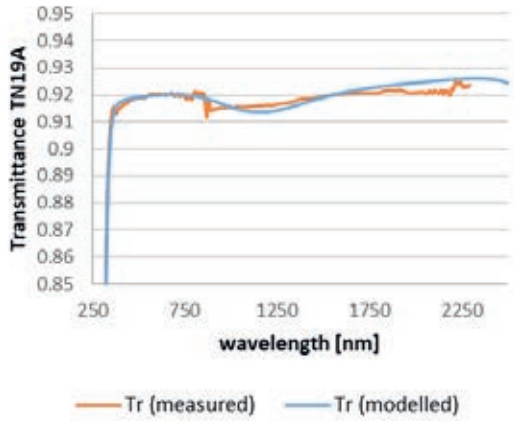

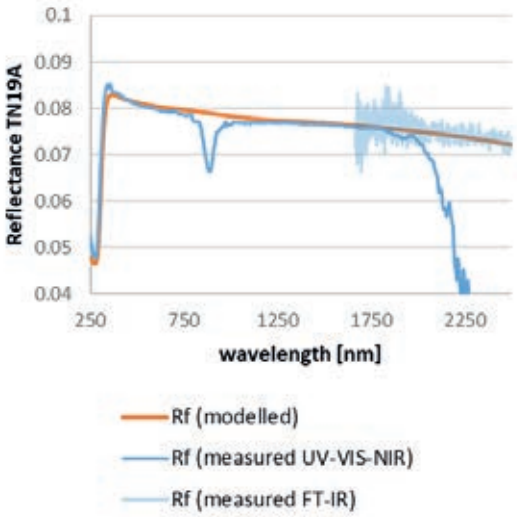

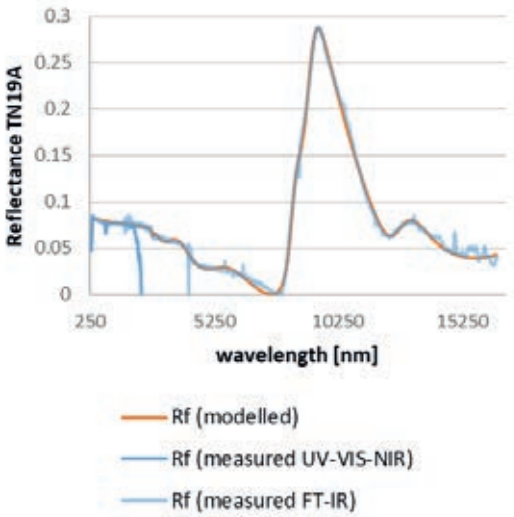

As can be observed in the spectra some deviations do occur. For instance, the spike around 800nm which is not modelled because this is a measurement artifact from the grating change over in the spectroscope. As well as the area between 1750nm and 2500nm where the smoothly modelled reflection is more reasonable than the measurement data from which it is derived, the noise in the FT-IR measurement is ignored and the fitting procedure was set to ignore the UV/VIS/NIR data above 2000nm where the signal to noise ratio starts to collapse.

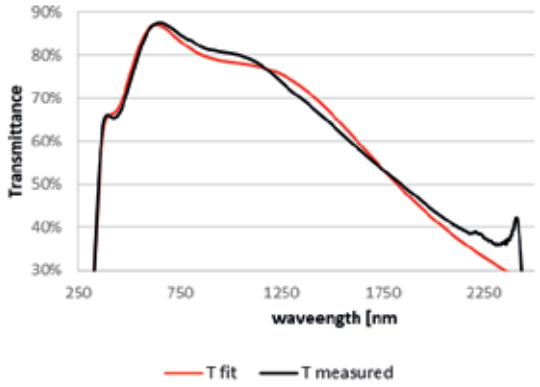

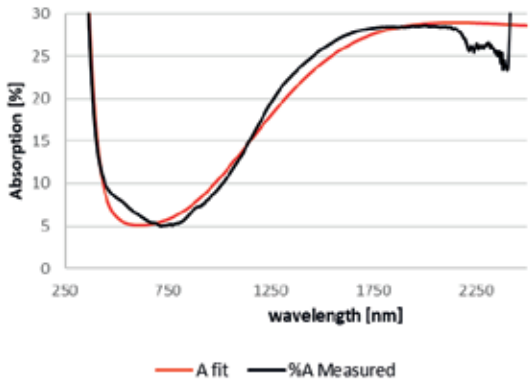

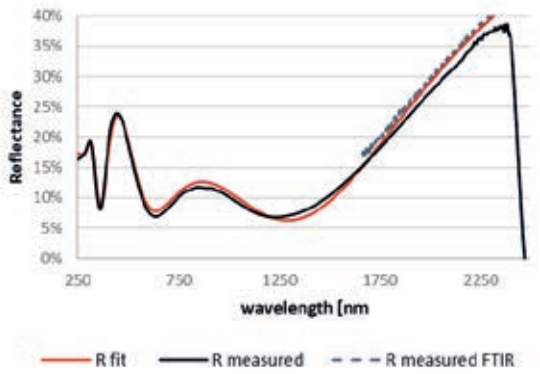

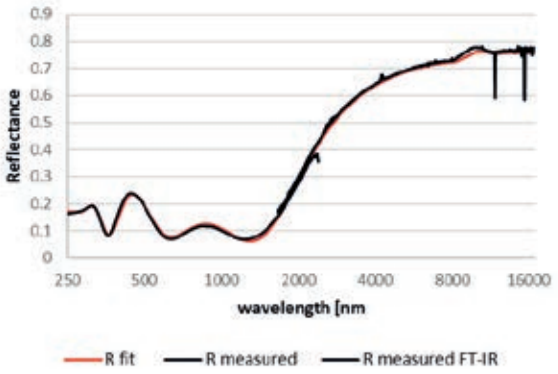

	Measured	Fitted and modelled
NEN2675 weighted Transmission	78.6(58)%	79.4(79)%
NEN2675 weighted Reflection	13.6(55)%	14.0(42)%
NEN2675 weighted Absorption	7.6(87)%	6.4(79)%

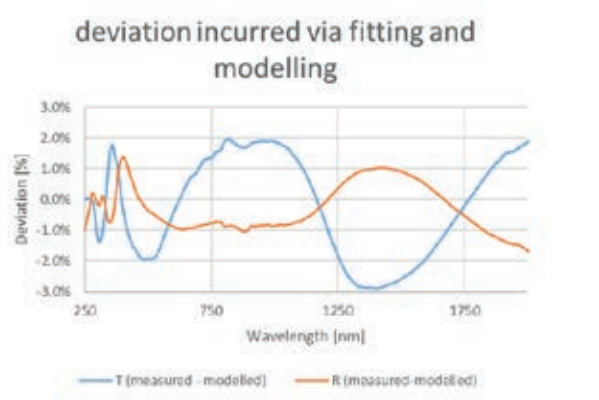

For glass the largest deviation occurs for the reflection with 0.0373% difference between measured and fitted value while for an ITO layer on glass the largest deviation occurs for the Absorption with 1.21% difference between measured and fitted value.

In this procedure small spectral features will be lost but since we are interested in broad spectral ranges like the NEN2675 PAR, NIR and Solar range or the Max Planck weighted emissivity which are useful for greenhouse design this is deemed acceptable. In the results section the measured and modelled NEN2675 PAR values will be provided as an indication of the uncertainty that was introduced by the fitting procedure.

5.2 Effects of deposition parameters and processing conditions (Investigation 1)

The optical Transmission and electrical resistivity of ITO and IZO are known to be sensitive to the partial pressure of O_2 as well as to the sample temperature during deposition ref. Also the deposition speed can have an impact on the TCO qualities. In turn, the resistivity is linked to the IR emissivity via the Drude model. We therefore tested different process parameters combinations. This preliminary Investigation 1 aimed at finding the best process parameters to achieve the targeted properties.

5.2.1 Sample preparation

Two sputtering tools were used by TNO Solliance for experimental glass production. The AJA sputtering tool allows for high quality TCO deposition but only at low deposition speed and on a few centimetres sample scale. Therefore, this tool has no industrial relevance for coating greenhouse glazing but it was used to set a reference point for the best quality deposition that can practically be expected.
Hereunder the process parameters tested for the first investigation (Investigation 1) are listed. The aim was to compare two metal oxides (ITO and IZO) grown in different conditions of O_2 content and deposition temperature. The following recipes were investigated:

- Type A (standard recipe):
  - Substrate is at room temperature.
  - Atmosphere 9sccm pure Argon + 6 sccm 97.5% Argon mixed with 2.5% O_2.
- Type B (high O_2):
  - Substrate is at room temperature.
  - Atmosphere 5 sccm pure Argon + 10 sccm 97.5% Ar mixed with 2.5% O_2.
- Type C (high temperature):
  - Substrate is at 300 degrees Celsius.
  - Atmosphere 9sccm pure Argon + 6 sccm 97.5% Argon mixed with 2.5% O_2.

A tempering process was simulated in the lab by loading the samples in a furnace pre-heated at 625°C, heating them for either 440 s (4mm thick substrates) or 150 s (1mm thick substrate) and pulling them out in <10 s and letting them cool down at room temperature. In the table below the samples used for this exploratory Investigation 1 are listed.

Table 16

Samples used for investigating different deposition equipment, thin layer thicknesses and processing conditions.

Code*	Used deposition equipment	Size [mm]	Material	Thin layer thickness deposited	Tempered	Processing conditions
TN19A**	-	50x50x1	Base glass	-	No	
TN19D	AJA	30x30x1	ITO	180nm	No	Type A
TN19E						Type B
					Yes	Type A
						Type B
TN19C	MRC	50x50x1	AZO	270nm	No	
TN19B			ITO	150nm	No	Type A
TN19F						
					Yes	
TN19G						
					No	Type B
					Yes	
					No	Type C
					Yes	
TN19H			MgF_2	100nm		Magnesium fluoride
TN19N		25x50x1	IZO	160nm	No	Type A
TN19O				320nm		
		50x50x1		270nm		
					yes	

* samples without a WUR code were prepared and analysed at Solliance and not send to WUR for further analysis

** TN19A is the substrate glass used for all other samples in this table

5.2.2 Results and discussion

The most important characterisation on those samples was the optical characterisation, since the crop yield model from WUR clearly indicates that very high Transmission in the useful wavelength range was a strict requirement. Next to that the thermal properties have been characterised, the thermal infrared reflection is a good indicator for energy saving properties, A high thermal infrared reflection (TIR) (thus a low emissivity) is desired.

Table 17

Optical properties (PAR light transmission T, reflection R, absorption A) and thermal properties (thermal infrared reflection TIR) of samples prepared with different deposition equipment, different thin layer thicknesses and processing conditions, both measured and modelled.

	Code	PAR light reflection RNEN2675		PAR light transmission TNEN2675		PAR light absorption ANEN2675 (A minus A substrate)		Max Planck weighted TIR reflection
		Measured [%]	Fitted in Model [%]	Measured [%]	Fitted in Model [%]	Measured [%]	Fitted in Model [%]	Measured [%]
Substrate	TN19A	8.0	8.1	91.9	91.9	0.043	0.0062	
MgF2	TN19H	5.9	5.7	94.8*	94.1*	-0.7*	0.2*	
AJA	TN19D	18.1*	17.1*	79.7	79.4	2.2*	3.4*	59
	TN19E	17.2*	16.6*	80.5	80.3	2.3*	3.1*	76
IZO	TN19N	17.8	17.6	81.5	81.3	0.7	1.1	53
	TN19O	16.8	16.6	80.2	80.1	3.0	3.3	76
AZO	TN19C	13.8	13.7	80.9	81.1	5.3	5.1	68
ITO type A	TN19B	13.7	14.0	78.7*	79.5*	7.6*	6.5*	75
	TN19F	13.6	14.0	72.7	72.6	13.7	13.4	67
ITO type A tempered	TN19G	15.5	15.2	83.8	83.3	0.7*	1.5*	49

*deviation between the fitted model and the measurement is larger than 0.5%

The PAR light Transmission and reflection values are reported to give a sense of the quality of the fitting procedure but are on their own not a consequential indicator of performance except for the deduced absorptance via A=1-R-T. The PAR light absorption on the other hand is a clear indicator of performance since absorption cannot be reduced via interference in the AR stack design.

Table 18

Refractive index N of samples prepared with different deposition equipment, different thin layer thicknesses and processing conditions, modelled.

	Code	Refractive index NThin Layer NEN2675	Thin layer thickness
		Fitted in Model [n+ik]	Fitted in Model [nm]
Substrate	TN19A	$1.5160+i2.739\cdot10^{-9}$	
MgF2	TN19H	1.3769	111.1
AJA	TN19D	$2.0758+i8.278\cdot10^{-3}$	180.7
	TN19E	$2.0653+i7.941\cdot10^{-3}$	175.2
IZO	TN19N	$2.0673+i3.924\cdot10^{-3}$	95.0
	TN19O	$2.0687+i5.110\cdot10^{-3}$	274.0
AZO	TN19C	$1.8747+i1.030\cdot10^{-2}$	224.9
ITO Type A	TN19B	$1.9857+i1.830\cdot10^{-2}$	164.1
	TN19F	$2.0194+i3.936\cdot10^{-2}$	163.6
ITO type A tempered	TN19G	$2.0383+i3.387\cdot10^{-3}$	162.1

From the first results shown above, we can conclude that the AJA deposited ITO clearly shows superior quality relative to ITO deposited via the MRC tool and could serve its role as a point of reference for maximum attainable deposition quality. Looking at the as deposited properties it seems that AZO and IZO have less intrinsic absorption in the PAR region relative to ITO under the same deposition conditions.

While the observations about the as deposited layer properties are definitely interesting the most important result to observe is the TN19G, the MRC deposited ITO type A that had been post processed with an tempering step to explore the coating's survivability of the post deposition tempering process. The low-e effect is slightly diminished but the absorption in the PAR region is also greatly reduced and shows an absorptance lower than the point of reference for quality deposition that was set by the AJA deposition.

The positive effect of tempering on the PAR absorption was further investigated via a set of MRC deposited ITO samples and one IZO sample. These were analyzed in the UV VIS NIR range directly at TNO Solliance.

In Figure 40 the absorptance (A=1-Reflection -Transmission) of the four types of coatings is plotted., It shows the following:

- Before tempering,
  - For ITO: the type B (High T) and C (high O_2) samples perform the best.
  - For IZO: the absorption is very low, compared to non-tempered ITO, however, with more absorption in the 400-450nm range than ITO, due to its lower bandgap.
- After tempering,
  - The absorption is close to 0% for most of the PAR spectrum, regardless of the initial process parameters used during deposition. Only IZO still suffers from a slight loss in the 400-450nm range.

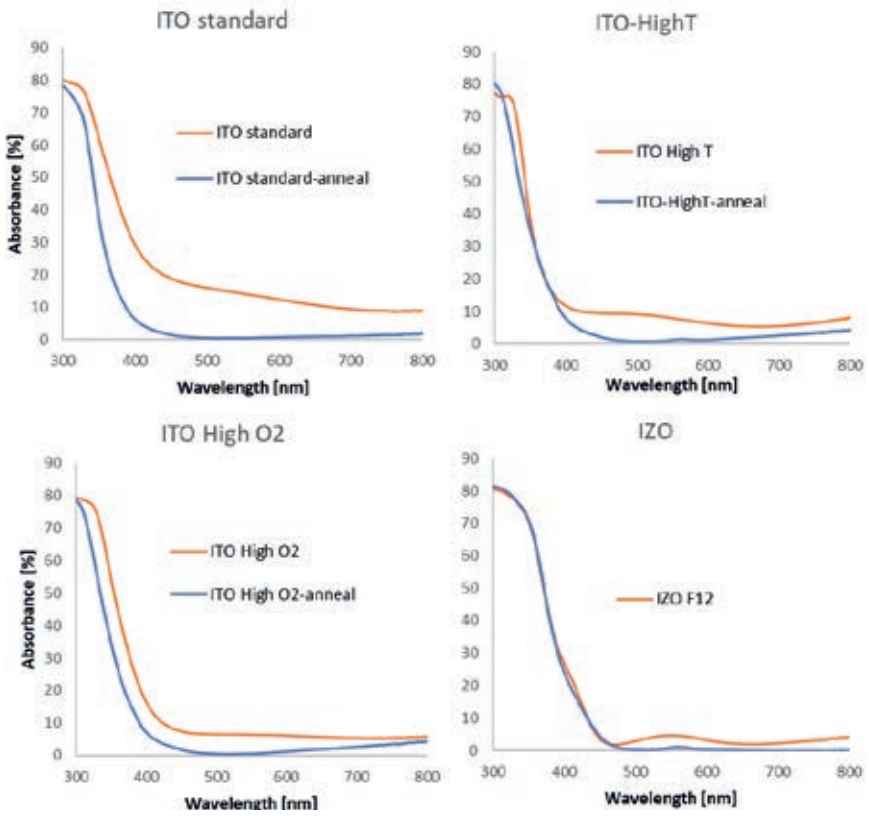

Figure 40 *PAR light absorption of the different samples deposited in Investigation 1.*

The PAR absorption of the post deposition tempered ITO layer deposited glasses shows the tempering step consistently improves the layer properties in the PAR region and that the final properties in this region are made approximately independent of the deposition process.

The effect of tempering was further investigated by looking at the bandgap of the coated TCOs. This was assessed via the Tauc plot of the absorptance (Figure 41).

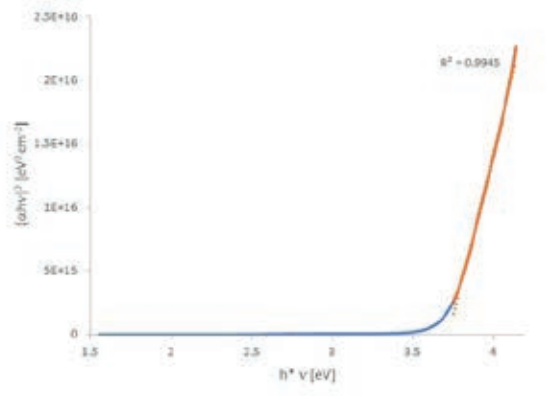

Figure 41 *Example of Tauc plot to determine the band gap from the absorption a=1-T- R.*

Table 19

Bandgap values Eg calculated from the light transmission T and light reflection R for different glass samples with different TCOs (ITO and IZO).

Samples with TCO	Bandgap Eg (eV)
ITO standard non-tempered	3,68
ITO standard tempered	3,69
ITO high O_2 non-tempered	3,70
ITO high O_2 tempered	3,79
ITO high T non-tempered	3,72
ITO high T tempered	3,79
IZO F12 non-tempered	3,63
IZO F12 tempered	3,63

For the ITO samples a slight increase in bandgap is observed upon tempering, this indicates that the conduction band is filled with more electrons after tempering, this is consistent with the reduction in below bandgap defect states that contribute to the absorptance in the PAR region before tempering. For IZO the bandgap seems to be unaffected.

The sheet resistance of the samples was also measured, as it is known to scale with the emissivity. The results indicate a substantial increase upon tempering.
Two possible reasons were proposed:

- Micro-cracks in the TCO, which impede the lateral conductivity measured by 4-point probe, but not necessarily the emissivity.
- Defects migrating into the TCO, e.g. Na from the glass.

Table 20

Sheet resistance R of the samples (measured by 4-point probe).

Samples with TCO	Sheet resistance R (Ω.sq-1)
ITO standard non-tempered	44
ITO standard tempered	109
ITO high O_2 non-tempered	33
ITO high O_2 tempered	81
ITO high T non-tempered	15
ITO high T tempered	83
ITO AJA non-tempered	48
ITO AJA tempered	58

When we look at the modelled refractive index of an as deposited ITO glass type (TN19F) and a post deposition tempered ITO glass types (TN19G) it can be observed that the extinction coefficient k is indeed greatly reduced in the PAR region for the tempered ITO but there is also a later onset of the increase in extinction coefficient[2] that is responsible for the low-e effect and causes the low-e effect of the tempered ITO to be less compared to the non-tempered ITO.

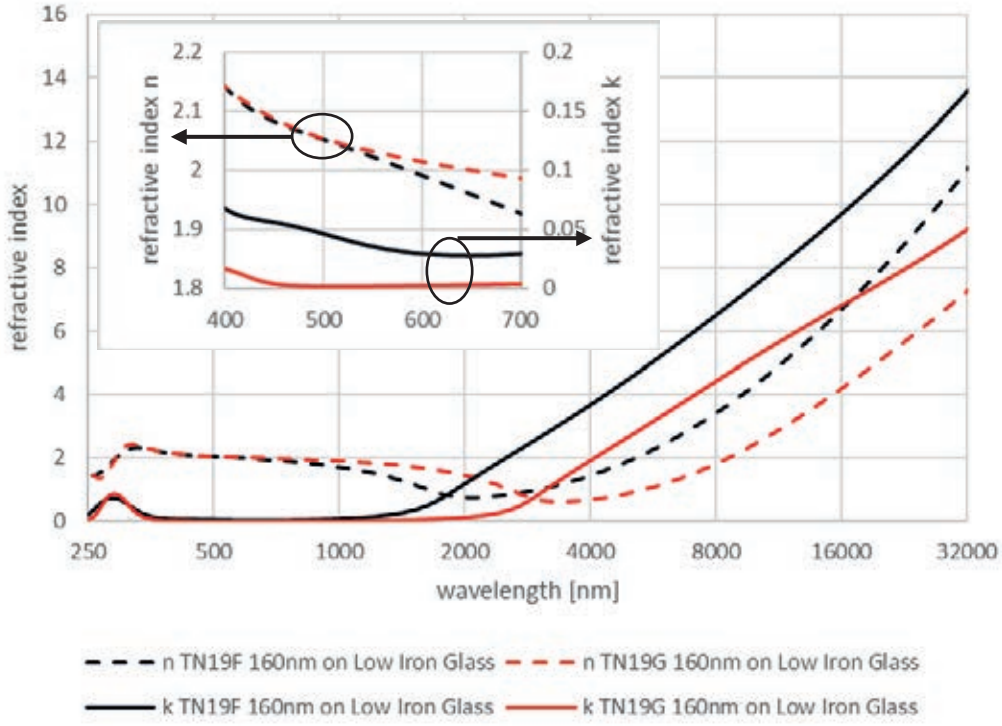

Figure 42 *Refractive index spectrum of as deposited ITO and post deposition tempered ITO.*

[2] A later onset of the increase of k indicates a lower free electron density and thus a lower plasma resonance frequency and conflicts with the observed increase in bandgap energy that indicates there should also be a higher free electron density in the conduction band. Possible explanations could be bound electrons in the conduction band or the extensive below bandgap absorption from defect states causing a misreading of the Taucplot. These conflicting observations were not further investigated.

5.2.3 Conclusion

- Exploratory Investigation 1 shows there is extensive influence of the deposition conditions on the TCO qualities important for greenhouse applications like PAR absorption and emissivity reduction.
- Despite the fact that the effects of deposition conditions on quality was large these turned out to be of relatively little consequence because the differences in PAR absorptance disappeared upon tempering.
- PAR absorptance almost completely disappeared after tempering (PAR absorptance smaller than 1%).
- Tempering did not show a significant effect on layer thickness and neither on the real part of the refractive index in the PAR range indicating the layers are able to survive and withstand the tempering process.
- Some properties are affected by tempering, it was shown that:
  - The bandgap increases slightly.
  - The sheet resistance increases dramatically indicating an increase in emissivity.
  - The increase in emissivity was also measured directly and shows a lower plasma frequency evidenced by the change over from Transmission to reflection to occur at a larger wavelength.
- In this exploratory Investigation 1 the thermal infrared properties which determine the emissivity was only measured for one tempered TCO the evaluation of the characterized as deposited TCOs was omitted because these properties were shown to be impacted by tempering as well.

5.3 Effects of industrial tempering (Investigation 2)

For insurance and safety purposes, virtually all greenhouse glass used today is tempered. However, since most industrial lines for glass and coating fabrication require that the coatings be deposited prior to tempering, the coatings deposited on this glass must be resilient enough to survive industrial tempering. We therefore decided to study the effect of tempering on the TCO coatings deposited in this project.

In Investigation 1 (5.2), we had observed a significant increase of emissivity upon tempering in the experimental glasses. One potential explanation for this increase was the diffusion of sodium or other alkalis from the glass substrate. For the following experiment (Investigation 2), we therefore decided to use an alkali barrier layer on top of the glass. For this, AGC provided one of their commercial glasses already coated with this barrier layer (Luxclear).
We then compared the samples deposited on Luxclear to the ones deposited on glass without barrier layer after tempering. Since diffusion of alkali elements also happens at room temperature it is part of the natural aging process of glass, so if an alkali diffusion barrier in between the substrate and the coating has an impact on the performance it will likely be necessary to ensure long term stability as well.

5.3.1 Sample preparation

The same types of samples as in Investigation 1 (5.2.1) were deposited, except for the IZO type B', which was this time omitted because it didn't show any significant difference with the room temperature deposited IZO in Investigation 1. In order to test conditions during industrial tempering, the three types of ITO described in 5.2.1 were deposited on 10 cm x 10 cm, 4 mm thick Luxclear substrates from AGC and tempered at AGC in harsh tempering conditions.

Process parameters for Investigation 2 are the same as for Investigation 1:

- Type A (standard recipe):
  - Substrate is at room temperature.
  - Atmosphere 9sccm pure Argon + 6 sccm 97.5% Argon mixed with 2.5% O_2.
- Type B (high O_2):
  - Substrate is at room temperature.
  - Atmosphere 5 sccm pure Argon + 10 sccm 97.5% Ar mixed with 2.5% O_2.
- Type C (high temperature):
  - Substrate is at 300 degrees Celsius.
  - Atmosphere 9sccm pure Argon + 6 sccm 97.5% Argon mixed with 2.5% O_2.

All depositions were carried out in the MRC RF sputtering tool. All samples were tempered at AGC with tempering conditions: 670°C, 180s, no forced convection, 85% blow speed.

Table 21

Samples used for industrial tempering with different deposition equipment, thin layer thicknesses and processing conditions.

Code	Size [mm]	Substrate	Material	Thin layer thickness	Processing conditions
TN19J Luxclear	100x100x4	89+ glass	SiO_x	30nm	Tempered
TN19K	100x100x4	TN19J	ITO		Type A and tempered
TN19L	100x100x4	TN19J	ITO		Type B and tempered
TN19M	100x100x4	TN19J	ITO		Type C and tempered

In this Investigation 2, the aim was to test more industrially relevant sample sizes and this time also characterise the thermal infrared emissivity. The deposition parameters applied are summarised above. Since doping elements like sodium can, during the tempering process, diffuse from the substrate and affect the electrical, and therefore emissivity, properties of the TCOs, we compared TCOs grown on regular soda lime glass (where no barrier prevents alkali like Na from migrating), to TCOs grown on special glass with an alkali barrier between the glass and the TCO (Luxclear from AGC). However, a failure of the samples during tempering made this comparison impossible.
Process parameters for Investigation 2. All depositions were carried out in the MRC RF sputtering tool and all samples were tempered at AGC.

Table 22

Samples used for industrial tempering with different deposition equipment, thin layer thicknesses and processing conditions.

Code	Size [mm]	Substrate	Material	Thin layer thickness	Processing conditions
TN19P	300x300x4	Luxclear	ITO	150nm	Type A Tempered
TN19Q		Plain Glass			
TN19R		Luxclear		300nm	
TN19S		Plain Glass			
TN19T		Luxclear	IZO	150nm	Type A Tempered
TN19U		Plain Glass			
TN19V		Luxclear		300nm	
TN19W		Plain Glass			

5.3.2 Results and discussion

The results of optical measurements (PAR light transmission, reflection and absorption) and thermal properties (thermal infrared reflection) are shown in Table 23. The as-deposited deposited trends are very similar to the results of section 0, i.e. decrease of the absorptance upon tempering. One noticeable difference, however, is that the absorptance in the 400-700 nm range is slightly higher than for Investigation 1. This is mainly a difference in the absorption of the substrate, the difference in absorptance of the ITO thin layer is likely due to the higher temperature and shorter duration used for tempering at AGC compared to the lab-scale tempering in the previous investigation.

Table 23

Optical properties (PAR light transmission T, reflection R, absorption A) and thermal properties (thermal infrared reflection TIR) of samples prepared with different deposition equipment, different thin layer thicknesses and processing conditions, both measured and modelled.

Code	PAR light reflection RNEN2675		PAR light transmission TNEN2675		PAR light absorption ANEN2675 (A minus A substrate)		Max Planck weighted TIR reflection
	Measured [%]	Fitted in Model [%]	Measured [%]	Fitted in Model [%]	Measured [%]	Fitted in Model [%]	Measured [%]
TN19J	9.5	9.5	87.5*	88.3*	3.0*	2.2*	
TN19K	14.5	14.4	81.1	81.4	1.4**	1.9**	52.5
TN19L	14.2	14.1	81.6	81.8	1.2**	1.9**	49.8
TN19M	14.3	14.2	81.9	81.9	0.8**	1.7**	52.5

Luxclear is a float glass with a dense SiO_x barrier coated on top to prevent the diffusion of mobile alkali elements in soda lime glass, the most important being Sodium which plays an important role in glass corrosion. Despite our best efforts a perfect fit was not obtained for the substrate with a significant deviation between the measured and modelled Transmission, the introduced error propagates in the analysis of all other samples that were deposited on Luxclear since the modeled Luxclear is necessarily part of the model.

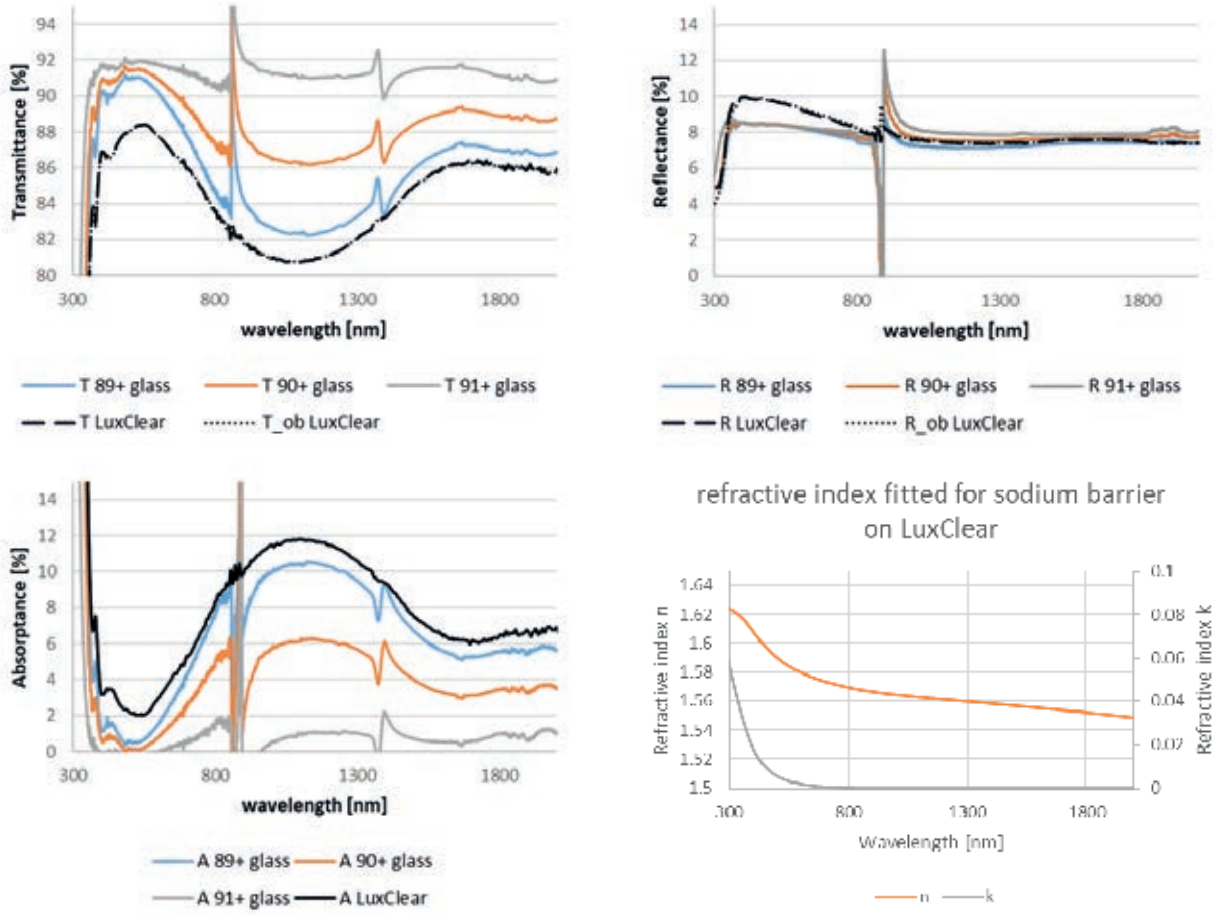

Figure 43 *Measurements on the Luxclear substrate with sodium barrier, top left: PAR light Transmission, top right: PAR light reflection, bottom left: PAR light absorption. 89+, 90+ and 91+ base glass measurements are added for comparison. Bottom right the best fit refractive index based on 89+ substrate glass and a SiO – SiO2 mixture thin layer.*

Spectral features in the Luxclear glass like the broad absorption peak around 1100nm and narrow absorption peak at 380nm are best explained by selecting a 89+ base glass which has some Iron content that cause these features. The barrier coating is slightly reflecting and absorbing in the blue range which is the only remaining feature not explained by the base glass.
Since the sodium barrier consists of a dense SiO_x layer a mixture of SiO and SiO_2 was modelled, this gave the best fit relative to other models that were tried. Fitting resulted in a 15% SiO fraction in the sodium barrier thin layer with a 74 nm thickness.

As expected from investigation 1 the PAR absorptance of the three differently deposited ITO layers converged to roughly the same low value around 1%.

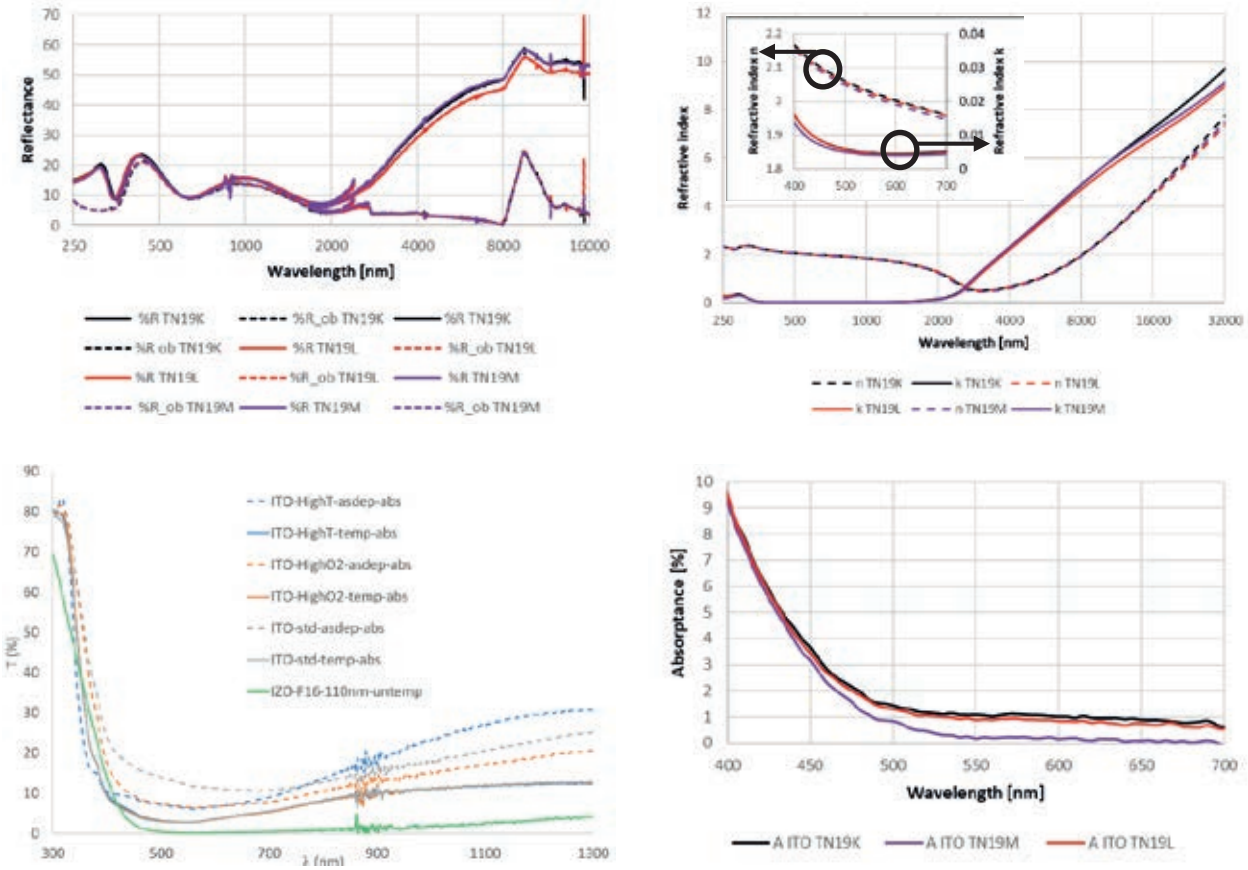

Figure 44 *Measurements on the tempered samples of ITO deposited on Luxclear using different deposition parameters. Top left: the reflection from UV to TIR for the tempered samples, top-right: the fitted refractive index for the tempered ITO thin layers, below-left: the absorption of the ITO thin layers on Luxclear before and after tempering, below-right: the absorptance in the PAR range of the ITO layer only (Luxclear substrate absorption has been subtracted).*

Once tempered the ITO layers on Luxclear converge to become roughly identical, the absorption in the PAR range converges to close to zero and the reflection in the thermal infrared converge to roughly the same performance.

Table 24

Refractive index N and sheet resistance R of samples before and after industrial tempering.

Code	Refractive index NThin Layer NEN2675	Thin layer thickness	Sheet resistance Rs [W/sq]1 before tempering	Sheet resistance Rs [W/sq]1 after tempering
	Fitted in Model [n+ik]	Fitted in Model [nm]	Measured[2]	Measured[2]
TN19J	$1.5860+i4.794\cdot10^{-3}$	73.9		
TN19K	$2.0358+i6.192\cdot10^{-3}$	157.2	33.3±1.6	51.7±3.2
TN19L	$2.0320+i6.010\cdot10^{-3}$	153.8	30±0.6	60.5±2.1
TN19M	$2.0238+i5.300\cdot10^{-3}$	156.8	15.4±0.6	52.7±2.1

[1] measured using a four point probe

As can be seen in Figure 44, a similar convergence of properties is observed for the fitted refractive index over the entire spectrum. Sample TN19L shows a slight deviation: 2.5% lower thermal infrared reflection and ~15% larger sheet resistance this could be caused either by the slightly lower layer thickness or slightly lower extinction coefficient in this range. In either case the differences in properties of the ITO thin layers can be considered negligible after tempering, especially in relation to the differences observed before tempering caused by different deposition conditions.

The effect of alkali diffusion from the glass substrate to the TCO thin layer was investigated using a set of 8 samples with and without an alkali diffusion barrier. A concurrent aim for this investigation was to test more industrially relevant sample sizes and tempering conditions.

One major hurdle during the tempering tests carried out at AGC on this set of samples was that, unlike in the previous study, which was with smaller samples, most of the samples coated with ITO shattered upon tempering. This is a commonly observed phenomenon in the glass industry. It generally occurs when the glass is too cold when entering the cooling phase of the tempering process: when the glass is not hot enough (i.e. soft enough) to develop the stress gradient expected for the tempering to be effective, the assisted cooling phase that follows is likely to cause sample breakage where local weaknesses pre-existed (e,g, scratches, hairline cracks).

In our case, a too low sample temperature is indeed likely, because of the low emissivity of the ITO: low emissivity means that the coating reflects a large part of the infrared, therefore limiting the amount of IR and thus heating power that can reach the glass underneath the TCO.

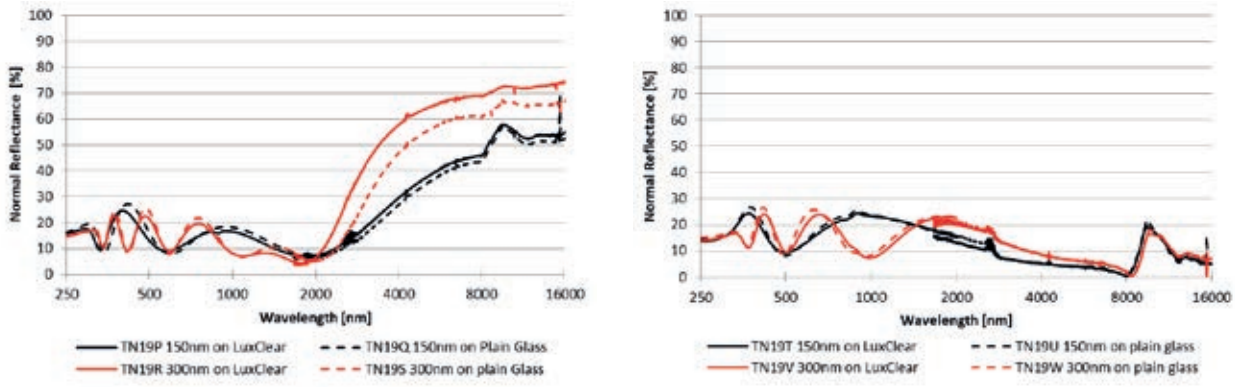

Figure 45 *Measured reflection spectra of, left: the ITO thin layers and right: the IZO thin layers. Black lines are used for the 150 nm layers and red for the 300 nm layers, dashed lines represent the layers on plain glass and solid lines those coated on a substrate glass with an alkali diffusion barrier.*

The reflection spectra in Figure 45 shows that the reflection in the thermal infrared for the IZO layers has completely disappeared. While undesirable in the context of this project, this explains why the IZO samples underwent the tempering process without issue where the ITO samples suffered breakage undergoing the exact same process.

Table 25

Integral properties measured and modelled for the sample set investigating the effect of an alkali diffusion barrier.

Code	PAR light reflection RNEN2675		PAR light transmission TNEN2675		PAR light absorption ANEN2675 (A minus A substrate)		TIR reflection RMIR
	Measured [%]	Fitted in model [%]	Measured [%]	Fitted in model [%]	Measured [%]	Fitted in model [%]	Measured [%]
TN19P 150nm on Luxclear	13.0	13.4	82.4	82.4	1.6	2.0	51.6
TN19Q 150nm on plain glass	13.9	14.0	83.7	83.4	1.5	1.7	49.6
TN19R 300nm on Luxclear	14.7	14.7	80.7	80.3	1.64	2.74	71.3
TN19S 300nm on plain glass	15.4	15.2	81.3	81.3	2.4	2.5	64.1
TN19T 150nm on Luxclear	13.4	13.7	82.7	82.3	0.94	1.84	7.9
TN19U 150nm on plain glass	13.8	14.0	83.73	83.23	1.5	1.9	7.8
TN19V 300nm on Luxclear	18.3	18.1	77.53	77.03	1.33	2.73	8.3
TN19W 300nm on plain glass	19.7	19.4	75.43	74.43	4.03	5.33	8.6

[3] deviation between the fitted model and the measurement is larger than 0.5%

[4] deviation in absorption between model and measurement was caused by the less than optimal fit of the Luxclear sodium barrier substrate.

Table 23 shows the optical properties in the PAR range and thermal properties by the Max Planck weighted reflection. As shown in the table the Luxclear samples show a lower quality of fit due to the less than perfect fit for the Luxclear substrate itself. It can also be noted that the TCO layers show a consistently low absorptance in the PAR range. Another trend that can be observed is that the thicker ITO layer show a less than proportional increase in absorptance with layer thickness, if this is a random effect seen here or if the extinction coefficient has a direct relation with the layer thickness has not been investigated further.

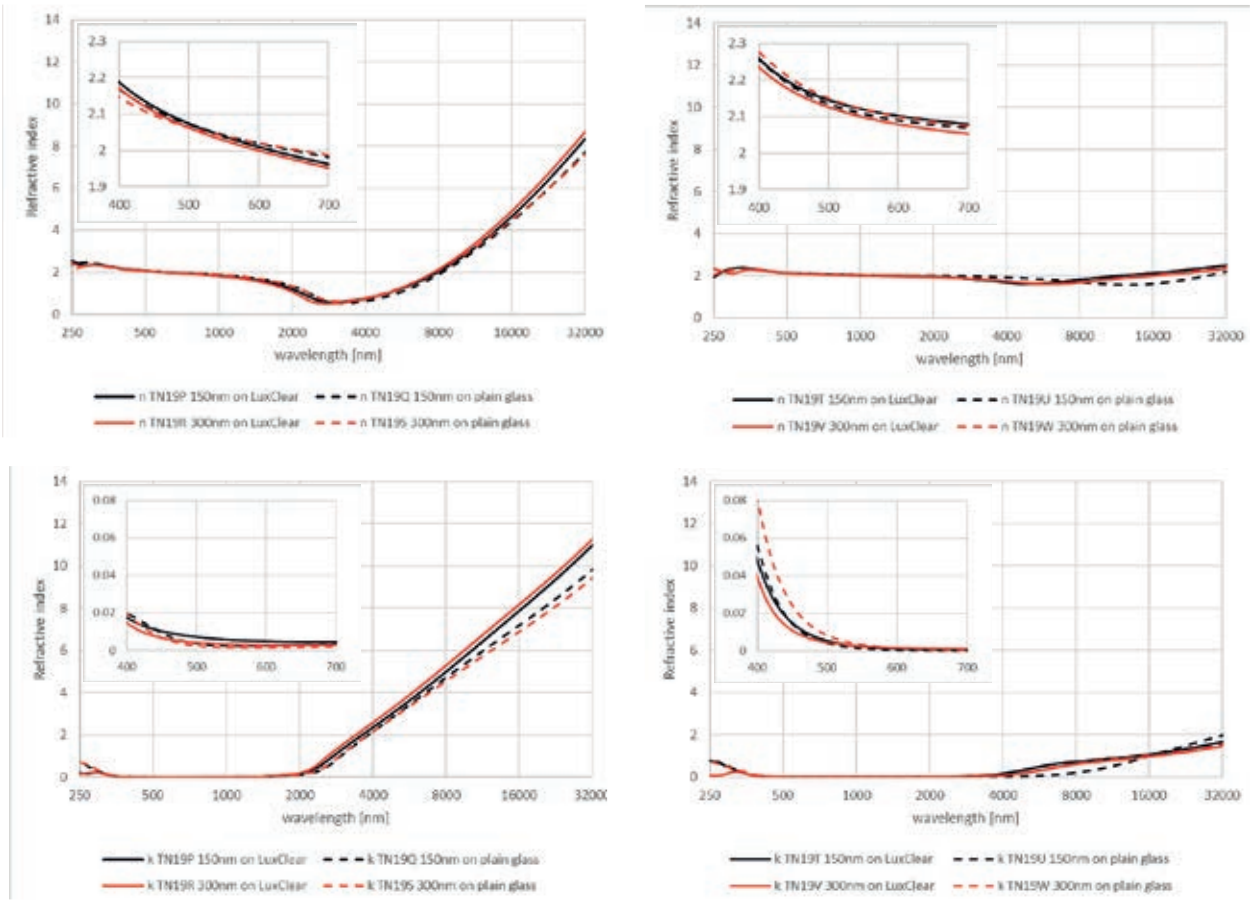

Figure 46 *Fitted refractive index spectra of left the ITO thin layers and right the IZO layers. At the top the real part and at the bottom the extinction coefficient of the refractive index is plotted. Black lines are used for the 150 nm layers and red for the 300 nm layers, dashed lines represent the layers on plain glass and solid lines those coated on a substrate glass with an alkali diffusion barrier.*

The 300nm IZO thin layer seems to show an anomalously high absorptance in the PAR range, looking at the refractive index data it seems that the tail of the bandgap has moved considerably into the PAR range.

Table 26

Refractive index N and sheet resistance R of samples before and after industrial tempering.

Code	Refractive index NThin Layer NEN2675	Thin layer thickness
	Fitted in Model [n+ik]	Fitted in Model [nm]
TN19P	$2.0455+i6.847\cdot10^{-3}$	141.6
TN19Q	$2.0492+i4.972\cdot10^{-3}$	147.1
TN19R	$2.0343+i4.384\cdot10^{-3}$	292.0
TN19S	$2.0448+i3.633\cdot10^{-3}$	294.5
TN19T	$2.1307+i6.663\cdot10^{-3}$	117.2
TN19U	$2.1207+i6.394\cdot10^{-3}$	116.9
TN19V	$2.1087+i5.649\cdot10^{-3}$	237.7
TN19W	$2.1334+i1.065\cdot10^{-2}$	230.5

The most notable effects are seen for TNO Solliance "standard" IZO samples (i.e. deposited at room temperature), although the tempering did not significantly affect the Transmission, it led to a dramatic increase of the sheet resistance and emissivity, with post-tempering emissivity values close to that of glass.
This observation explains why, unlike for ITO, none of the IZO samples shattered during tempering. Indeed, the increase in emissivity occurred during the heating stage of the process, so that very little of the IR was being reflected and most was absorbed by the glass. The temperature achieved by the samples was therefore significantly higher than that of the ITO samples, that is, hot enough to temper without damage.
To understand the dramatic change in emissivity, XRD was carried out on the tempered IZO and compared to the non-tempered one (Figure 47). Although TNO Solliance standard, as-deposited IZO is almost completely amorphous, the tempered IZO shows a much more crystalline structure. The tempering therefore led to crystallisation of the In_2O_3 phase. Why the crystallised phase has a higher emissivity is not elucidated by the data. One possibility is that the doping defects that normally provide low sheet resistance and low emissivity in IZO were "healed" by the high temperature step, hence increasing both sheet resistance and emissivity.

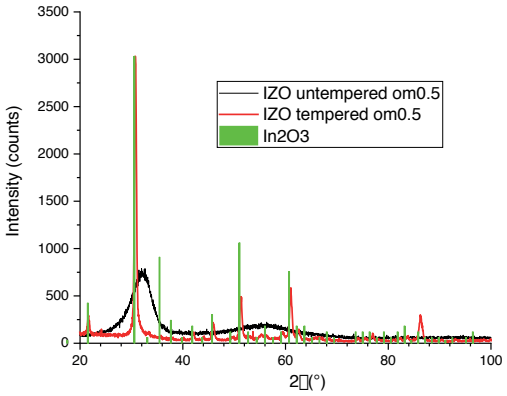

Figure 47 *XRD patterns of the IZO sample before (black) and after (red) tempering, as well as the In2O3 powder diffraction reference file.*

5.3.3 Conclusion

ITO and IZO show a large variation in its properties after deposition under varying conditions. Tempering after deposition changes the properties considerably, for ITO:

- The PAR absorption is reduced to close to zero regardless of its absorption post deposition before tempering.
- Properties like sheet resistance, refractive index and emissivity each converge to become roughly the same after tempering regardless of deposition conditions.

The low-e properties are affected by alkali diffusion from the substrate into the ITO thin layer during tempering. The ITO thin layers deposited on an alkali diffusion barrier show an onset of the rise in the extinction coefficient at shorter wavelengths and a steeper rise throughout the thermal infrared leading to better low-e properties. Alkali diffusion does not show an effect on PAR absorption of the ITO thin layer.

IZO shows very little absorption before tempering and remains to be highly transparent after tempering. Contrary to ITO - which showed limited increase in sheet resistance and emissivity - the low-e properties of IZO completely disappeared upon tempering, this coincides with a morphological change from an amorphous to a crystalline phase for the indium oxide.

5.4 Demonstrator glass with low-e AR coatings using TCOs (Investigation 3)

The aim of the last series of experiments (Investigation 3) was to provide a demonstrator for the project, drawing on the lessons learnt from the first series of experiments.

5.4.1 Experimental sample preparation

The samples deposited were the ones that had demonstrated the most promising optical properties, but had not fully yet succeeded in achieving the researched properties.

For the ITO, we needed to achieve a better tempering process, i.e. without the 30 cm x 30 cm samples breaking. The workaround to this breaking was a more careful tuning of the tempering process to ensure sufficient heating in spite of the low ITO emissivity.

For the IZO, we needed to preserve the low emissivity intact upon tempering. As a possible workaround to the dramatic emissivity increase observed in Investigation 2, we therefore tested IZO depositions at 150°C. The idea was to "pre-crystallize" the IZO in more favourable conditions, rather than the harsher conditions of a tempering process, in the hope that the tempering would then have a milder effect on the defect chemistry of the IZO.

The following samples were used for Investigation 3, producing a series of demonstrators.

Table 27

Overview demonstrator samples with different deposition parameters for Investigation 3.

Code	Size [mm]	Substrate	Material	Thin layer thickness	Processing info
TN20A	300x300x4	Extra clear glass (AGC19G)	ITO	130nm	* Type B (standard recipe) only: T=300°C , 9sccm pure Ar + 6 sccm (97.5% Ar , 2.5% O_2)
TN20B					
TN20C					
TN20D					
TN20H				300nm	
TN20E			IZO	150nm	*Type B' only: T=150°C, 9sccm pure Ar + 6 sccm (97.5% Ar , 2.5% O_2)
TN20F					
TN20G					

5.4.2 Results

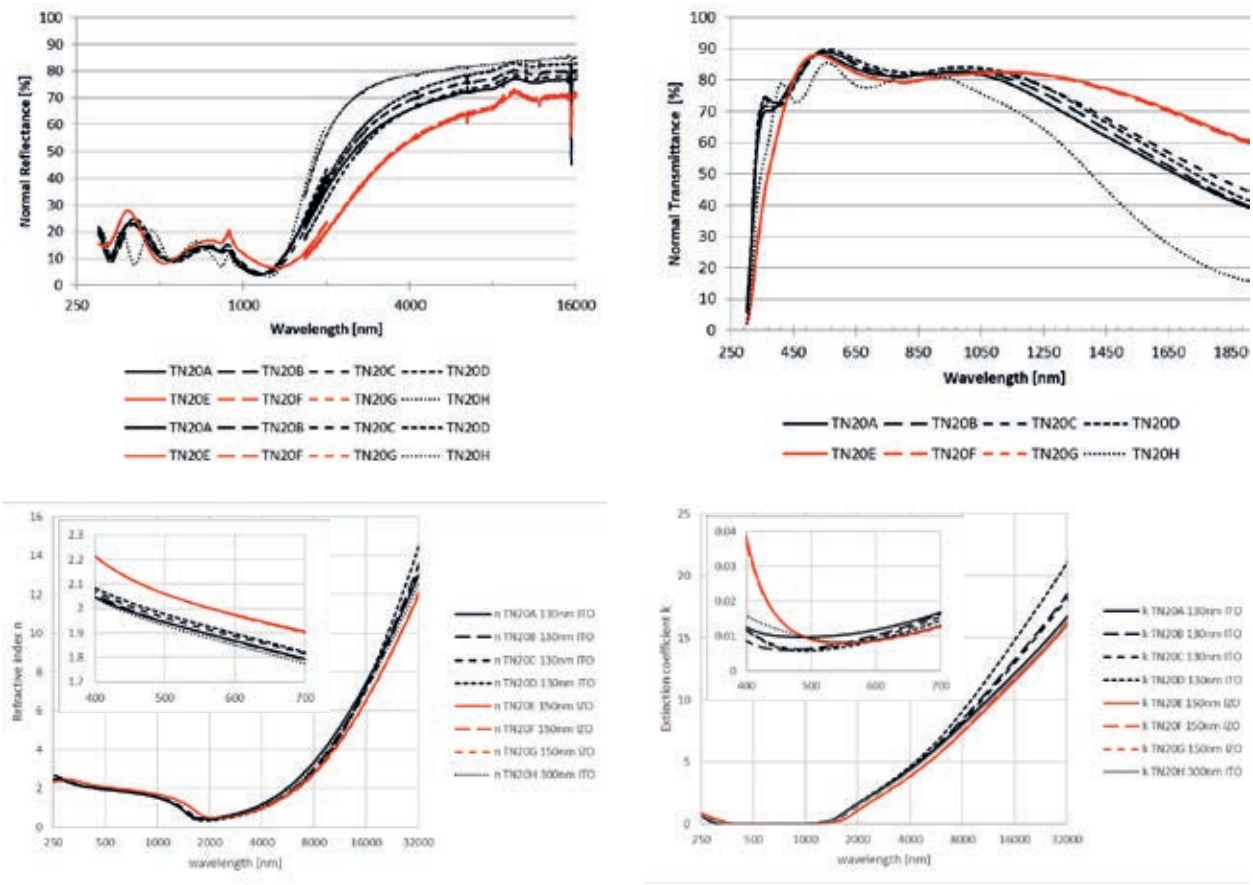

Figure 48 *Measured optical and thermal properties of different demonstrator glasses. Upper left: Thermal reflection, upper right: PAR light Transmission, lower left: refractive index, lower right: extinction coefficient.*

Table 28

Optical and thermal properties of different demonstrator glasses.

	PAR light reflection RNEN2675		PAR light transmission TNEN2675		PAR light absorption ANEN2675 (A minus A substrate)		Max Planck weighted TIR reflection
	Measured [%]	Fitted in Model [%]	Measured [%]	Fitted in Model [%]	Measured [%]	Fitted in Model [%]	Measured [%]
TN20A	12.9	11.7	84.2	84.4	2.7	3.6	75.3
TN20B	12.8	12.2	84.5	84.5	2.4	3.0	78.5
TN20C	12.9	12.2	84.7	84.7	2.1	2.9	76.4
TN20D	12.9	12.5	84.8	84.6	2.0	2.7	81.4
TN20E	12.7	13.0	83.2	83.5	3.9	3.3	68.4
TN20F	12.7	13.0	83.2	83.5	3.8	3.4	69.4
TN20G	12.7	13.0	83.3	83.5	3.7	3.3	69.1
TN20H	14.0	13.2	79.4	80.0	6.3	6.6	83.4

For the ITO samples the fitting procedure let to an absorption 0.6% to 0.9% larger than what was actually measured on the samples. For tempered samples we've seen the absorption being reduced further than for ITO, consequently in the table below a column was added with the predicted hemispherical Transmission corrected for the deviation caused by fitting and the expected reduction in absorption from tempering.

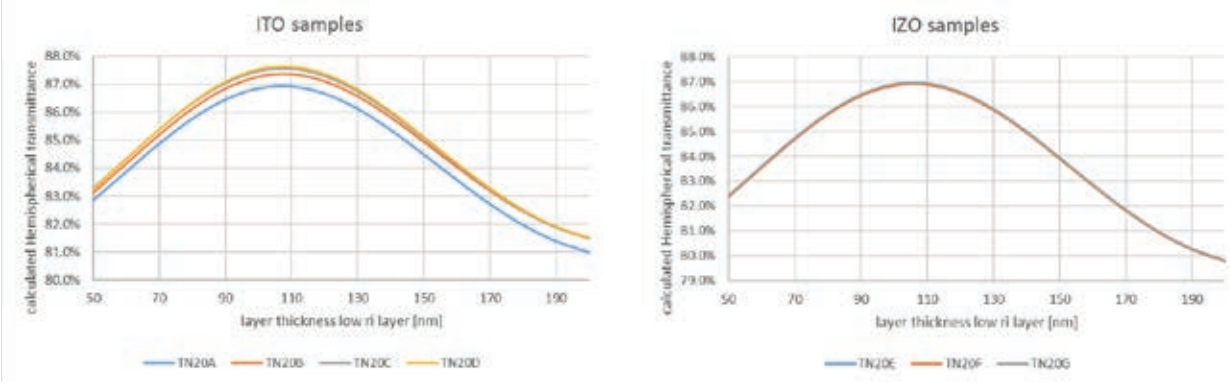

Figure 49 *Calculated hemispherical Transmission of different TCO glasses with ITO (left) and IZO (right) depending on thickness of the layer.*

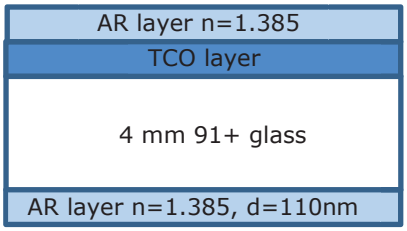

Figure 50 *Composition of the demonstrator glass consisting of a 4 mm 91+ basic glass with a TCO layer and with two AR coatings on both sides with a refractive index N of 1.385.*

Table 29

Refractive index and expected hemispherical transmission (Them) modelled, corrected and measured.

Code	Refractive index NThin Layer NEN2675	Thin layer thickness	Calculated Them for double AR stack combined with n=1.385 low RI layer	Calculated Them corrected for deviation from fitting and effect of tempering *	THem measured after AR deposition and tempering
	Fitted in Model [n+ik]	Fitted in Model [nm]			
TN20A	$1.905+i1.166\cdot10^{-2}$	143.8	86.9	89.3%	
TN20B	$1.905+i9.357\cdot10^{-3}$	151.2	87.4	89.2%	
TN20C	$1.925+i9.275\cdot10^{-3}$	145.9	87.5	89.2%	
TN20D	$1.936+i8.615\cdot10^{-3}$	147.3	87.6	89.1%	88.6%
TN20E	$2.022+i1.184\cdot10^{-2}$	125.6	86.9	86.4%	
TN20F	$2.020+i1.183\cdot10^{-2}$	126.5	86.9	86.4%	
TN20G	$2.020+i1.166\cdot10^{-2}$	126.3	86.9	86.6%	88.9%
TN20H	$1.890+i1.034\cdot10^{-2}$	297.8	83.0	87.2%	86.7%

* it was assumed that after tempering the absorption of the ~150nm ITO layer would become 1.2%, this was estimated based on the absorptance measured for ITO samples TN19K, -L, -M, -P, -Q after tempering. IZO was only corrected for the deviation caused by fitting since not enough data was available on the effect of tempering on absorption to make an estimate.

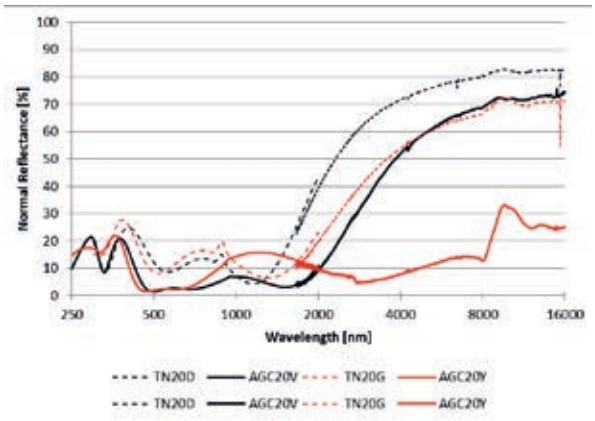

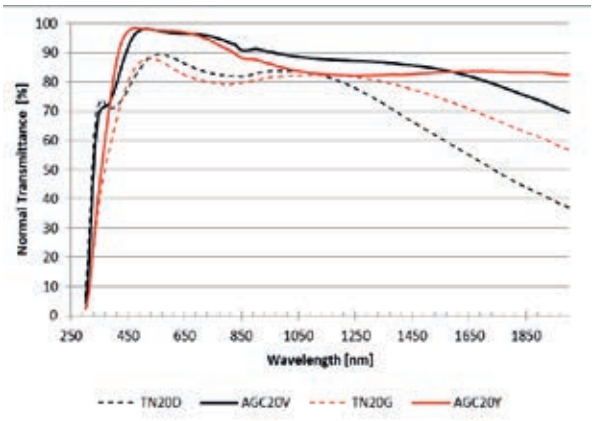

Table 30

Optical properties (Direct PAR light reflection, Transmission, absorption and hemispherical PAR light Transmission) and thermal properties (thermal reflection) measured of different demonstrator glasses with only TCO coating (either ITO or IZO) and after adding a 2AR coating on both sides of the samples.

Code	Type of coating	PAR light reflection R*	PAR light Transmission*	PAR light absorption* minus substrate	Hemispherical PAR light Transmission*	Max Planck weighted TIR reflection
TN20A	ITO	12.9	84.2	2.7	77.5	75.3
AGC20S	ITO & 2AR	3.3	95.7	0.7		66.8
TN20D	ITO	12.9	84.8	2.0	78	81.4
AGC20V	ITO & 2AR	3.5	95.3	1.0	88.6	70.9
TN20G	IZO	12.7	83.3	3.7	76.1	69.1
AGC20Y	IZO & 2AR	2.8	96.7	0.2	88.9	23.4
TN20H	ITO	14.0	79.4	6.3	73	83.4
AGC20Z	ITO & 2AR				86.7	79

*perpendicular, NEN2675 PAR weighted in [%]

From Table 30 we can observe that adding a 2AR coating on top of the TCO coating resulting in a substantial increase of light transmission on all samples. The highest light transmission could be reached on the IZO 2AR sample. At the same time the 2AR coating also reduced the thermal properties, unfortunately the highest reduction could be observed on the IZO 2AR sample.

We can conclude that we were able to produce a high transmission and low emissivity glass with TCOs from ITO 2AR with a good performance of hemispherical light transmission of 88.6% and a thermal infrared reflection of 70.9% (sample AGC20V).

5.5 Industrial samples and preparation

During this project Asahi Glass Company developed a coating stack with the same aim of combining low-e and antireflective properties but than based on established industrial processes that can already be used for multi-hectare scale production.

For this demonstration Fluor doped Tin oxide (FTO) was deposited on high temperature 89+ glass using an in line CVD coater located close to the glass smelter.

The usage of existing production facilities has some obvious advantages - like proven scalability - but also some disadvantages. For instance, the CVD coater used to deposit Fluor doped tin oxide (FTO) is situated in the production line of the glass furnace, this makes an obvious optimization like switching from 89+ to 91+ base glass a prohibitively expensive task when the only purpose it serves is to make an optimized demonstrator.

Table 31

Overview of demonstrator samples.

Code	Size [mm]	description	THem [%]	e [%]
AGC18A	500x500x4		82.8	16
AGC18B	500x500x4		78.1	16
AGC18C	500x500x4	89+ base glass coated with fluor doped tin oxide low-e layer and antireflective layer on the top side and AR layer at the bottom side	86.0	16
AGC18N	170x170x4			16
AGC19E	500x500x4	89+ base glass without AR coating	82.8	86
AGC19F	500x500x4	90+ base glass without AR coating	83.5	86
AGC19G	500x500x4	91+ base glass without AR coating	84.3	86
AGC19N	500x500x4	91+ base glass with double sided AR coating	89.8	86
AGC19O	500x500x4	91+ base glass with double sided AR coating	89.5	86
AGC20R	500x500x2	Physical vapor deposited indium tin oxide low-e layer and AR layer on the top side and AR layer on the bottom side	75.8	25

6 Conclusion and future perspectives

6.1 Material development

The goal of this project was to develop and explore the potential of new greenhouse glass types, combining high light transmission for crop production with high energy saving. We explored experimental and industrially relevant transparent conducting oxides (TCOs) in order to reduce the thermal emissivity of greenhouse covers combined with an antireflective stack for high light transmissivity.

As a **result,** an experimental scale prototype sample was fabricated that demonstrates a hemispherical PAR Transmission of 88.6% and an emissivity of 31% and an industrial scale prototype was realized with 86% hemispherical PAR Transmission and 16% emissivity.

The integration of low-e properties in AR coatings is a novel pursued for greenhouse applications and the prototypes developed in this project represent a best effort performance with the current technology and time available within this project. This is of course not equal to the maximum attainable performance with this technological approach, so also the **future perspectives** have been investigated based on theoretical calculations.

- To combine low emission with anti-reflective properties, a coating structure with at least 2 thin layers is required. To gain insight into the potential of 2- and 3-layer AR stacks, hypothetical AR coatings with 1, 2 and 3 layers were calculated, assuming 0% absorption.
  - Coatings with 1 thin layer can theoretically achieve a hemispherical PAR transmission of 94%, in practice the maximum performance is around 91%.
  - With 2-layer coatings, slightly more than 92% hemispherical PAR transmission can be achieved.
  - With 3-layer coatings, slightly less than 92% hemispherical PAR transmission can be achieved.
- For a single layer AR coating the theoretical maximum performance requires a refractive index of 1.18. For a conventional silica-based AR coating this necessitates a porosity of 63%. In practice, a maximum of 91% is achieved with single-layer coatings (n = 1.34 and porosity 29%). This difference can likely be explained by the high porosity required for a lower refractive index which probably leads to a coating that is too fragile.
- For the calculations on 2- and 3-layer AR coatings a refractive index of 1.34 has been used as a practical lower limit for the outermost layer. Also, the hemispherical PAR transmission of 2 and 3 layer coatings is much less sensitive to the refractive index of the outer layer, if non-porous quartz (n = 1.48) is used for this, it can be slightly more than 91% for a 3 layer system and for a 2 layer system 90.5% hemispherical PAR transmission can be achieved. (still using a single layer n=1.34 AR coating on the inside).

- Transparent conductive oxides (TCOs) have been investigated for the layer that should contribute low-e properties to the AR stack. A suitable TCO should: have the lowest possible absorption in the PAR region, show a significant reduction in emissivity and be able to withstand the further production process for safety glass.
  - Indium Tin Oxide (ITO) and Indium Zinc Oxide (IZO) were investigated. Differences in properties that arise from variation in deposition conditions largely disappear with a thermal after-treatment that is common in tempering glass. The high temperature tempering treatment causes the PAR absorption to become suitably low (<1%). This high temperature treatment also caused a reduction in thermal infrared reflection for ITO and the low-e properties of IZO was shown to be severely degraded.

- Low-e integrated AR coatings for greenhouse application will necessarily be optimised for maximum hemispherical PAR Transmission. This limits the thickness that can be used for the TCO layer and this is also what limits the thermal infrared reflection that could be reached with the TCOs investigated in this project, this is not a fundamental limit.

- Fluor doped Tin Oxide (FTO) deposited via in line spray pyrolysis was investigated on an industrial scale.

The following **open research questions** have been identified from a material development perspective:

- The durability of the coating stack performance should be further investigated.
- TCO performance:
  - Tuning n to be lower would be great because it enables us to go to an optimal double layer AR stack, however, this seems to be very difficult.
  - Increasing electron density in TCO would negatively affect the properties in the PAR range.
  - Increasing electron mobility would help lower the emissivity for the same layer thickness and further improve energy saving.
- A possible future development could be to employ resonant doping of metal oxides which shows promise in regards to combining high electron mobility with moderate electron density. An example is molybdenum doped indium oxide which shows less hybridisation of the dopant's donor state with the conduction band resulting in less ionized impurity scattering.
- The properties of TCOs can be manipulated further to find an improved optimum.
  - By increasing the doping concentration of the TCOs the properties of the TCO could be tuned to start reflecting at shorter wavelengths but care has to be taken to not move the absorption tail into the PAR region.
  - Higher electron mobility would improve the low-e properties without the risk of moving the absorption tail too much into the PAR range. Although beneficial, pursuing would entail researching other material combinations and would entail a risk of failure since.
  - Molybdenum doped indium oxide seems to be promising in this regard.
  - Tuning n.

We can **conclude** that more detailed material development by industrial companies is possible in the near future. However, having developed the current industrial protoype glass, we have shown that is already has a good performance combining low-e properties for energy saving and high light transmission for crop production. We have shown, that the current industrial prototype glass has already a good technical performance and economic perspective for growers.

6.2 Greenhouse application

The **goal** of this project was to develop and explore the potential of new greenhouse glass types, combining high light transmission for crop production with high energy saving. We explored experimental and industrially relevant transparent conducting oxides (TCOs) in order to reduce the thermal emissivity of greenhouse covers combined with an antireflective coating for high light transmissivity.

As a **result,** an experimental scale prototype glass sample was fabricated during this project with a hemispherical PAR Transmission of 88.6% and an emissivity of 29% and an industrial scale prototype was realized with 86% hemispherical PAR Transmission and 16% emissivity.

The **energy saving potential** of new glass types was investigated. For a model cultivation, a tomato crop in a Venlo type greenhouse without artificial lighting but equipped with an energy saving screen in the Dutch climate. The experimental and industrial scale glass prototypes can reduce natural gas consumption respectively from 33.6 to 28.7 $m^3_{gas}/m^2_{greenhouse}$ and from 33.6 to 27.3 $m^3_{gas}/m^2_{greenhouse}$ or -15 and -19% respectively. This is compared to a current high-performance greenhouse cover consisting of a double-sided AR coated single glass with a hemispherical PAR Transmission of 90% and an emissivity of 86%.
The demonstrated prototypes will not only reduce energy consumption but will also affect the production, the experimental and industrial scale prototypes will reduce the production by 2.1 and 4.4 %, the difference in hemispherical PAR Transmission explains 1.1 and 3.2% respectively and 0.7 and 1.2% this reduction is due to a lower CO_2 concentration caused by an increased need for ventilation.

From an **economic perspective** our model cultivation is at the break-even point for an energy saving screen to make economic sense at the current price of natural gas (0,20 €/m^2 incl. taxes). To be a competitive alternative option for saving energy the premium price on top of that for double sided AR coated glazing should be below 20 and 16 €/m^2 for the experimental and industrial scale prototypes, respectively. This assumes a 15-year depreciation period and no change in energy prices.

From a **sustainability** point of view the development of low emission high transmission glasses can deliver a serious contribution to the climate goals of the Dutch government towards fossil-free climate neutral greenhouse production in 2050. Depending on the speed of material development towards market-ripe products these glasses might also contribute to the goal of CO_2 emission reduction with 1,8 – 2,9 Mton in 2030. If we assume a reduction primary gas use with 5 $m^3/m^2/y$, this results in a CO_2 emission of 8,5 $kg/m^2/y$ (8,5 t/ha/y). If we further assume that yearly 100 ha new greenhouses would be newly built during a period of 10 years, this will lead to a CO_2 emission reduction of 8500 t CO_2 emission reduction.
The new type of glass can be estimated to be interesting for at least all crops not using artificial lighting and not being a "cold" crop which represents an area of 3500 ha in The Netherlands. If the whole area would be equipped with the new type of glass in the future this would lead to a CO_2 emission reduction of ca. 30.000 t per year.

References

Bot, G. (1983).
Greenhouse climate: From physical processes to a dynamic model. PhD Thesis. In Wageningen Agricultural University. Institute Of agricultural and environmental engineering and physics (Vol. 43)The Netherlands: AA Wageningen University. P. O. B NL-6700.

Breuer, J. J. G., & van de Braak, N. J. (1989).
Reference year for Dutch greenhouses. Acta Horticulturae, 248, 101e108. https:// doi.org/10.17660/ ActaHortic.1989.248.9. https://doi.org/ 10.17660/ActaHortic.1989.248.9.

Jong, T. De (1990).
Natural ventilation of large multispan greenhouses, De Jong. PhD Thesis. Wageningen University.

Goudriaan, J., & Van Laar, H. H. (1994).
Modelling potential crop growth processes. Textbook with exercises. Dordrecht: Kluwer Academic Publishers.

Graamans, L., Baeza, E., van den Dobbelsteen, A., Tsafaras, I., & Stanghellini, C. (2018).
Plant factories versus greenhouses: Comparison of resource use efficiency. Agricultural Systems, 160, 31e43. https://doi.org/10.1016/j.agsy.2017.11.003.

Gueymard, C. (2001).
"Parameterized Transmission Model for Direct Beam and Circumsolar Spectral Irradiance." Solar Energy (71:5); pp. 325–346.

Guillemot, F., A. Brunet-Bruneau, E. Bourgeat-Lami, T. Gacoin, E. Barthel, J.-P. Boilot (2010a).
Latex-templated porous silica films for antireflective applications. Proceedings Volume 7725, Photonics for Solar Energy Systems III; 77250G (2010) https://doi.org/10.1117/12.853514

Guillemot, F., A. Brunet-Bruneau, E. Bourgeat-Lami, T. Gacoin, E. Barthel, J.-P. Boilot (2010b).
Latex-Templated Silica Films: Tailoring Porosity to Get a Stable Low-Refractive Index. Chem. Mater. 2010, 22, 9, 2822–2828. https://doi.org/10.1021/cm^{9}03754k

Hemming, S., Hemming, S.; Waaijenberg, D.; Bot, G.; Sonneveld, P.; Zwart, F. de; Dueck, T.A.; Dijk, C.J. van; Dieleman, J.A.; Marissen, N.; Rijssel, E. van; Houter, G. (2004).
Optimaal gebruik van natuurlijk licht in de Glastuinbouw. Rapport WUR 100. https://edepot.wur.nl/40067

Katsoulas, N., Sapounas, A., De Zwart, F., Dieleman, J. A., & Stanghellini, C. (2015).
Reducing ventilation requirements in semiclosed greenhouses increases water use efficiency. Agricultural Water Management, 156, 90e99. https://doi.org/10.1016/j.agwat.2015.04.003.

Löbmann, P. (2017).
Antireflective coatings by sol–gel processing: commercial products and future perspectives. J Sol-Gel Sci Technol 83, 291–295 (2017). https://doi.org/10.1007/s10971-017-4408-x

Ludvig Svensson (2020a).
https://www.ludvigsvensson.com/en/climate-screens/climate-screens-products/luxous/luxous-1347-fr/

Ludvig Svensson (2020b).
https://www.ludvigsvensson.com/en/climate-screens/climate-screens-products/all-climate-screen-products/tempa-8672-d

Luo, W., de Zwart, H. F., Daii, J., Wang, X., Stangehllini, C., & Bu, C. (2005).
Simulation of greenhouse management in the subtropics. art I: Model validation and scenario study of the winter season. Biosystems Engineering, 90, 307e318.

Monteith, J. L. (1973).
Principles of environmental physics, 241. London: Edward Arnold. Vanthoor, B. H. E. (2011). A model-based greenhouse design method. Ph.D. Thesis. Wageningen, The Netherlands: Wageningen University.

Simonis, F. *et al.* (1979).
Physics of doped tin dioxide films for spectral-selective surfaces. Solar Energy Materials 1, 221-231

Stanghellini, C., Dai, J., & Kempkes, F. L. K. (2011).
Effect of nearinfrared- radiation reflective screen materials on ventilation requirement, crop transpiration and water use efficiency of a greenhouse rose crop. Biosystems Engineering, 110(3), 261e271. https://doi.org/10.1016/j.biosystemseng.2011.08.002. ISSN 1537-5110.

Thomas, I.M. (1992).
Method for the preparation of porous silica antireflection coatings varying in refractive index. Applied Optics Vol. 31, Issue 28, pp. 6145-6149 (1992). https://doi.org/10.1364/AO.31.006145

Timothy J. Coutts, David L.Young and Xiaonan Li (2000). Characterization of Transparent Conducting Oxides. MRS BULLETIN/AUGUST 2000, 58-65.

Zwart, H. F. de (1996). Analysing energy-saving options in greenhouse cultivation using a simulation model. PhD Thesis. Wageningen, The Netherlands: Agricultural University.

Annex 1 Refractive index spectrum for different base glasses

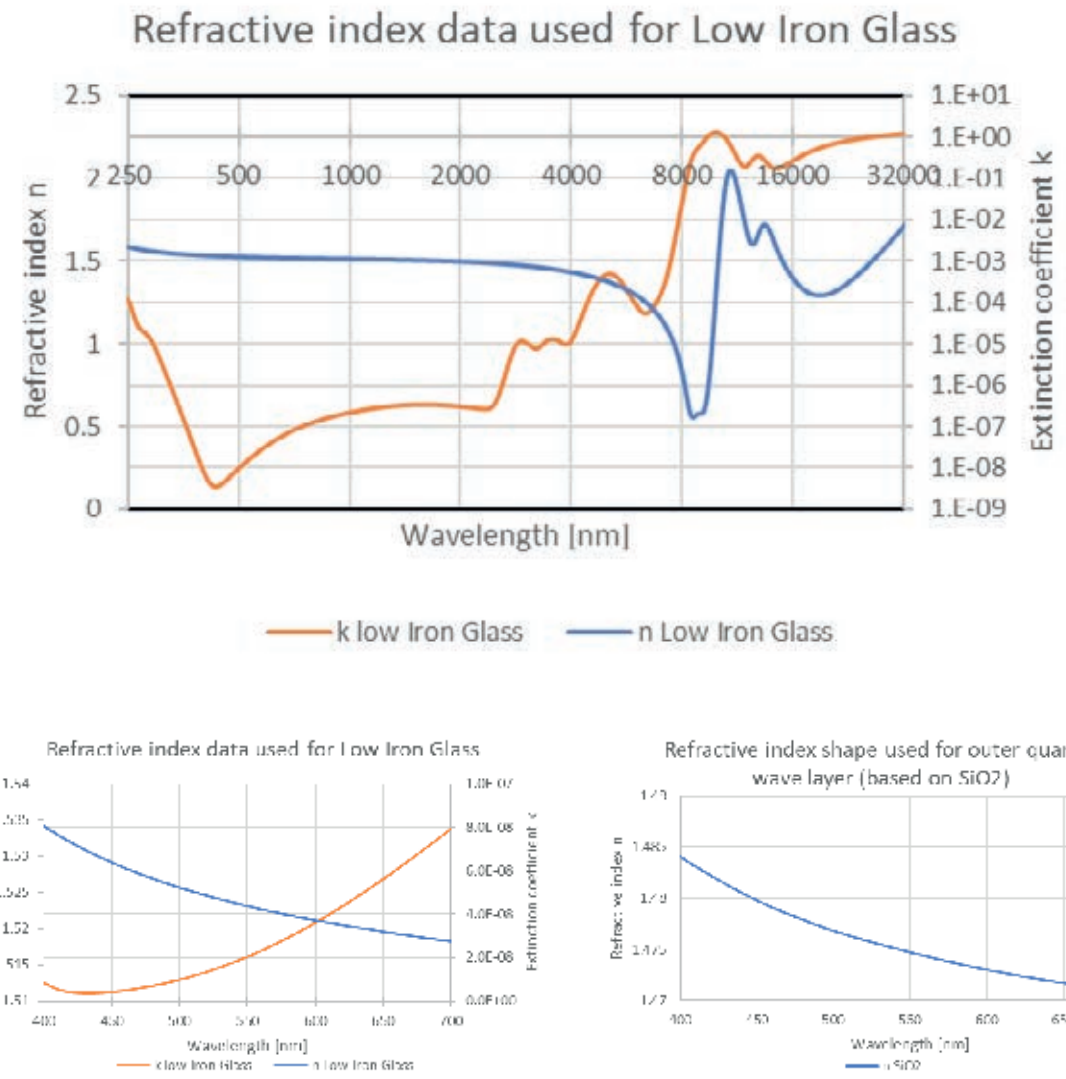

Figure 51 *Refractive index for low iron glass for the solar spectrum (above) and in more detail for the visible light c.q. PAR light spectrum (below).*

To explore the potential of nature to improve the quality of life

Wageningen University & Research,
BU Greenhouse Horticulture
P.O. Box 20
2665 ZG Bleiswijk
Violierenweg 1
2665 MV Bleiswijk
The Netherlands
T +31 (0)317 48 56 06
www.wur.nl/glastuinbouw

Report WPR-1040

The mission of Wageningen University and Research is "To explore the potential of nature to improve the quality of life". Under the banner Wageningen University & Research, Wageningen University and the specialised research institutes of the Wageningen Research Foundation have joined forces in contributing to finding solutions to important questions in the domain of healthy food and living environment. With its roughly 30 branches, 5,000 employees and 12,000 students, Wageningen University & Research is one of the leading organisations in its domain. The unique Wageningen approach lies in its integrated approach to issues and the collaboration between different disciplines.